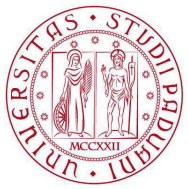

UNIVERSITÀ
DEGLI STUDI
DI PADOVA

Università degli Studi di Padova

Department of Industrial Engineering

Master Degree Course in Electrical Engineering

Master Thesis

Investigation of the sensorless capability of an Induction Motor with intentionally created saliency. Simulations and measurements

Supervisor: Prof. Nicola Bianchi

Graduate: Renzo Zeni

Session 2012−2013

Contents

List of Figures

List of Tables

Abstract

Field Oriented strategy for induction motor control are usually realized with position and speed sensors, that are expensive and are a source of fault. Sensorless drives are a good solution to avoid these disadvantages, but to implement this type of drive on induction motor there are no valid large scale industrial solution. In this thesis work, a new model for induction motor sensorless application is considered and the industrial construction feasibility of the motor is analyzed. At first, new conception induction motor rotors are analyzed with finite elements simulation. In order to validate the results of simulations, a prototype has been realized and a series of measurements has been performed. In addiction a rotor sensorless capability optimization is carried out.

Work presentation

Introduction

Variable speed drives (VSD) operation of the motor systems can save energy as well as provide better and optimal control over the process. The elimination of position and velocity transducers in AC drives has been an attractive prospect since they are a significant source of failure and cost. This is not desirable in applications like transportation systems and electrical vehicles, in which a high grade of fault tolerance is required. In large-scale production indeed the absence of the position sensor implies a worthwhile cost reduction. The greatest success has been with synchronous and reluctance machines that are considerably less complex than an induction motor (IM) and have inherent spatially dependent properties that can be tracked easily. Particular care has to be given during operating conditions so as to avoid to demagnetize the permanent magnet.

On the other hand, the induction motor represents the workhorse of electrical machines thanks to its robustness and reliability. Moreover, the absence of expensive components makes it cheap and easy of being manufactured. However, there are not only advantages. When an IM drive is compared with a PM motor drive, the power electronic has to be slightly oversized due to the lower power factor of the IM.

Position and speed estimation in IM represent a great potential but are complicated due to the machine symmetric smooth rotor, induced rotor currents and slip. Has been demonstrated that a spatial modulation of the rotor leakage inductance can be a detectable form of magnetic saliency for high frequency signals, allowing the continuous estimation of the rotor position and flux angle. However experimental validation of the sensorless control of the IM has not been investigated yet and deep studies of the detrimental effect on torque or main flux introduced by the modulation of the rotor leak-

age inductance do not exist in literature. Neither the effect of saturation at steady state operation on sensorless control of IM has not been studied yet.

Objective of thesis work

This thesis work investigates the potential sensorless capability of induction motor. After prototype construction, measure are performed to obtain high frequency parameters and compared with simulation results. Such a comparison could give some hints to propose new geometries in order to improve the knowledge in this research sector.

Chapter outlines

The contents of the chapters are following briefly exposed.

Chapter 1 exposes the main data of the studied Induction motor. The analytical analysis is then performed in order to have valid data for comparison. After that, finite elements simulation are carried out and the parameters of induction motor are obtained. At last, based on the obtained parameters, the steady state behaviour and dynamic performance of the machine is investigated.

Chapter 2 deal with field oriented control simulation with finite element software. The optimal current angle to control IM, similary to a synchronous motor is also investigated. At least the torque ripple, the mean torque and the constant torque loci of the three types of rotor are explained.

Chapter 3 deal with the high frequency response of induction motor rotor. The study is performed in two reference frames, dq and $\alpha\beta$.Last, difference between simulation and measure are investigated.

Chapter 4 examines the potential of the optimization algorithms in increasing sensorless capability of the induction motor with the choose saliency geometry. The optimizer takes also in account the mean torque of the motor, in order to maximize both objectives.

Chapter 5 explains the measurement procedures used for the characterization of induction motor prototypes. At first classical measure procedure are explained, like no-load and locked rotor test. Then the procedures to

retrieve the rotor parameters at high frequency are illustrate. The high frequency parameter can be used to implement a sensorless field oriented control of the induction motor.

Chapter 6 contains a comparison of the three motors under evaluation. The data of previous chapters are summarized in Tables, in order to have a complete view of obtained results.

Chapter 1

Estimation of the IM parameters

In this chapter main data of the proposed induction motors are introduced. The analytical analysis is performed in order to have analytical prediction data, for measures and simulation comparing. After that, finite elements simulations are carried out and the parameters of induction motor are obtained. At last the steady state behaviour and dynamic performance of the machine is investigated.

1.1 Main data of the machine

The main data of the machine are reported in the following table. In Table 1.1 are listed the nominal data of the IM. In Table 1.2 the main stator geometrical data are listed , and in Table 1.3 the winding data are reported. Table 1.4 shows the geometrical data of the rotor prototypes 1 and 2.

Table 1.1: Machine nominal data

Parameter	Value
Nominal voltage [V]	400
Nominal current [A]	3.63
nominal frequency [Hz]	50
pole pairs	4

In fig 1.3, fig 1.2, fig 1.1, are represented stator rotors of the three motors. In fig and fig the difference of rotor are zoomed for better understand the differences.

Table 1.2: stator parameter

Parameter	Value
Stator package length [mm]	110
External stator diameter [mm]	150
Stator slot number	36
Slot height [mm]	13.8
Teeth width [mm]	4.44
Slot open width [mm]	2.5
Slot open height [mm]	0.7
Wedge height [mm]	2.2
Slot cross section [mm^2]	66.33
External rotor diameter [mm]	95.2
Shaft diameter [mm]	95.2
Rotor slot number	28

Table 1.3: Winding data

Parameter	Value
numbers of turns per slot	44
single wire section [mm^2]	0.6

Table 1.4: Prototype data

Parameter standard Motor	*hsor*	*wsor*
Value	0.5[mm]	1.0[mm]

Parameter Motor #01	*hsor*		*wsor*	
	d	q	d	q
Value	4.0[mm]	0.95[mm]	0.5[mm]	0.5[mm]

Parameter Motor #02	*hsor*		*wsor*	
	d	q	d	q
Value	4.0[mm]	0.95[mm]	0.5[mm]	3.0[mm]

In fig 1.1, fig 1.2, fig 1.3, the differences between the three considered rotor are highlighted.

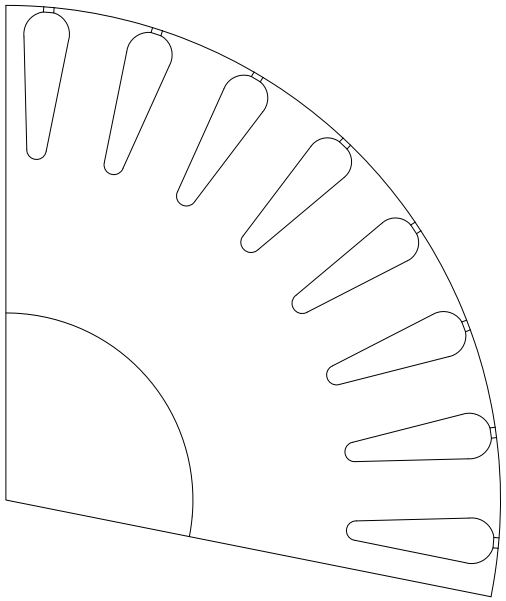

Figure 1.1: Standard Motor

1.1.1 Stator data

The material used for the stator is laminated iron. For some computation the material is considered to be linear, with a $\mu_r = 7000$ and for others, where iron saturation is important, the BH curve is used.

The simulation in which the current is small, can be computed with linear iron; the iron flux density doesn't reach high value, so a linear characteristic can be adopted. All the simulation used to compute the rotor parameters are carried out with linear iron characteristic. Hence superposition of the effect can be applied. This is suitable for the estimation of the rotor parameters that are assumed to be independent of the magnetizing flux. [1]

If the current is close to the nominal, such in the simulation for foc torque evaluation, the real BH curve is used. This is very important, because at nominal current the iron flux density is higher and saturation occurs. Also for the No-load simulation the iron used present non linear characteristic.

There are some data, which are not reported in the above Tables, but are however important. They are:

the stator and rotor teeth pitch

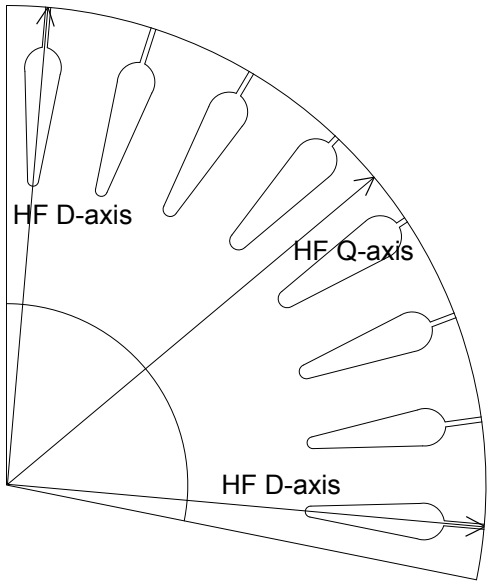

Figure 1.2: Prototype 01

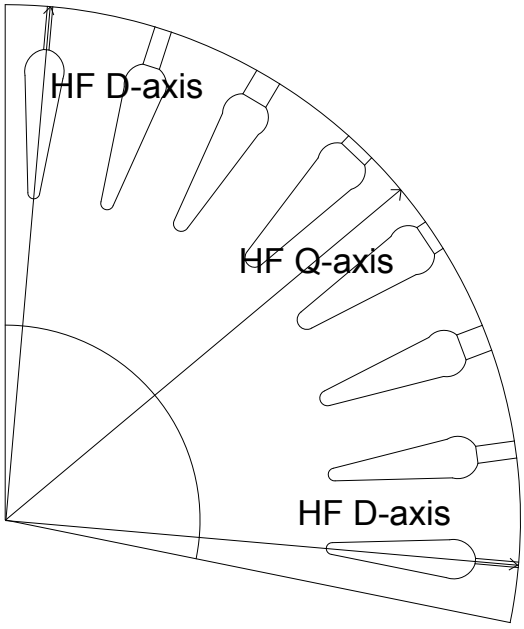

Figure 1.3: Prototype 02

$$p_s = \frac{\pi \cdot D}{Q_s} = \frac{\pi \cdot 96}{36} = 8.38\, mm$$

$$p_{sr} = \frac{\pi \cdot D_{er}}{Q_r} = \frac{\pi \cdot 95.2}{28} = 10.68\, mm$$

the air gap

$$g = \frac{(D_{is} - D_{er})}{2} = 0.40\, mm$$

In according to these geometrical values, the carter factor results in:

$$\begin{aligned} k_c &= \frac{p_s}{p_s + g - \frac{3}{4}\, w_s o} \\ &= \frac{8.38}{8.38 + 0.40 - \frac{3}{4} \cdot 2.5} = 1.21 \end{aligned} \tag{1.1}$$

1.1.2 Stator current

It is important to estimate the maximum current permissible in the stator winding.

After drawing the machine geometry, from FE software it is simple to extract the slot section:

$$S_{slot} = 66.33 mm^2$$

Assuming a current density:

$$J_{cu} = 6 A/mm^2$$

and a fill factor of the slot:

$$k_{fill} = 0.4$$

The total current in the slot is equal to:

$$I_{slot} = J_{cu} \cdot S_{slot} \cdot k_{fill} = 160 A$$

The maximum current in each phase conductor should be less than:

$$I_{rms} = \frac{I_{slot}}{n_{cs}} = 3.63\, A$$

The maximum peak current is:

$$\hat{I} = \sqrt{2} \cdot I_{rms} = 5.15\, A \tag{1.2}$$

1.1.3 Winding

According to the stator slot number $Q_s = 36$ the slot angle results in:

$$\alpha_s = 360/36 = 10^\circ$$

that is, in electrical degrees:

$$\alpha_{se} = p \cdot \alpha_s = 20^\circ$$

The number of slot per poles per pair is

$$q = \frac{Q_s}{2 \cdot p \cdot 3} = \frac{36}{2 \cdot 2 \cdot 3} = 3 \tag{1.3}$$

The coil throw of a non-chorded winding is:

$$y_q = (\frac{Q_s}{2 \cdot p}) + 1 = 10$$

Therefore, the pitch factor is:

$$k_p = 1$$

the distribution factor:

$$k_d = \frac{\sin(q \cdot \frac{\alpha_{se}}{2})}{q \cdot \sin(\frac{\alpha_{se}}{2})} = 0.9597 \tag{1.4}$$

and the winding factor:

$$k_w = k_p \cdot k_d = 0.96$$

The number of equivalent series conductors per phase is:

$$N_s = n_{cs} \cdot \frac{Q_s}{3} = 44 \cdot \frac{36}{3} = 528 \tag{1.5}$$

From the slot area and the fill factor, is simple obtain the copper area. Dividing it by the number of conductors per slot, the equivalent copper section of a single wire is equal to $0.6mm^2$.

For automatic computation and current setting in the stator slot, a slot matrix is implemented. This is constructed using a +1 where the current is entering and -1 where the current is going out. The induction motor has 36 stator slots and 4 poles, and hence the slot matrix exhibits a periodicity. Table 1.5 reports the matrix used for this motor.

Table 1.5: Stator slot Matrix

slot	1	2	3	4	5	6	7	8	9	10	11	12	13	14	15	16	17	18
ka	0	0	0	1	1	1	0	0	0	0	0	0	-1	-1	-1	0	0	0
kb	-1	-1	-1	0	0	0	0	0	0	1	1	1	0	0	0	0	0	0
kc	0	0	0	0	0	0	-1	-1	-1	0	0	0	0	0	0	1	1	1

1.2 Analytical prediction of IM parameters

In the purpose to verify FEM results, machine parameters are obtained here by analytical method. Based on the machine geometry, the IM parameters (such stator and rotor leakage inductances and resistances, air gap magnetic field and magnetizing inductance) are computed.

In addition, stator resistance and end winding leakage inductance, that are not considered in the FEM analysis, are computed below.

1.2.1 Magnetizing Inductance

The fundamental harmonic of the total electric loading is:

$$\hat{K_{s\mu}} = \frac{3 \cdot k_w \cdot N_s \cdot \hat{I}}{\pi \cdot D} \tag{1.6}$$

where $\hat{I}$ is the peak of the magnetizing current calculated in (1.2); supposing in order of $i_0 = 50\%$

$$\hat{I_\mu} = \sqrt{2} \cdot I_{nom} \frac{50}{100} = \sqrt{2} \cdot 1.8 = 2.54\ A$$

The total electric loading is, for (1.6):

$$\hat{K_{s\mu}} = \frac{3 \cdot 0.96 \cdot 528 \cdot 2.54}{\pi \cdot 0.096} = 12835\ A/m \tag{1.7}$$

Only the fundamental harmonic of the air gap flux density is considered in order to obtain machine parameters. The main harmonic of the air gap magneto-motive-force (mmf) is:

$$\begin{aligned} \hat{U} &= \hat{K_s} \frac{D}{2 \cdot p} \\ &= 12835 \frac{0.096}{2 \cdot 2} = 308\ A \end{aligned} \tag{1.8}$$

Therefore, the amplitude of the fundamental harmonic of the air gap flux density is obtained as:

$$\begin{aligned}\hat{B}_g &= \mu_0 \frac{\hat{U}}{k_c \cdot k_s \cdot g} \\ &= \mu_0 \frac{308}{1.2136 \cdot 1.10 \cdot 0.4 \cdot 10^{-3}} = 0.725\, T\end{aligned} \tag{1.9}$$

assuming the carter coefficient in according to (1.1) and a saturation coefficient equal to $k_s = 1.10$. The flux can now be computed as:

$$\begin{aligned}\Phi &= \frac{\hat{B} \cdot D \cdot L_s tk}{p} \\ &= \frac{0.7248 \cdot 0.096 \cdot 0.11}{2} = 3.83 \cdot 10^{-3}\, Wb\end{aligned} \tag{1.10}$$

therefore, the flux linkage is

$$\begin{aligned}\hat{\Lambda} &= \frac{k_w \cdot N_s}{2} \Phi \\ &= \frac{0.96 \cdot 528}{2} \cdot 3.83 \cdot 10^{-3} = 0.969\, Vs\end{aligned} \tag{1.11}$$

The magnetizing inductance can now be computed as:

$$\begin{aligned}L_m &= \frac{\hat{\Lambda}}{\hat{I}} \\ &= \frac{0.9686}{\sqrt{2} \cdot 1.8} = 0.380\, H\end{aligned} \tag{1.12}$$

or with the equation:

$$\begin{aligned}L_m &= \frac{3}{\pi} \cdot \mu_0 L_{stk} \left(\frac{k_w N_s}{2p}\right)^2 \frac{D}{k_c k_s g} \\ &= \frac{3}{\pi} \cdot \mu_0 \cdot 0.11 \left(\frac{0.96 \cdot 528}{4}\right)^2 \frac{0.096}{1.2136 \cdot 1.10 \cdot 0.40 \cdot 10^{-3}} = 0.381\, H\end{aligned} \tag{1.13}$$

that leads to the same result.

With this value of flux linkage, the value of the stator voltage is equivalent to:

$$\begin{aligned}V_{rms} &= \frac{\omega \cdot \hat{\Lambda}}{\sqrt{2}} \\ &= \frac{314 \cdot 0.9686}{\sqrt{2}} = 215\, V\end{aligned} \tag{1.14}$$

1.2.2 Stator resistance

The stator winding material is copper and the reference temperature is for assumption $120°C$.

$$\rho_{cu-20^\circ} = 0.0169 \cdot 10^{-6}\,\Omega m$$

$$\alpha_{cu} = 0.0042 \quad 1/°C$$

$$\begin{aligned}\rho_{cu-120^\circ} &= \rho_{cu-20^\circ} \cdot (1 + \alpha_{cu} \cdot (T - T_0)) = \\ &= 0.024 \cdot 10^{-6}\,\Omega m\end{aligned}$$

$$\sigma_{cu-120} \cong 41\ MS/m$$

For compute the stator resistance, it is necessary to estimate the total length of the conductor in according to [2]:

$$\begin{aligned}L_{tot} &= L_{stk} + \left(\frac{y_q \cdot \pi \cdot D_{es}}{Q_s}\right) \\ &= 0.11 + \left(\frac{10 \cdot \pi \cdot 0.15}{36}\right) = 0.24\,m\end{aligned} \tag{1.15}$$

so that the total stator winding resistance can be obtained by:

$$\begin{aligned}R_s &= \rho_{cu-120^\circ} \cdot \frac{N_s \cdot L_{tot}}{S_{c-eq}} \\ &= 0.024 \cdot 10^{-6} \cdot \frac{528 \cdot 0.24}{0.6 \cdot 10^{-6}} = 5.068\,\Omega\end{aligned} \tag{1.16}$$

If the temperature of the motor is $20°C$ the stator resistance is:

$$R_s = 0.0169 \cdot 10^{-6} \cdot \frac{528 \cdot 0.24}{0.6 \cdot 10^{-6}} = 3.57\,\Omega \tag{1.17}$$

An other possible way to find the rotor resistance is to use the weight and the losses in the entire winding. The result has to be the same.

$$\begin{aligned}G_{cu} &= \gamma_{cu} \cdot Q_s \cdot n_{cs} \cdot S_{c-eq} \cdot L_{tot} \\ &= 8900 \cdot 36 \cdot 44 \cdot 0.6 \cdot 10^{-6} \cdot 0.24 = 2.03\,kg\end{aligned} \tag{1.18}$$

$$\begin{aligned} P_{s-j} &= \rho_{cu} \cdot Vol_{cu} \cdot J^2 = \frac{\rho_{cu}}{\gamma} \cdot G_{cu} \cdot J^2 \\ &= \frac{0.024 \cdot 10^{-6}}{8900} \cdot 2.03 \cdot (6 \cdot 10^6)^2 = 197\, W \end{aligned} \tag{1.19}$$

$$R_s = \frac{P_{s-j}}{3 \cdot I^2} = \frac{197}{3 \cdot 3.63^2} = 4.98\, \Omega \tag{1.20}$$

1.2.3 Rotor resistance

The die-cast rotor is made in Aluminium and the reference temperature is obviously the same of the stator.

$$\rho_{al-20^\circ} = 0.026 \cdot 10^{-6}\, \Omega m$$
$$\alpha_{al} = 0.0043\, 1/^\circ C$$

$$\begin{aligned} \rho_{al-120^\circ} &= \rho_{al-20^\circ} \cdot (1 + \alpha \cdot (T - T_0)) = \\ &= 0.037 \cdot 10^{-6}\, \Omega m \end{aligned}$$

$$\sigma_{al-120^\circ} \cong 25.5\, MS/m$$

For the evaluation of the rotor current, the starting equation is:

$$m_S \cdot N_s \cdot k_{ws} \cdot I_{sr} = m_R \cdot N_r \cdot k_{wr} \cdot I_{bar} \tag{1.21}$$

$$I_{sr} = I_s \cdot cos\varphi = 3.63 \cdot 0.8 = 2.90\, A$$

$$\begin{aligned} I_{bar} &= \frac{m_S \cdot N_s \cdot k_{ws} \cdot I_{sr}}{m_R \cdot N_r \cdot k_{wr}} \\ &= \frac{3 \cdot 528 \cdot 0.96 \cdot 2.90}{28 \cdot 1 \cdot 0.998} = 157.81\, A \end{aligned} \tag{1.22}$$

The bar current density can be obtain from:

$$J_{bar} = I_{bar}/S_{bar} = 157.81/42 = 3.75\, A/mm^2 \tag{1.23}$$

The ring current can be estimated as:

$$\begin{aligned}\hat{I}_{ring} &= (\frac{2}{\pi} \cdot \hat{I}_{bar}) \cdot \frac{Q_R}{2 \cdot 2p} \\ &= \frac{Q_R}{2p \cdot \pi} \cdot \hat{I}_{bar}\end{aligned} \tag{1.24}$$

$$I_{ring} = \frac{Q_R}{2p \cdot \pi} \cdot I_{bar} = \frac{28}{2p \cdot \pi} \cdot 157.81 = 351.62\ A \tag{1.25}$$

Supposing a ring current density

$$J_{ring} = J_{bar} = 3.75\ A/mm^2$$

The section of the ring should be approximately:

$$S_{ring} = I_{ring}/J_{bar} = 351.62/3.75 = 93.76\ mm^2$$

Therefore the ring is supposed has a section

$$15 \cdot 6 \rightarrow S_{ring} = 90\ mm^2$$

.

$$\begin{aligned}P_{j-r} &= \rho_{al-120^\circ} \cdot \left[S_{bar} \cdot L_{stk} \cdot Q_r \cdot J_{bar}^2 + 2 \cdot S_{ring} \cdot \pi \cdot (D_{er} - h_s) \cdot J_{ring}^2\right] \\ &= \frac{1}{25.5} \cdot 10^3 \cdot 10^{-6} \cdot \left[41.99 \cdot 110 \cdot 28 \cdot 3.75^2 + 2 \cdot 90 \cdot \pi \cdot (95.2 - 14) \cdot 3.75^2\right] \\ &= \frac{1}{25.5} \cdot 10^3 \cdot 10^{-6} \cdot \left[1.8187 \cdot 10^6 + 0.6457 \cdot 10^6\right] = 96.64\ W\end{aligned} \tag{1.26}$$

From the Joule losses is simple to compute the rotor resistance. The value of the rotor current is assumed as the only active part of the current:

$$I_{sr} = I_s \cdot cos\varphi = 3.63 \cdot 0.8 = 2.90A \tag{1.27}$$

$$R_r = \frac{P_{j-r}}{3 \cdot I_{sr}^2} = \frac{97}{3 \cdot 2.90^2} = 3.83\ \Omega \tag{1.28}$$

1.2.4 Leakage inductance

The total leakage inductance of the motor can be computed by summing vary components:

- stator leakage inductance
- rotor leakage inductance
- zig-zag leakage inductance
- stator coil end-winding leakage inductance
- belt leakage inductance
- skewing leakage inductance

stator leakage inductance

For calculation of this inductance, some data are necessary:

$$\begin{aligned} w_s &= \frac{\pi\left(D + 2h_{wed} + 2hso\right)}{Q_s} - w_t \\ &= \frac{\pi \cdot (96 + 2 \cdot 2.2 + 2 \cdot 0.7)}{36} - 4.44 = 4.443\, mm \end{aligned} \tag{1.29}$$

$$\begin{aligned} h_{si} &= h_s - h_{so} - h_{wed} \\ &= 13.7 - 0.7 - 2.2 = 10.8\, mm \end{aligned} \tag{1.30}$$

$$\begin{aligned} k_{slot-s} &= \frac{h_{so}}{w_{so}} + \frac{h_{wed}}{w_s - w_{so}} \cdot \ln\left(\frac{w_s}{w_{so}}\right) + \frac{h_{si}}{3w_s} \\ &= \frac{0.7}{2.5} + \frac{2.2}{4.443 - 2.5} \cdot \ln\left(\frac{4.443}{2.5}\right) + \frac{10.8}{3 \cdot 4.443} = 1.741 \end{aligned} \tag{1.31}$$

Now can be finally compute the leakage inductance with:

$$\begin{aligned} L_{\sigma slot-s} &= 2p \cdot q \cdot n_{cs}^2 \cdot \mu_0 \cdot L_{stk} \cdot k_{slot-s} \\ &= 4 \cdot 3 \cdot 44^2 \cdot 4 \cdot \pi \cdot 10^{-7} \cdot 0.11 \cdot 1.741 = 5.59 \cdot 10^{-3}\, H \end{aligned} \tag{1.32}$$

rotor leakage inductance standard rotor

Like for the stator is necessary to find some data before calculating leakage inductance:

$$\begin{aligned} w_{s-r} &= \frac{\pi\left(D + 2h_{wed} + 2h_{so}\right)}{Q_r} - w_{tr} \\ &= \frac{\pi \cdot (95.2 + 2 \cdot 2.5 + 2 \cdot 0.5)}{28} - 5.71 = 4.29\, mm \end{aligned} \tag{1.33}$$

$$\begin{aligned} h_{si} &= h_s - h_{so} - h_{wed} \\ &= 17 - 0.5 - 2.5 = 14\, mm \end{aligned} \tag{1.34}$$

$$\begin{aligned} k_{slot-r} &= \frac{< h_{so-r} >}{3 \cdot w_{so-r}} + \frac{h_{wed-r}}{w_{s-r} - w_{so-r}} \cdot \ln\left(\frac{w_{s-r}}{w_{so-r}}\right) + \frac{h_{si}}{3w_s} \\ &= \frac{0.5}{3 \cdot 1} + \frac{2.5}{4.29 - 1} \cdot \ln\left(\frac{4.29}{1}\right) + \frac{14}{3 \cdot 4.29} = 2.35 \end{aligned} \tag{1.35}$$

and the leakage inductance:

$$\begin{aligned} L_{\sigma slot-r} &= 2p \cdot q \cdot ncs^2 \cdot \mu_0 \cdot L_{stk} \cdot k_{slot-r} \\ &= 4 \cdot 3 \cdot 44^2 \cdot 4 \cdot \pi \cdot 10^{-7} \cdot 0.11 \cdot 2.65 = 7.54 \cdot 10^{-3}\, H \end{aligned} \tag{1.36}$$

It can be inferred that the leakage inductance of the rotor is closely related with the slot opening. So this portion is very important for the total leakage inductance.

Zig-Zag leakage inductance standard rotor

The zig-zag leakage inductance is due to the interaction between stator and rotor teeth.

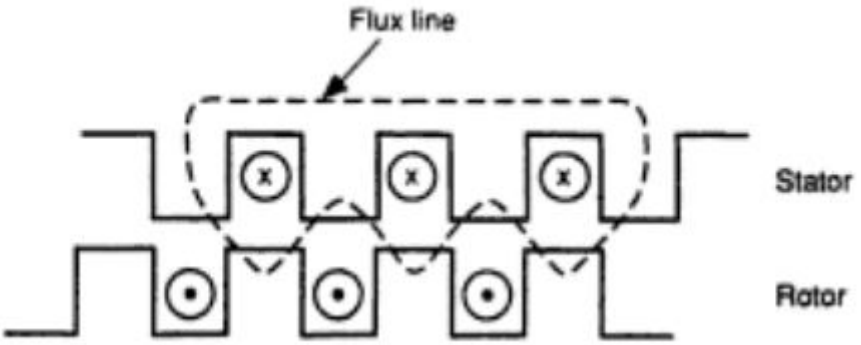

Some data are necessary to compute those inductance:

$$w_{t-s} = p_{s-s} - w_{so-s} = 8.3776 - 2.5 = 5.87\,mm$$

$$w_{t-r} = p_{s-r} - w_{so-r} = 10.6814 - 1 = 9.68\,mm$$

and the zig-zag factor:

$$\begin{aligned} k_{zig-zag} &= \frac{1}{12 \cdot g} \cdot \frac{(w_{t-s} + w_{t-r})^2}{p_s + p_{sr}} \\ k_{zig-zag} &= \frac{1}{12 \cdot 0.4} \cdot \frac{(5.87 + 9.68)^2}{8.37 + 10.68} = 2.64 \end{aligned} \tag{1.37}$$

finally the leakage inductance can be computed:

$$\begin{aligned} L_{\sigma zig-zag} &= 2p \cdot q \cdot ncs^2 \cdot \mu_0 \cdot L_{stk} \cdot k_{zig-zag} \\ \#1 &= 4 \cdot 3 \cdot 44^2 \cdot 4 \cdot \pi \cdot 10^{-7} \cdot 0.11 \cdot 2.64 = 8.47 \cdot 10^{-3}\,H \end{aligned} \tag{1.38}$$

End winding stator leakage inductance

The length of end-winding can be estimate in:

$$L_{ew} = \left(2.5\frac{D}{p}\right) = \left(2.5\frac{0.096}{2}\right) = 0.12\,m$$

The first formulation is due to Shuisky:

$$\begin{aligned} L_{\sigma-ew} &= \mu_0 \cdot ncs^2 \cdot q^2 \cdot 2p \cdot \lambda''_{ew} \cdot L_{ew} \\ &= 4 \cdot \pi \cdot 10^{-7} \cdot 44^2 \cdot 3^2 \cdot 4 \cdot 0.35 \cdot 0.12 = 3.6784 \cdot 10^{-3}\,H \end{aligned} \tag{1.39}$$

whilst the second is due to Someda:

$$\begin{aligned} L_{\sigma-ew} &= \mu_0 \left(ncs^2 \cdot q^2 \cdot 2p\right) \cdot \lambda'_{ew} \cdot \tau_p \\ &= 4 \cdot \pi \cdot 10^{-7} \cdot \left(44^2 \cdot 3^2 \cdot 4\right) \cdot 0.50 \cdot 0.07539 = 3.30 \cdot 10^{-3}\,H \end{aligned} \tag{1.40}$$

A compromise is take a mid value, $L_{\sigma-ew} = 3.50 \cdot 10^{-3}\,H$

Belt leakage inductance

This leakage flux results from the non-sinusoidal mmf distribution of the winding. To compute it, some data are necessary:

$$\frac{Q_s + Q_r}{2p} = \frac{36 + 28}{4} = 16$$

and from the diagram in fig 1.4

$$k_B = 1.23$$

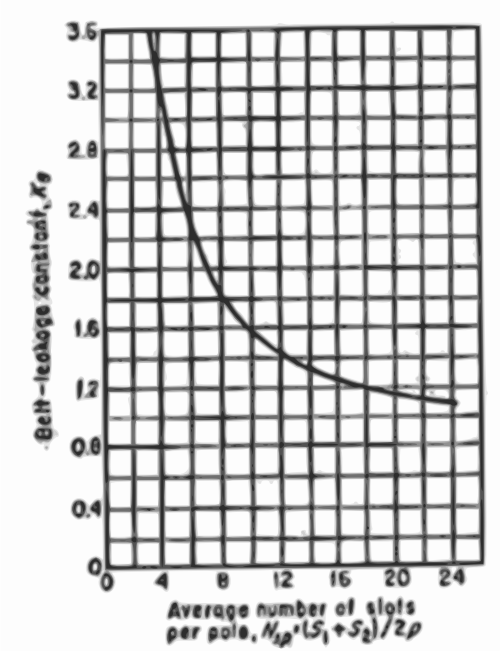

Figure 1.4: Belt Factor

$$\begin{aligned} L_{\sigma-belt} &= L_m \cdot \left(3.65 \cdot 10^{-3} \cdot k_B\right) \\ &= 0.38 \left(3.65 \cdot 10^{-3} \cdot 1.23\right) = 1.70 \cdot 10^{-3}\ H \end{aligned} \tag{1.41}$$

skewing leakage inductance

The rotor is skewed of 1.5 times rotor slot. Then the skewing angle of the rotor is:

$$\alpha_{sk}^{e} = p \cdot 1.5 \cdot \frac{2\pi}{Q_r} = 2 \cdot 1.5 \cdot \frac{2\pi}{28} = 0.673$$

$$\begin{aligned} k_{skw} &= \frac{sin\left(\frac{\alpha_{sk}^{e}}{2}\right)}{\frac{\alpha_{sk}^{e}}{2}} \\ &= \frac{sin\left(\frac{0.673}{2}\right)}{\frac{0.673}{2}} = 0.981 \end{aligned} \tag{1.42}$$

$$\begin{aligned} L_{\sigma-sk} &= \left(1 - k_{skw}^2\right) \cdot L_m \\ &= \left(1 - 0.981^2\right) \cdot 0.38 = 14.30 \cdot 10^{-3}\ H \end{aligned} \tag{1.43}$$

Total leakage inductance

The total leakage inductance are obviously different for the three motors. The bast way to compare is to put the value in a table 1.6.

The total leakage inductance is obtained by summing all the components:

$$L_{\sigma-total} = L_{\sigma slot-s} + L_{\sigma slot-r} + L_{\sigma-zig-zag} + L_{\sigma-ew} + L_{\sigma-belt} + L_{\sigma-sk}$$

Table 1.6: Leakage inductance

Parameter	Standard	Prototype 01		Prototype 02	
		d	q	d	q
$L_{\sigma slot-s}[mH]$	5.59				
$L_{\sigma-ew}[mH]$	3.50				
$L_{\sigma-belt}[mH]$	1.70				
$L_{\sigma-sk}[mH]$	14.30				
$L_{\sigma slot-r}[mH]$	7.54	23.35	9.69	16.92	6.03
$L_{\sigma-zig-zag}[mH]$	8.47	9.02	9.02	9.02	6.42
$Total[mH]$	41.05	57.5	43.8	68.17	37.54

The value of the leakage inductance should be approximately 10% of the magnetizing inductance. If a motor has two leakage inductance, the average value is considered and the ratio with respect the magnetizing inductance is computed.

Table 1.7: Magnetizing inductance in percent

Motor	Lm [mH]	L_σ [mH]	%
Standard	381	42.10	11.04
Prototype 01	381	50.65	13.30
Prototype 02	381	52.85	13.87

Looking at Table 1.6, it can be observed that the $L_{\sigma-sk}$ is very high and it influences a lot the total leakage inductance. Nevertheless the total inductance of the standard motor is in the range and the inductance of the other two motors is a bit greater, due to introduced the anisotropy.

On the q axis inductance a little note must be made. From fig 1.1 it can be see that there are no slots in correspondence of q-axis. The parameter referred to the q-axis are the value in the case it the rotor slot exist.

The value of total leakage inductance of standard motor is similar to those obtained from fem simulation:

$$L_{\sigma-total} = L_{\sigma slot-s} + L_{\sigma slot-r} + L_{\sigma-zig-zag} + L_{\sigma-belt} = 23.25 \cdot 10^{-3}\, H$$

. This value can compare with fig 1.10 and the value are approximately the same.

1.2.5 Nominal Power

After finding the nominal current, the nominal power can be computed, assuming $\cos\varphi = 0.8$ and the nominal voltage $V = 400\, V$.

$$\begin{aligned} P_n &= 3 \cdot E_{avv} \cdot I_{nom} \cdot \cos\varphi \\ &= 3 \cdot \frac{400}{\sqrt{3}} \cdot 3.63 \cdot 0.8 \approx 2000\, W \end{aligned} \tag{1.44}$$

1.2.6 Mechanical Losses

The mechanical losses of this electric motor are obtained by an empirical equation:

$$\begin{aligned} P_{mec} &= 0.6 \cdot P_{nom} \cdot \sqrt{n_{rpm}} \\ &= 0.6 \cdot 2 \cdot \sqrt{1500} \approx 50\, W \end{aligned} \tag{1.45}$$

1.2.7 Nominal torque

For the calculation of the nominal torque it is necessary to compute $\hat{K_s}$ using the total current in the winding machine and not only the magnetizing current. With the calculated nominal current $I_n = 3.63\ A_{rms}$, the total electric load for the torque computation is:

$$\begin{aligned} \hat{K_s} &= \frac{3 \cdot k_w \cdot N \cdot \hat{I}}{\pi \cdot D} \\ &= \frac{3 \cdot 0.96 \cdot 528 \cdot 3.63 \cdot \sqrt{2}}{\pi \cdot 0.096} = 25884\ A/m \end{aligned} \tag{1.46}$$

The torque can now be compute with the equation that is based on the energy in the machine air gap:

$$\begin{aligned} T &= \frac{\pi}{4} \cdot D^2 \cdot L_{stk} \cdot \hat{K_s} \cdot \hat{B_g} \cdot \cos\varphi \\ &= \frac{\pi}{4} \cdot 0.096^2 \cdot 0.11 \cdot 25884 \cdot 0.7248 \cdot 0.8 = 11.94\ Nm \end{aligned} \tag{1.47}$$

This value of torque is a good evaluation of the expected torque, useful for a check of the results of the FEM analysis.

1.3 Rapid Analysis

Finite element simulation are performed with simulation free software FEMM [3, 4].

When a drive is made with an Induction Motor, a key factor for the implementation of the control algorithm is an accurate model, so Finite Elements simulation to achieve the IM parameters is a mandatory choice. However, the FE approach requires a high computation time, particularly if the IM analysis is coupled with the simulation of the drive control. A good compromise is to combine analytical and FE models so as to get advantages and to reduce the drawbacks: the simulation time is reduced, and the iron saturation phenomena are better considered.

The rapid analysis results are made for the three motors, but are shown only the results for the standard motor. The result for all motors are compared in chapter 6.

1.3.1 No-load simulation

In this section the parameters of the machine are obtained from FEM simulation under no-load condition. These simulation are carried out in the rotor

reference frame, so that the frequency is zero and magneto-static simulation are done.

In the FEM simulation the field source is a set of current like:

$$\begin{cases} i_a = \hat{I} \\ i_b = -\dfrac{\hat{I}}{2} \\ i_c = -\dfrac{\hat{I}}{2} \end{cases} \tag{1.48}$$

in order to have the flow in the direction of the phase a.

The magnetizing inductance is computed through the integral of AJ. This is obtained from FEM solution with:

$$W_{AJ} = \int_{vol} A_z \cdot J_z \, dvol \tag{1.49}$$

$$L_m = \frac{W_{AJ}}{3I_{rms}^2} \tag{1.50}$$

From the magnetizing inductance the Flux can be computed using:

$$\Lambda = L_m \cdot I_{rms} \tag{1.51}$$

And now, knowing the flux, the phase voltage of the motor can be computed:

$$V_{rms} = \omega \cdot \Lambda \tag{1.52}$$

The simulation are carried out with a set of current starting from $I_{rms} = 0\,A$ to $I_{rms} = 10\,A$

The data resulting from the no-load simulation are shown in the fig 1.5, fig 1.6, fig 1.7, where the saturation effect of the magnetic circuit is visible.

Supposing a star connection of motor winding, and a grid connection at $V = 400\,V$, the voltage of the phase winding, deduced from losses:

$$\begin{aligned} E &= (1 - cdt) \cdot V_{(WINDING)} \\ &= (1 - 0.05) \cdot \frac{400}{\sqrt{3}} = 218.5\,V \end{aligned} \tag{1.53}$$

From the graph in fig 1.5 of the phase voltage, in correspondence of the value just found, is evidenced the magnetizing current of the motor.

$$I_\mu = 1.8\,A$$

In respect to the nominal current of the motor, the magnetizing is in the order of:

$$i_{0\,\%} = \frac{I_\mu}{I_n} \cdot 100 \cong 50\%$$

Assuming the magnetizing current of $I_\mu = 1.8\,A$, from fig 1.6, it is possible to achieve the value of the magnetizing inductance of the electrical motor.

In fig 1.7 in reported the magnetic flux versus the stator current.

Now, with the value of magnetizing current deduced above and set it into the fem simulation, is interesting examine the induction in the air gap. In fig 1.8 is displayed the effective value and the first harmonics of the induction. The value found fits very well with the estimated value in the analytical prediction, in equation (1.9).

The 1st harmonic amplitude value is

$$B_g = 0.7239\ T$$

respect to

$$B_g = 0.7248\ T$$

of the analytical prediction.

The iron losses can also be computed with this simulation, and then R_0 can be found. The best way is to use the specific iron losses, computing the losses in the stator teeth and in the back iron and sum them together to obtain the total iron losses. The specific iron losses must be reported at the work frequency and at the work flux density of the machine part.

In FE simulations it is simple to check and investigate the maximum flux density in the electric motor in every part. The B_{max} is investigated in the back iron and in the middle of the stator teeth.

The iron losses must be reported in the working condition with Steinmetz formulation:

$$P_{spec} = P_{spec-fe}\left[0.7\left(\frac{f}{f_{rif}}\right)\left(\frac{B}{B_{fe-rif}}\right)^{\alpha} + 0.3\left(\frac{f}{f_{rif}}\right)^{2}\left(\frac{B}{B_{fe-rif}}\right)^{2}\right]$$

In our case we have calculate the losses in the two part of the machine:

$$P_{fe-teeth} = k_{magg-t} \cdot P_{spec-t} \cdot Weight_t$$
$$P_{fe-backiron} = k_{magg-bi} \cdot P_{spec-bi} \cdot Weight_{bi}$$

with:

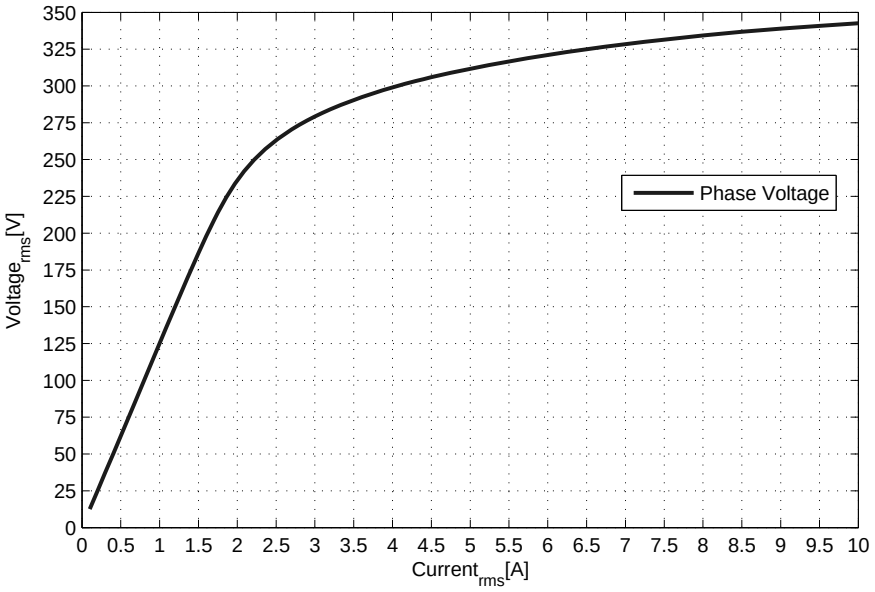

Figure 1.5: Phase voltage

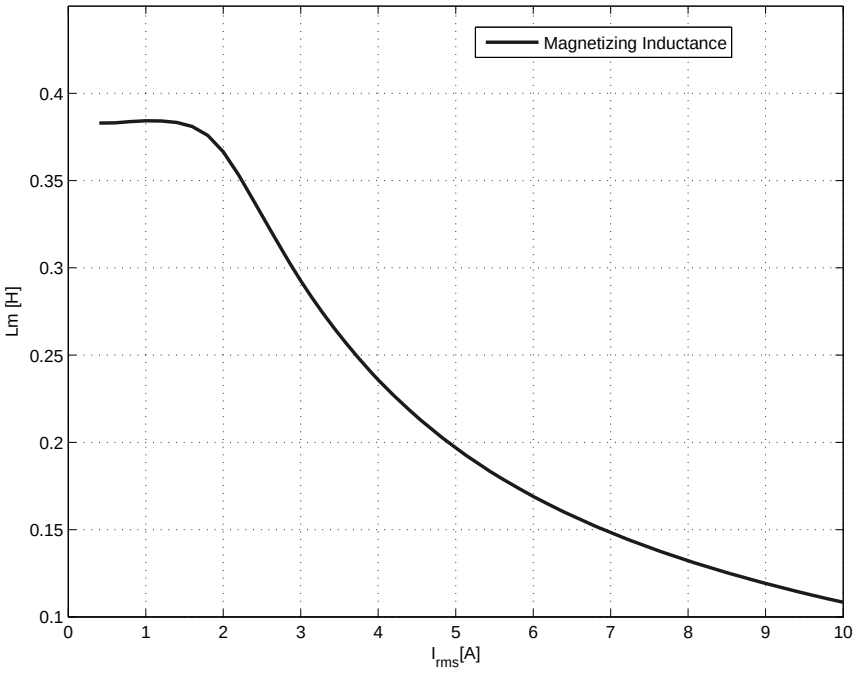

Figure 1.6: Magnetizing inductance

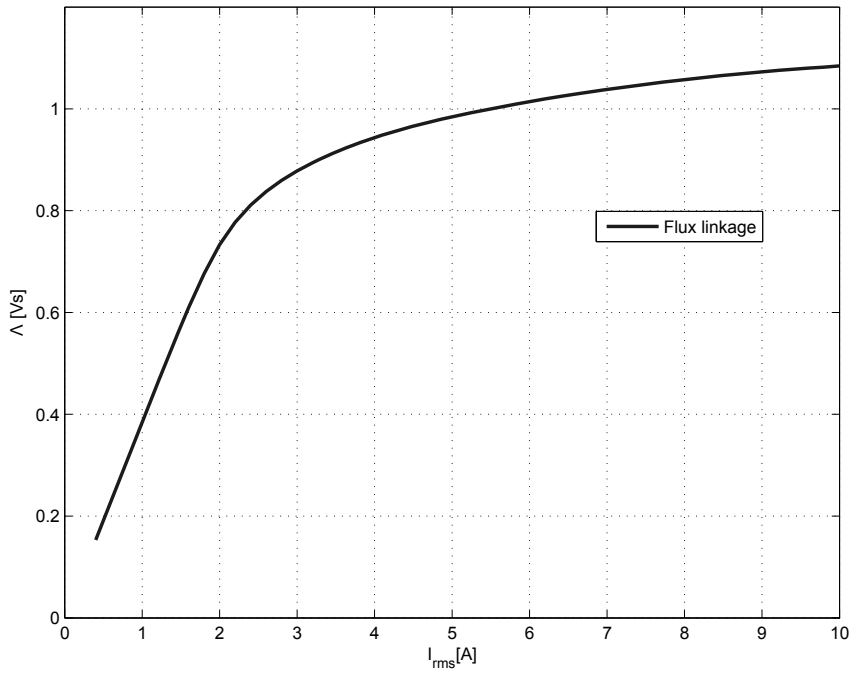

Figure 1.7: Magnetic flux

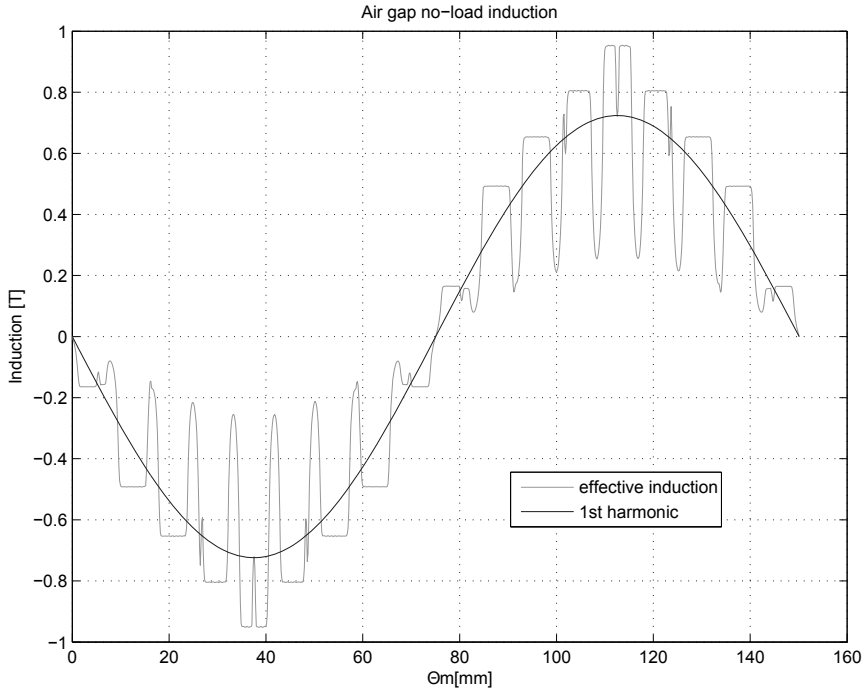

Figure 1.8: Air gap induction

$$k_{magg-t} = 2$$

$$k_{magg-bi} = 1.5$$

and $Weight_t$, $Weight_{bi}$ are the total weight of the iron stator machine.
$B_{fe-rif} = 2.3$ at $f_{rif} = 50\,Hz$

From simulation a value of $P_{fe} = 80\,W$ is obtained. So the resistance referred to the equivalent circuit is:

$$\begin{aligned} R_0 &= \frac{3 \cdot V_{avv}^2}{P_{fe}} \\ &= \frac{3 \cdot 215^2}{80} = 1733\Omega \end{aligned} \tag{1.54}$$

1.3.2 Locked rotor simulation

With locked rotor simulations, the rotor parameters are achieved. The simulation are carried out in the rotor reference frame, so that the simulation frequency is the slip frequency of the IM. The parameters are considered to

vary as a function of the frequency f_r used in simulation, due to the non uniform distribution of the current within the rotor slots.

It is very important highlight that the iron in the simulation is set to be *linear*, so superposition of the effect can be adopted. At the nominal current saturation does not appear, and simulations are made adopting a current $I_{n-rms} = 3.63\ A$. The current set into the simulations program have both real and imaginary part, to obtaining a rotating field with the desired frequency.

The equivalent circuit whence the equation are derived, is shown in circuit 1.1.

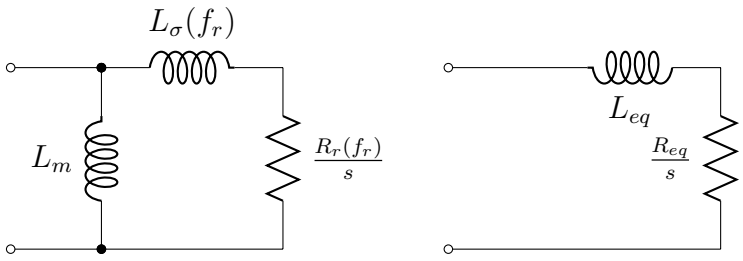

Circuit 1.1: Rotor equivalent circuit on Locked-rotor condition

From these simulation, the total leakage inductance and the rotor resistance can be obtained respectively with:

$$L_\sigma = L_m \frac{L_{eq}(L_m - L_{eq}) - (R_{eq}/\omega_r)^2}{(L_m - L_{eq})^2 + (R_{eq}/\omega)^2} \tag{1.55}$$

$$R_{r-bar} = R_{eq} \frac{L_m + L\sigma}{L_m - L_{eq}} \tag{1.56}$$

where

$$R_{eq} = \frac{P_{jr}}{3I_{rms}^2} \qquad L_{eq} = \frac{2W_m}{3I_{rms}^2} \tag{1.57}$$

and L_m come out from the no-load simulation carried out previously.

In fig 1.10 and fig 1.9 are respectively shown the Leakage inductance and the rotor resistance at nominal current condition and as a function of the rotor frequency.

The rotor resistance must be corrected including the ring resistance, so in according to [2]

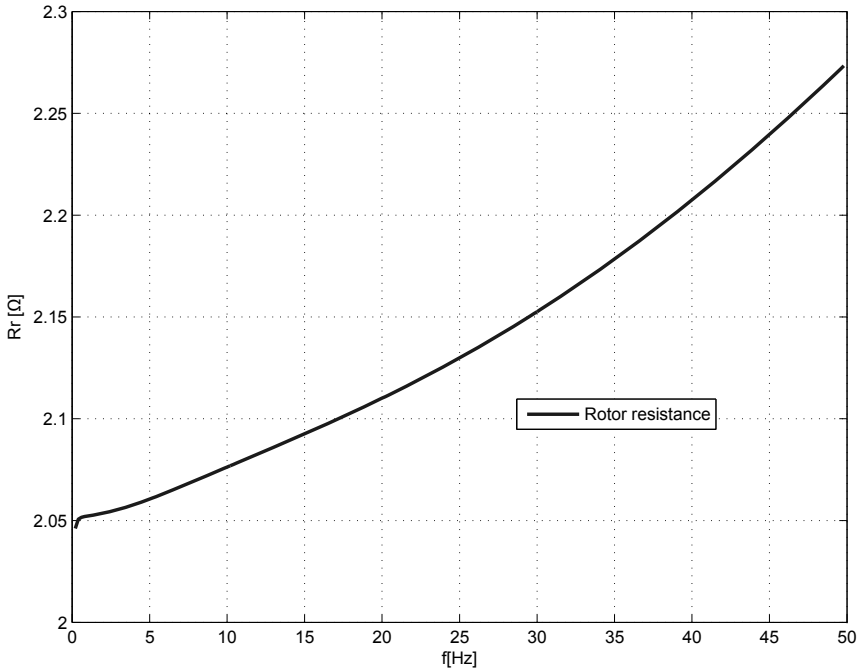

Figure 1.9: Rotor resistance vs rotor frequency

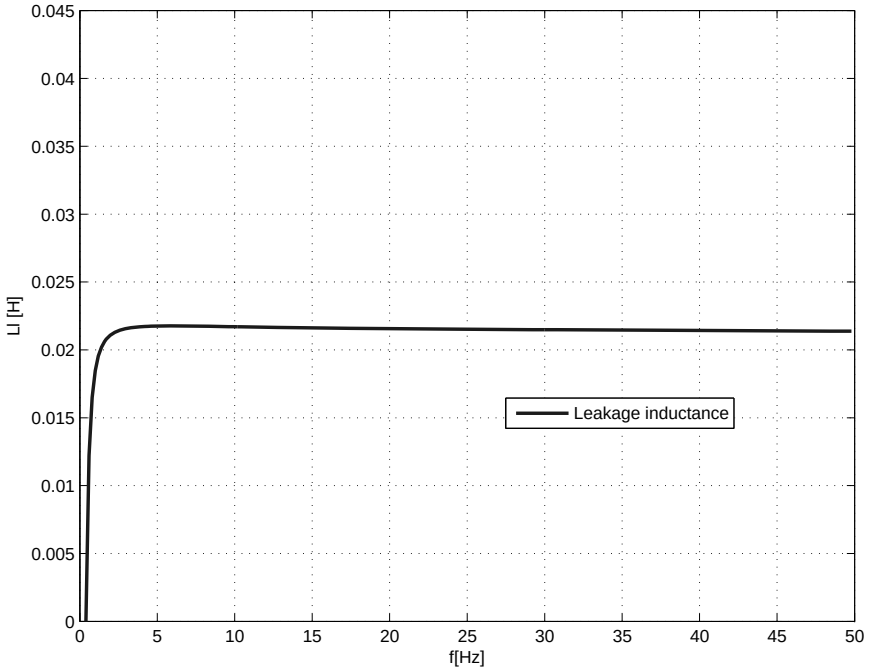

Figure 1.10: Leakage inductance vs rotor frequency

$$\begin{aligned} K_{ring} &= \frac{2 \cdot Q_r \cdot D_r \cdot S_{bar}}{\pi \cdot (2p)^2 \cdot L_{stk} \cdot S_{ring}} \\ &= \frac{2 \cdot 28 \cdot 0.0812 \cdot 41.99}{\pi \cdot 4^2 \cdot 0.11 \cdot 90} = 0.383 \end{aligned} \tag{1.58}$$

D_r is the average diameter of the ring.

The real rotor resistance can now be obtained with:

$$\begin{aligned} R_r &= R_{r-bar} \cdot (1 + K_{ring}) \\ &= 2.05 \cdot (1.383) = 2.83\ \Omega \end{aligned} \tag{1.59}$$

This correction however depends on the actual length of the motor, as shown in (1.58), so it is preferred to add the ring resistance to the rotor bar resistance in the equivalent circuit of the motor.

Also the leakage inductance has to be corrected, with the effect of the end ring in according also with [5]:

$$\begin{aligned} L_{\sigma,ring} &= \mu_0 \cdot k_r \left(\frac{k_{ws}}{k_{skew}}\right)^2 \cdot q^2 \frac{\pi \cdot D_r}{L_{stk}} \\ &= 4 \cdot \pi \cdot 10^{-7} \cdot 0.18 \cdot \left(\frac{0.96}{0.998}\right)^2 \cdot 3^2 \cdot \frac{\pi \cdot 0.0812}{0.11} = 4.36 \cdot 10^{-6}\ H \end{aligned} \tag{1.60}$$

where $k_r = 0.36$ if $2p = 2$, $k_r = 0.18$ if $2p > 2$, and k_{ws} is the stator winding factor.

The ring leakage inductance can be added to the inductance obtained earlier:

$$\begin{aligned} L_{\sigma-r} &= L_\sigma + L_{\sigma,ring} \\ &= 0.022 + 4.36 \cdot 10^{-6} 0.022\ H \approx L_\sigma \end{aligned} \tag{1.61}$$

$$\begin{aligned} L_{\sigma-tot} =& L_{\sigma-r} + L_{\sigma-sk} + L_{\sigma-ew} \\ & 0.022 + 0.0143 + 0.0035 = 0.039 \cdot 10^{-3}\ H \end{aligned} \tag{1.62}$$

Also the torque can now be computed, remembering this is not the true torque, but is the torque at nominal current calculated at several frequencies.

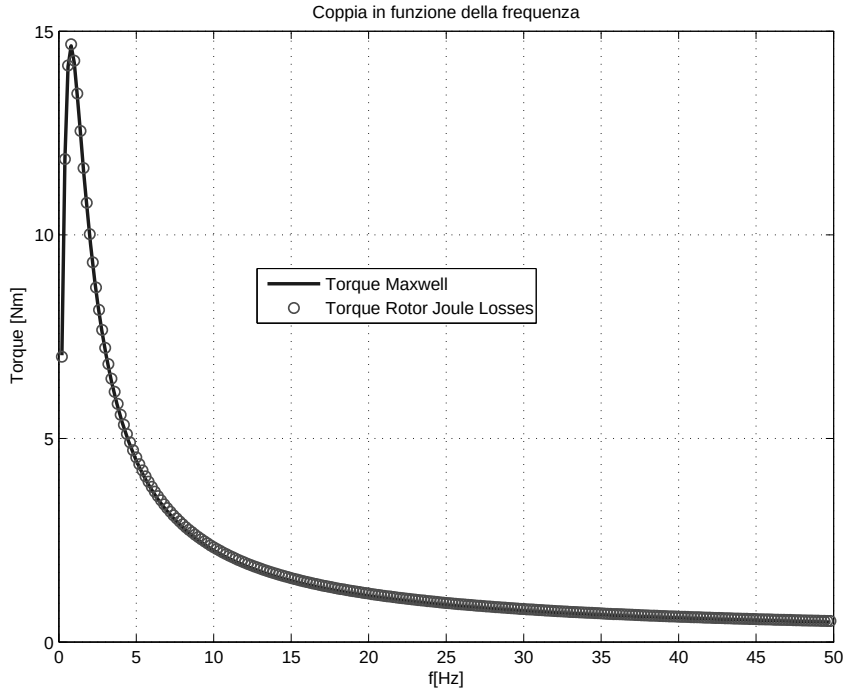

Figure 1.11: Electromagnetic torque vs rotor frequency

Figure 1.11 report the torque calculated with (1.63) and with the steady-state Maxwell weighted stress tensor torque.

$$T_{rl} = \frac{P_{jr} \cdot p}{2\pi f_r} \tag{1.63}$$

The two resultant torque are comparable between them.

1.4 Steady state IM performance

The Steady state electrical model of the machine is reported in circuit 1.2.

In Table 1.8 are shown the parameter of the machine, calculated by both method at $120°C$. On the other hand the simulation reported above, are referred at $40°C$ and a corrective factor must be used to refer the value at the reference temperature.

The performance of the motor can be derived from the equivalent circuit. In particular the torque can be computed from the Equivalent Circuit by the well known equation (1.64):

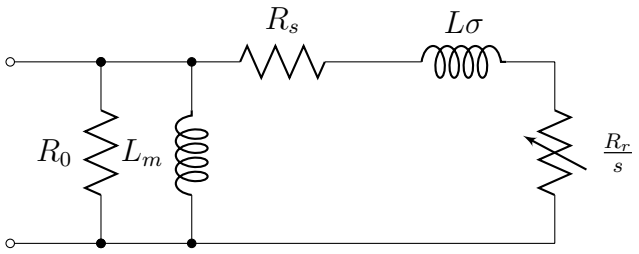

Circuit 1.2: IM equivalent Γ type circuit

Table 1.8: Summary of the electrical data motor

Parameter	Analytical analysis	Rapid analysis
$Lm[H]$	0.381	0.376
$R_0[\Omega]$	-	1733
$R_s[\Omega]$	5.06	-
$R_r[\Omega]$	3.83	3.79
$L_{\sigma-tot}[H]$	0.041	0.039

$$T_{em} = \frac{3 \cdot p}{\omega} \cdot \frac{V_w}{\left(\frac{R_s^2+X_\sigma^2}{R_r}\right) \cdot s + 2R_s + \frac{R_r}{s}} \tag{1.64}$$

The parameter used for computation are in Table 1.9

Table 1.9: Used data for steady state characteristic

Parameter	
$Lm[H]$	0.38
$R_0[\Omega]$	1733
$R_s[\Omega]$	5.00
$R_r[\Omega]$	3.8
$L_{\sigma-tot}[H]$	0.04

The temperature is set at $120°C$, i.e. the nominal, in order to see the performance at nominal operating condition.

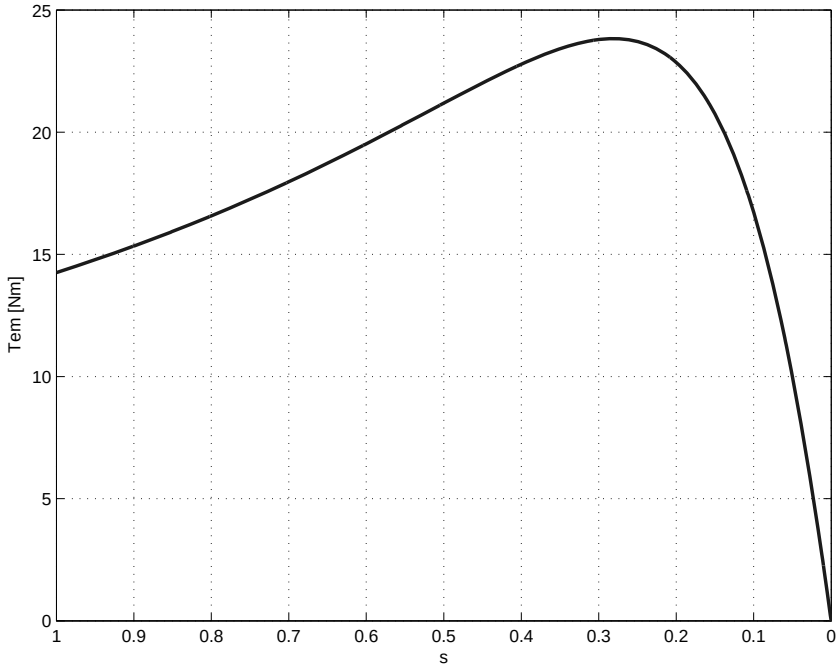

Figure 1.12: Electromagnetic torque

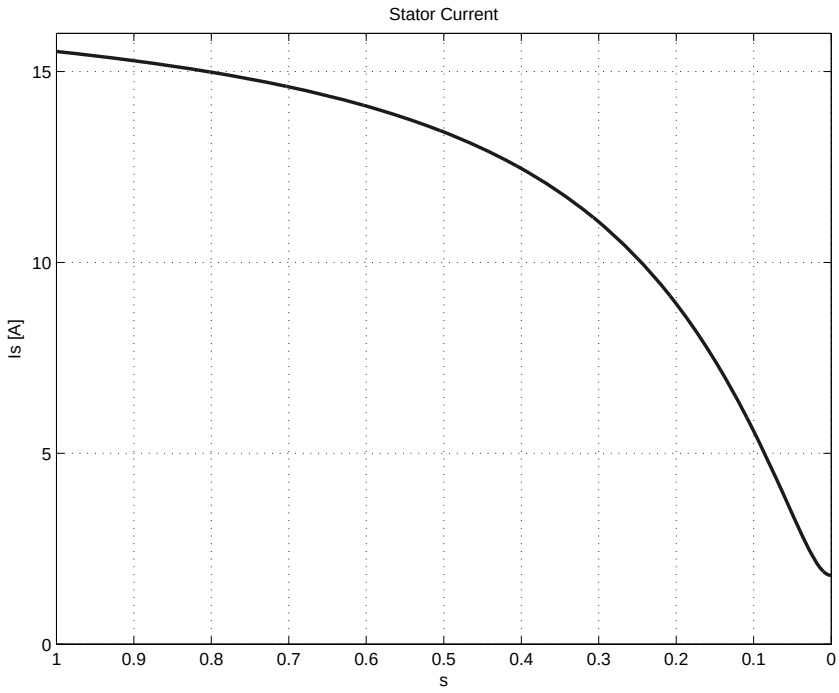

Figure 1.13: Starting current

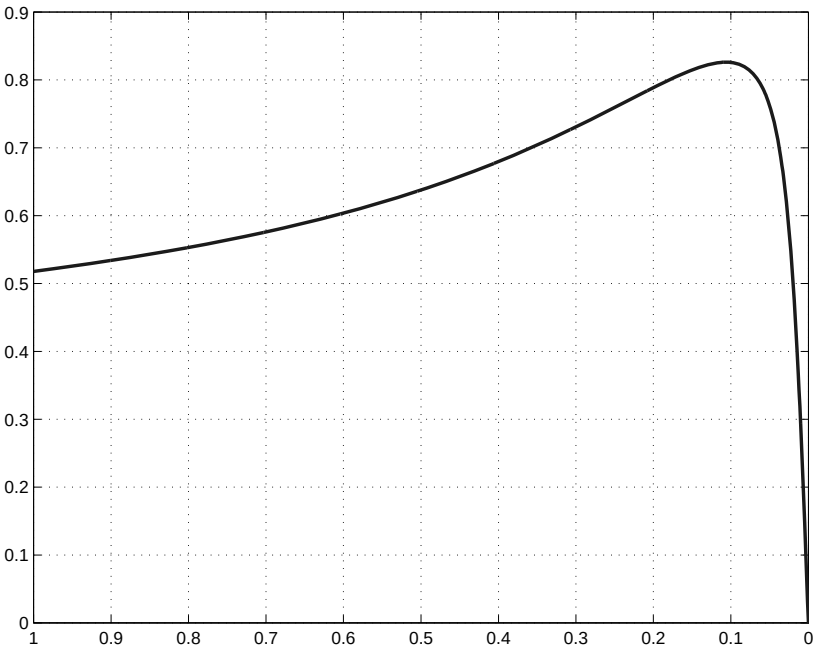

Figure 1.14: Power factor

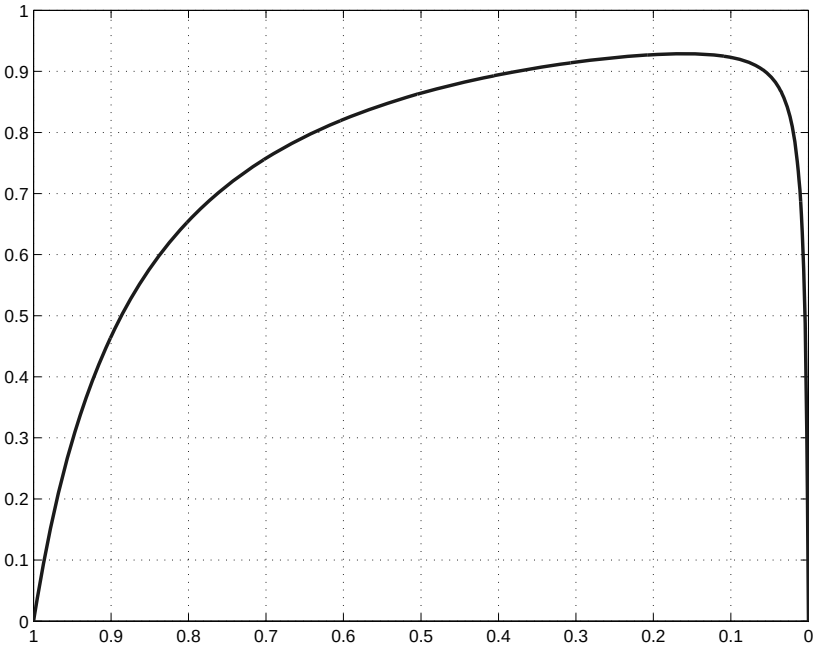

Figure 1.15: Efficiency

Chapter 2

Induction motor field oriented control

In this chapter the signal injection technique is rapidly explained. The field oriented control of an Induction Motor with FE analysis is then explained. The optimal current angle for control the IM, like in a synchronous motor is also investigated. At least the torque ripple, the mean torque and the constant torque loci of the three types of rotor are explained.

2.1 Sensorless Field Oriented Control

Full information can be found in paper [6].

The signal injection technique is considered. In particular, a rotating high frequency signal is injected in addition to the fundamental supply, and an intentionally created saliency is introduced in the rotor.

The interaction between the injected carrier signal and the rotor saliency, allows for a continuous estimation of the rotor position and flux angle.

Figure 2.1 shows a diagram of the control technique considered (the symbol $\sim$ over a letter indicates the estimated quantities). From the stator current reference $\overline{i}_s^*$, the current error is computed and the stator voltage reference $\overline{v}_s^*$ is generated. Then, a change of reference frame is operated and the voltage reference is reported to the stator frame by means of the operator $e^{j\tilde{\delta}}$, where $\tilde{\delta}$ is the estimated rotor flux angle computed from the estimated rotor angle $\tilde{\vartheta}_m^e$.

A high frequency carrier signal $\overline{v}_{sc}^{(s)}$ is added to the fundamental excitation using a PWM voltage source inverter. The high frequency voltage can be written in the stator reference frame as

$$\overline{v}_{sc}^{(s)} = V_{sc}\ e^{j\omega_c t} = v_{scd}^{(s)} + j\ v_{scq}^{(s)} \tag{2.1}$$

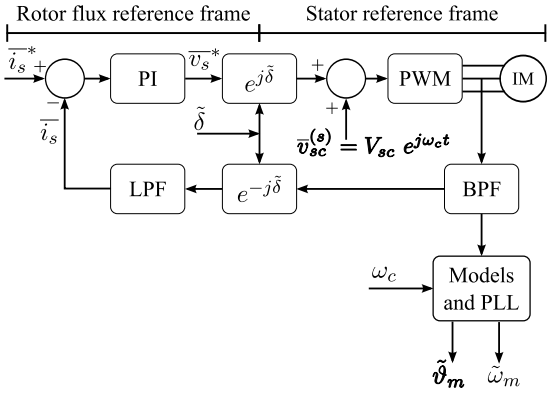

Figure 2.1: Diagram of the control scheme for sensorless control of IM

where the carrier voltage components along the two axes are

$$\begin{cases} v_{scd}^{(s)} = V_{sc} \cdot \cos\left(\omega_c t\right) \\ v_{scq}^{(s)} = V_{sc} \cdot \sin\left(\omega_c t\right) \end{cases} \tag{2.2}$$

and ω_c is the carrier signal angular speed.

The interaction between the carrier voltage $\overline{v}_{sc}^{(s)}$, and the rotor saliency produces a current signal that contains information related to the position of the rotor:

$$\overline{i}_{sc}^{(s)} = -jI_{cp}e^{j\omega_c t} - jI_{cn}e^{j(2\vartheta_m^e - \omega_c t)} \tag{2.3}$$

where

$$\begin{aligned} I_{cp} &= \frac{L_{\sigma d}^{(r)} + L_{\sigma q}^{(r)}}{2\ L_{\sigma d}^{(r)}\ L_{\sigma q}^{(r)}} \cdot \frac{V_{sc}}{\omega_c} \\ I_{cn} &= \frac{L_{\sigma d}^{(r)} - L_{\sigma q}^{(r)}}{2\ L_{\sigma d}^{(r)}\ L_{\sigma q}^{(r)}} \cdot \frac{V_{sc}}{\omega_c} \end{aligned} \tag{2.4}$$

The carrier current is composed by a positive–sequence and a negative–sequence components [7].

The negative–sequence component contains information about the rotor position ϑ_m^e which is proportional to the difference of the inductances along the two rotor axis. In order to extract the rotor position information from the negative–sequence component, the motor current is processed by the two blocks in the bottom–right corner of Fig. 2.1.

At first, the carrier current is multiplied by $e^{-j\omega_c t}$ and filtered to eliminate the positive–sequence component, as

$$HPF\left\{\bar{i}_{sc}^{(s)} \cdot e^{-j\omega_c t}\right\} = -jI_{cn}e^{j(2\vartheta_m^e - 2\omega_c t)} \tag{2.5}$$

Then this signal is elaborated by means of a signal $e^{j(2\tilde{\vartheta}_m^e - 2\omega_c t)}$ which contains an estimation $\tilde{\vartheta}_m^e$ of the rotor position. In this way, the following error signal is obtained

$$\varepsilon = \frac{V_{sc}}{\omega_c} \cdot \frac{L_{\sigma diff}}{L_{\sigma d}^{(r)}\ L_{\sigma q}^{(r)}} \cdot \sin 2(\vartheta_m^e - \tilde{\vartheta}_m^e) \tag{2.6}$$

When the error defined in (2.6) is zero, the estimated rotor position $\tilde{\vartheta}_m^e$ is equal to the actual rotor position ϑ_m^e, and the sensorless detection of the rotor position of the IM rotor is achieved. Then, the flux angle $\tilde{\delta}$ is computed elaborating $\tilde{\vartheta}_m^e$.

Equation (2.6) also shows the dependence of the error signal on the difference between the d– and q– axis leakage inductances $L_{\sigma d}$ and $L_{\sigma q}$.

In order to get the error signal, a proper value of such a difference has to be achieved by introducing a variation in the rotor slot geometry [8, 9].

2.2 Application of the Foc in finite element simulation

The field oriented strategy, is based on the cancellation of the rotor λ_{rq}. In this situation the torque is:

$$\tau_m = \frac{3}{2} \cdot p \cdot \lambda_{rd} \cdot i_{rq} \tag{2.7}$$

with

$$i_{rq} = -\frac{L_M}{L_r} i_{sq} \tag{2.8}$$

In finite element simulation this is made imposing the current on the rotor bars, in order to achieve $\Lambda_{rq} = 0$. The procedure and the steps to simulate FOC control technique are extensively and clearly discuss in [10].

2.3 Optimal current angle

Like in a synchronous motor, also for an induction motor with field oriented control, the current angle is important for the maximum exploitation of the motor. The current angle is investigated with the simulation script used for

Foc control. Many simulations at different current angle are made and the torque is calculated. The maximum of the torque is related with the optimal current angle. The limitation is the maximum magnitude of the current in the stator winding.

$$I_n = 3.6A \tag{2.9}$$

$$I_d = I_n \cdot \cos(\alpha_{ie}) \tag{2.10}$$

$$I_q = I_n \cdot \sin(\alpha_{ie}) \tag{2.11}$$

The α_{ie} is computed for the three motors, to investigate how change this angle in relation of the motor type. The results are reported in fig 2.2, fig 2.3 and fig 2.4.

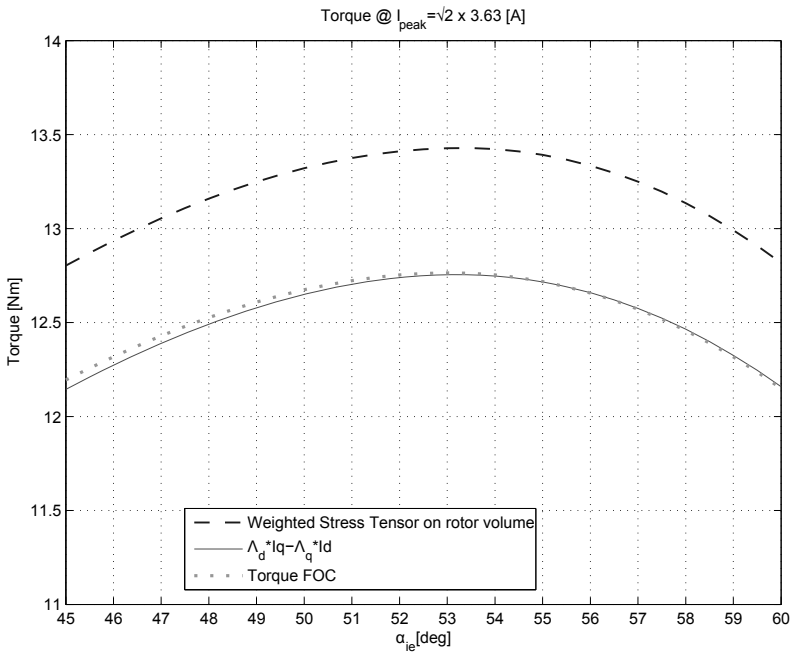

Figure 2.2: Torque as a function of α_{ie} for standard motor

It is immediate to see that the optimal angle isn't the same for the three motors. This is caused by the anisotropy introduced with the saliency. When a field oriented control is implemented, a preliminary evaluation of this angle is required.

In fig 2.2, fig 2.3, fig 2.4, the torque is computed by means of three methods. The Maxwell tensor give a different result with respect by the other two. The difference is due to the position of the rotor regard to the stator. Probably if the same simulation is made in another rotor position,

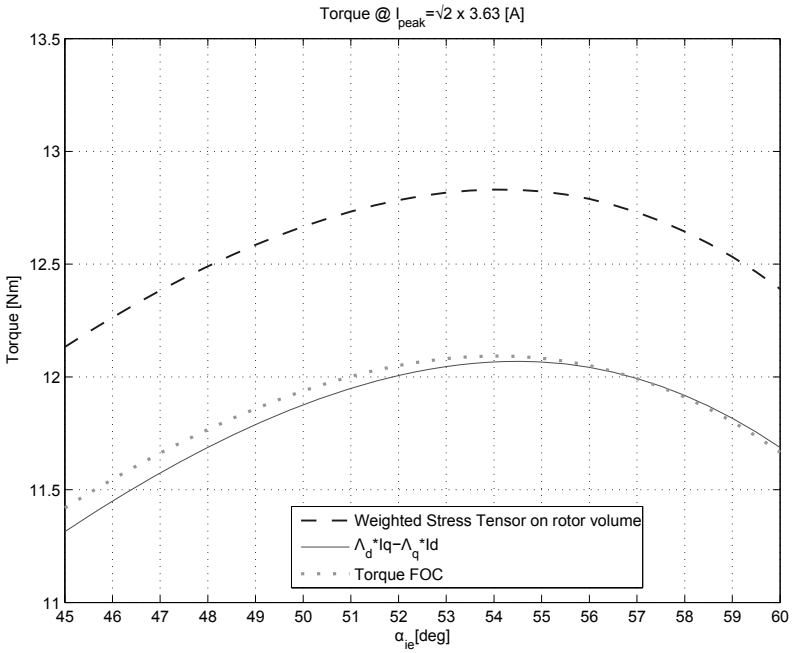

Figure 2.3: Torque as a function of α_{ie} for prototype 01

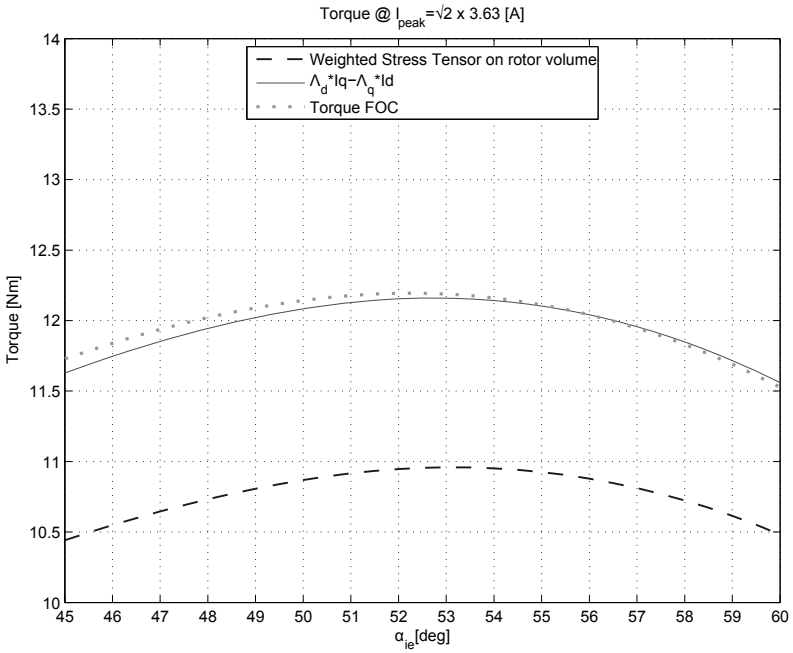

Figure 2.4: Torque as a function of α_{ie} for prototype 02

a different value would be obtained. The torque calculated with flux and current are less influenced by the rotor position and is a good evaluation of the torque.

For maximum exploitation of the motor, the current angle should be circa $\alpha_{ie} = 53 - 55$.

An other simulation is done, in which both α_{ie} and current are variable. This allow us to decide the right current angle in relation with the current value. Is immediate to see that the optimal α_{ie} has not a constant value but it's function of current. Those simulations are made for the three motors, in order to investigate the influence of the salience. Results are reported in fig 2.5

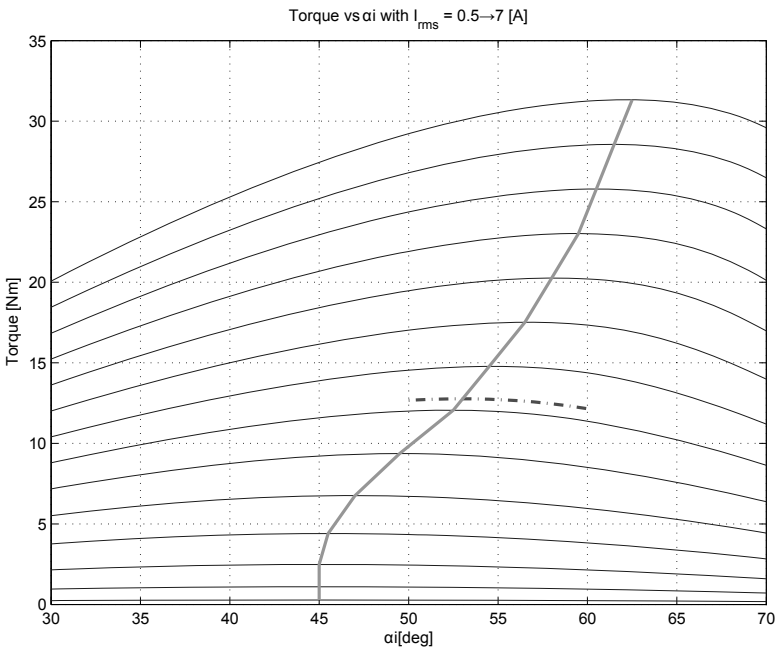

Figure 2.5: Relation between current angle and current value - Standard motor

2.4 Torque ripple

The simulation are made for the three motor in order to see how the introduced anisotropy affects the torque ripple.

- Standard Motor

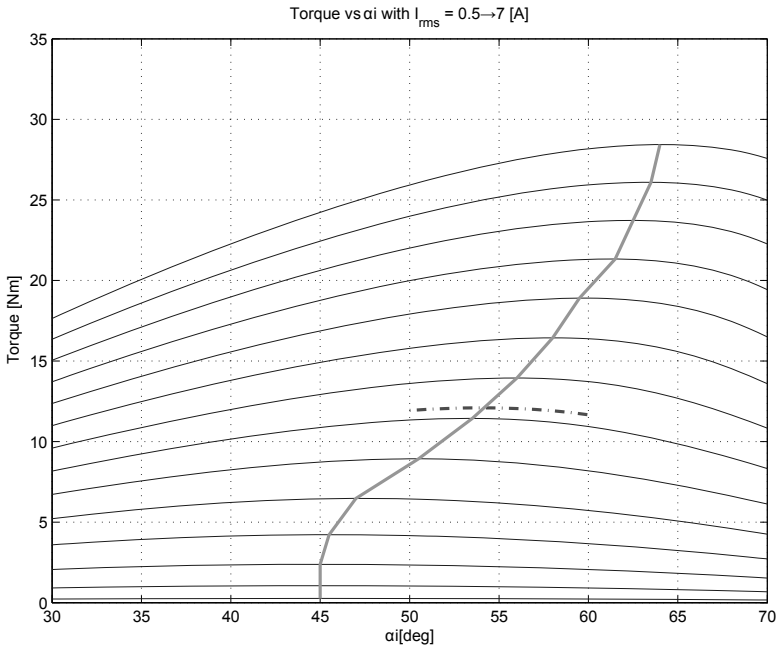

Figure 2.6: Relation between current angle and current value - Prototype 01

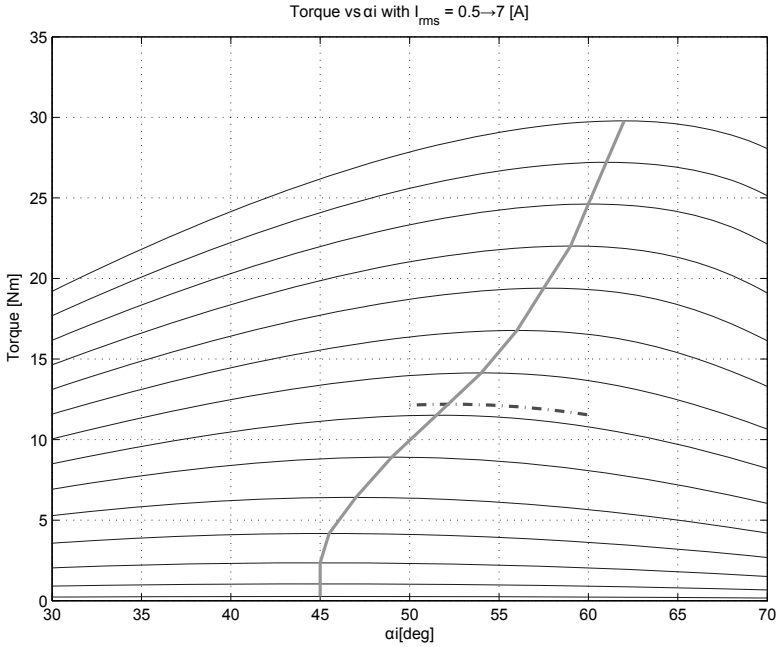

Figure 2.7: Relation between current angle and current value - Prototype 02

- Prototype n°01 (modified height slot open)
- Prototype n°02 (modified height and width slot open)

In fig 2.8, fig 2.9 and fig 2.10 are reported the torque of the motors calculated with the three methods. The Torque calculated with Maxwell tensor is major influenced by slot opening of the rotor and stator, but the mean is the same as the torque calculated with the flux and the current.

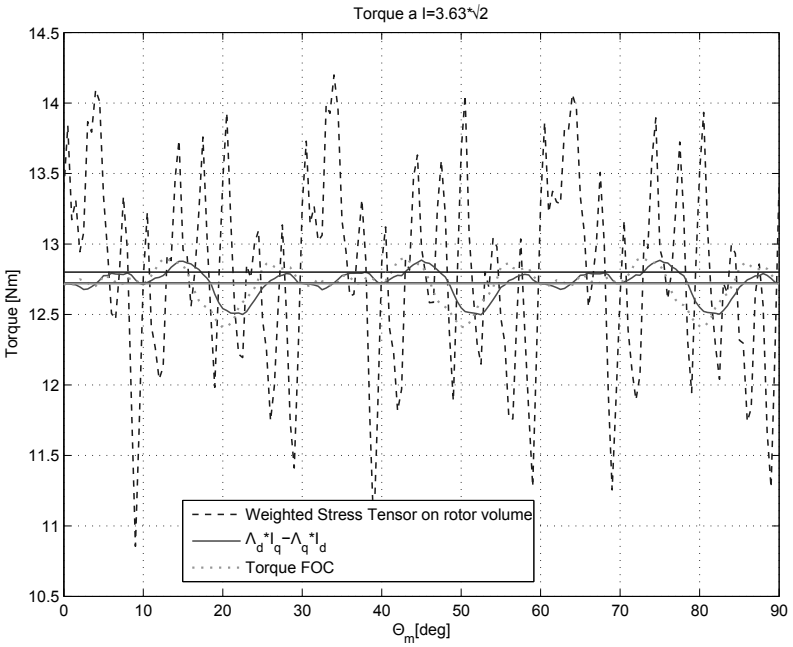

Figure 2.8: Torque vs mechanical angle, Standard Motor

The torque ripple calculated in this way is not totally correct. The real motor has the rotor skewed while the simulated does not.

The skew reduces the torque ripple very well, and a comparison is not possible. However the mean torque is correct and should be a good approximation.

2.5 Constant torque loci

The Foc script is also useful to get the constant torque loci. Results are show in fig 2.11, fig 2.12, fig 2.13.

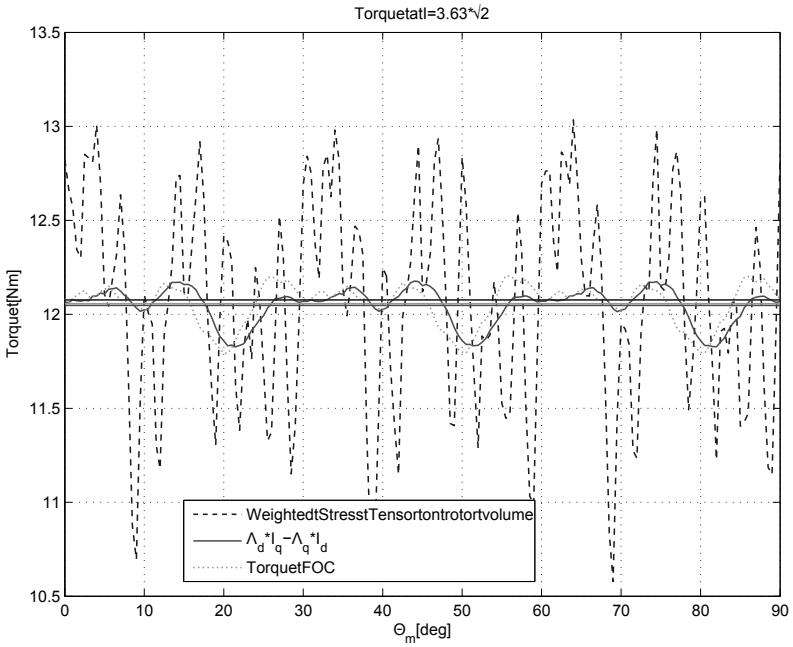

Figure 2.9: Torque vs mechanical angle, Prototype 01

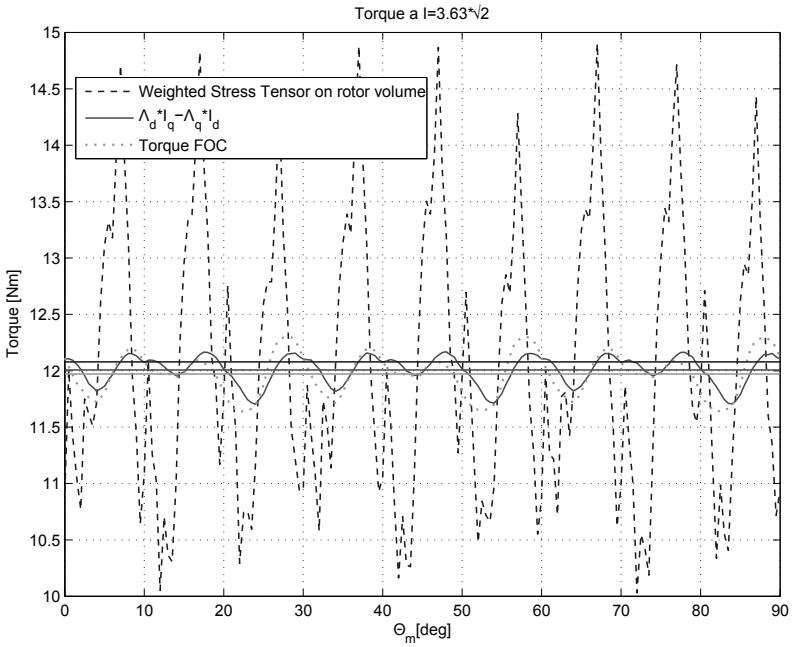

Figure 2.10: Torque vs mechanical angle, Prototype 02

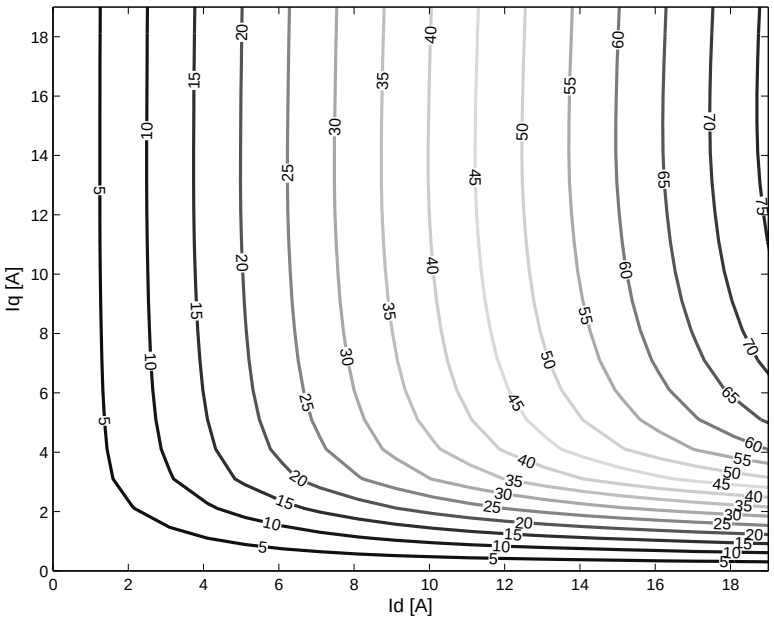

Figure 2.11: Constant torque loci, Standard Motor

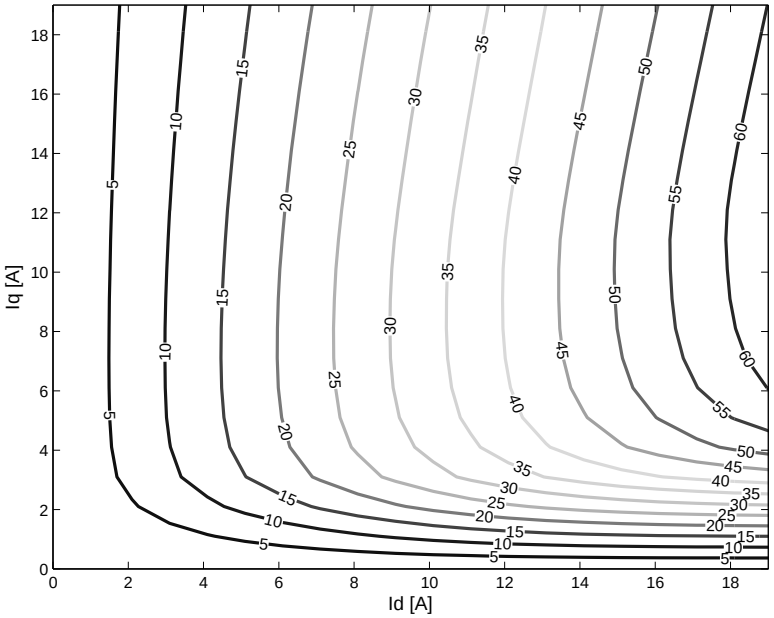

Figure 2.12: Constant torque loci, Prototype 01

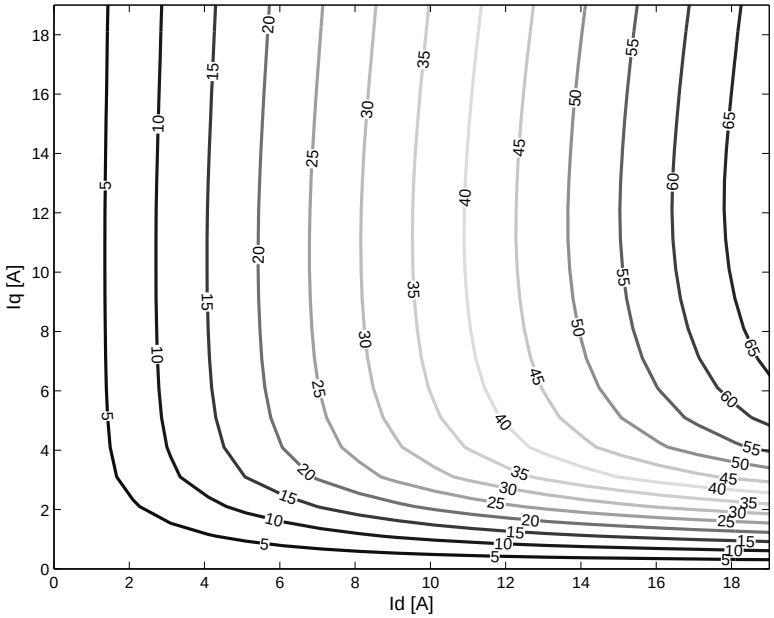

Figure 2.13: Constant torque loci, Prototype 02

Chapter 3

Induction Motor Finite Element parameters estimation

This chapter deal with the high frequency response of the induction motor rotor. The study is done for two reference frames, dq and $\alpha\beta$, in order to investigate the difference between them. Last, the possible reasons for the differences between simulations and measures are investigated.

3.1 Non Orthogonal transformation

Is worth note that we use the non-orthogonal transformation instead of orthogonal. So the transformation to one reference frame to another is not only the transpose of the initial matrix, but is the inverse. An orthogonal transformation preserve the dot product but not the magnitude of the parameter. Instead the non orthogonal transformation don't preserve lengths of vectors and angles between them.

Between *abc* and $\alpha\beta\gamma$ reference frame the relation are:

$$\begin{aligned} |\chi_{\alpha\beta\gamma}| &= |C|^{-1} \cdot |\chi_{abc}| \\ |Z_{\alpha\beta\gamma}| &= |C|^{-1} \cdot |Z_{abc}| \cdot |C| \end{aligned} \tag{3.1}$$

$$\begin{aligned} |\chi_{abc}| &= |C| \cdot |\chi_{\alpha\beta\gamma}| \\ |Z_{abc}| &= |C| \cdot |Z_{\alpha\beta\gamma}| \cdot |C|^{-1} \end{aligned} \tag{3.2}$$

with

$$|C|^{-1} = \frac{2}{3}\begin{bmatrix} 1 & -1/2 & -1/2 \\ 0 & \sqrt{3}/2 & -\sqrt{3}/2 \\ 1/2 & 1/2 & 1/2 \end{bmatrix} \tag{3.3}$$

and

$$|C| = \begin{bmatrix} 1 & 0 & 1 \\ -1/2 & \sqrt{3}/2 & 1 \\ -1/2 & -\sqrt{3}/2 & 1 \end{bmatrix} \tag{3.4}$$

Between the abc and $dq\gamma$ reference frame the relation are:

$$\begin{aligned} |\chi_{dq\gamma}| &= |D|^{-1} \cdot |\chi_{abc}| \\ |Z_{dq\gamma}| &= |D|^{-1} \cdot |Z_{abc}| \cdot |D| \end{aligned} \tag{3.5}$$

$$\begin{aligned} |\chi_{abc}| &= |D| \cdot |\chi_{dq\gamma}| \\ |Z_{abc}| &= |D| \cdot |Z_{dq\gamma}| \cdot |D|^{-1} \end{aligned} \tag{3.6}$$

with

$$|D|^{-1} = \frac{2}{3}\begin{bmatrix} cos(\theta_m^e) & cos(\theta_m^e - 120°) & cos(\theta_m^e - 240°) \\ -sin(\theta_m^e) & -sin(\theta_m^e - 120°) & -sin(\theta_m^e - 240°) \\ 1/2 & 1/2 & 1/2 \end{bmatrix} \tag{3.7}$$

and

$$|D| = \begin{bmatrix} cos(\theta_m^e) & -sin(\theta_m^e) & 1 \\ cos(\theta_m^e - 120°) & -sin(\theta_m^e - 120°) & 1 \\ cos(\theta_m^e - 240°) & -sin(\theta_m^e - 240°) & 1 \end{bmatrix} \tag{3.8}$$

Between the $\alpha\beta\gamma$ and $dq\gamma$ reference frame the relation are:

$$\begin{aligned} |\chi_{dq\gamma}| &= |E|^t \cdot |\chi_{\alpha\beta\gamma}| \\ |Z_{dq\gamma}| &= |E|^t \cdot |Z_{\alpha\beta\gamma}| \cdot |E| \end{aligned} \tag{3.9}$$

$$\begin{aligned} |\chi_{\alpha\beta\gamma}| &= |E| \cdot |\chi_{dq\gamma}| \\ |Z_{\alpha\beta\gamma}| &= |E| \cdot |Z_{dq\gamma}| \cdot |E|^t \end{aligned} \tag{3.10}$$

with

$$|E|^t = \begin{bmatrix} cos(\theta_m^e) & sin(\theta_m^e) & 0 \\ -sin(\theta_m^e) & cos(\theta_m^e) & 0 \\ 0 & 0 & 1 \end{bmatrix} \tag{3.11}$$

and

$$|E| = \begin{bmatrix} cos(\theta_m^e) & -sin(\theta_m^e) & 0 \\ sin(\theta_m^e) & cos(\theta_m^e) & 0 \\ 0 & 0 & 1 \end{bmatrix} \tag{3.12}$$

3.2 Flux distribution along rotor surface at 300 Hz

For better understand what happened when the motor is supplied with an high frequency current some figure could be very explicative.

In fig 3.2 and 3.1 are shown the two situation in which the motor has to work. The low frequency correspond to the normal functioning mode and the high frequency correspond to the signal injection to obtain the rotor position.

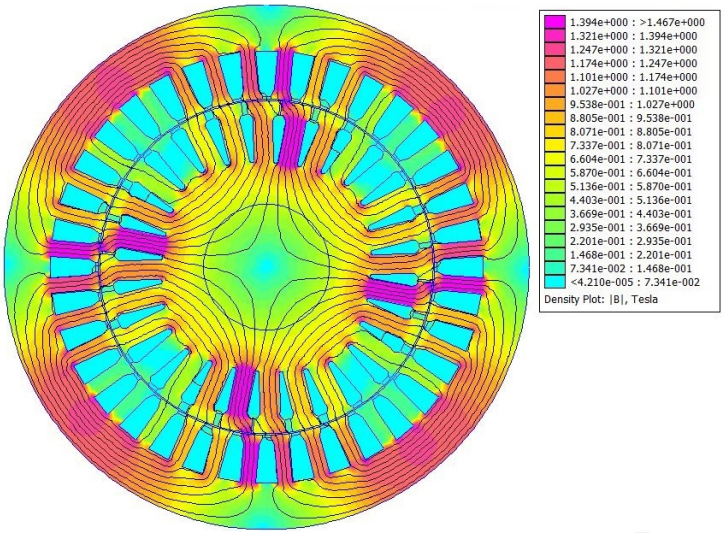

Figure 3.1: Flux distribution in the rotor at low frequency

In fig 3.3 a particular of the flux distribution on q-axis can be see.

Also the current are influenced by the frequency of the current injected on the stator. The current displacement on the rotor bars, especially on the rotor slot open, can be see in fig 3.4.

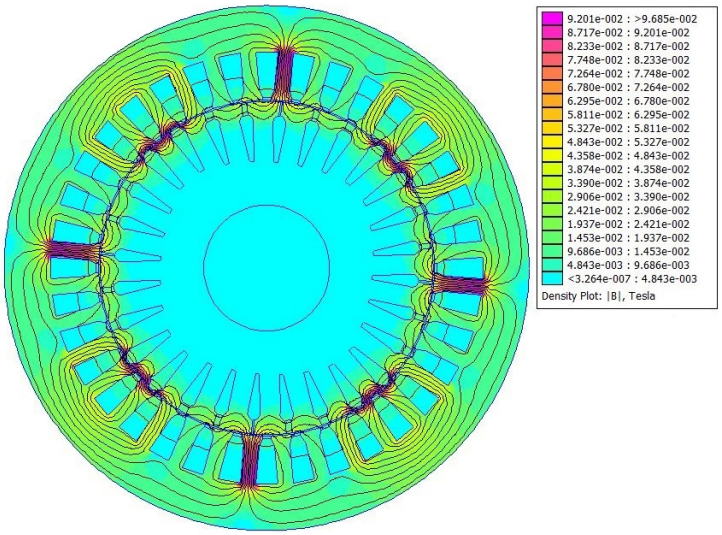

Figure 3.2: Flux distribution in the rotor at high frequency

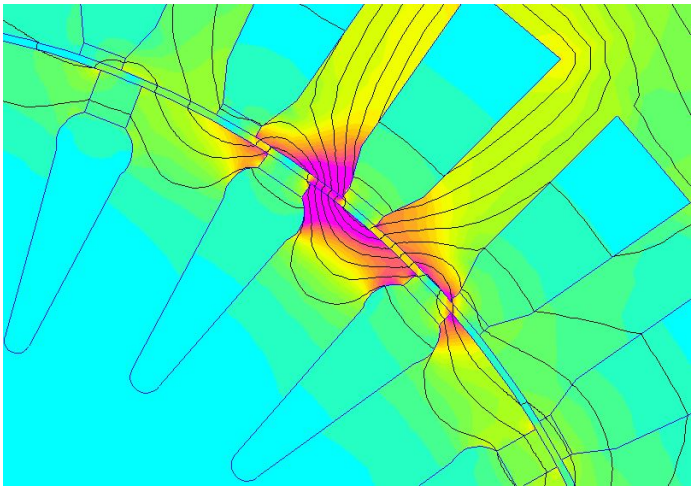

Figure 3.3: Zoomed view of flux distribution on q axis

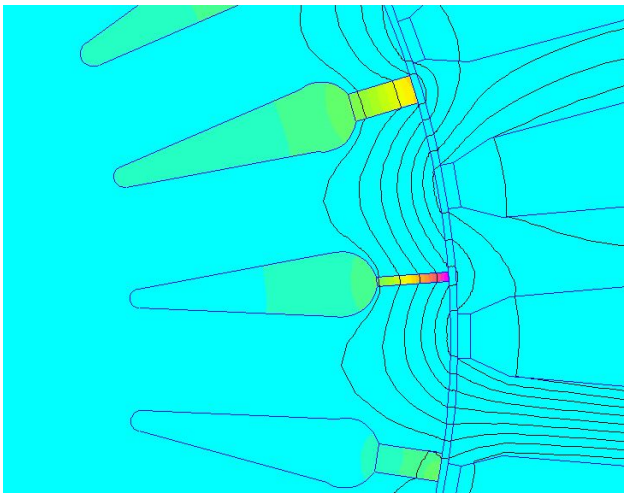

Figure 3.4: Current distribution in the rotor at high frequency

3.3 Induction motor model on dq model

Full paper over this arguments is [6].

The procedure to compute the IM parameters is based on the d and q axis model of the IM.

The analysis is carried out in the rotor reference frame, that is, the reference frame rotating at the same speed of the rotor, i.e., $\omega_{dq}^{e} = \omega_m$, in electrical radians per second. The electrical angle between the rotor d axis and the stator d axis is indicated as ϑ_r.

Both d and $q$axis are excited together, since a rotating magnetic field is imposed in the simulations and both d and q axis parameters of the IM are obtained simultaneously from the same field solution.

In the considered reference frame, the stator voltages are

$$\begin{aligned} v_{sd} &= R_s i_{sd} + \frac{d\lambda_{sd}}{dt} - \omega_m^e \lambda_{sq} \\ v_{sq} &= R_s i_{sq} + \frac{d\lambda_{sq}}{dt} + \omega_m^e \lambda_{sd} \end{aligned} \tag{3.13}$$

The corresponding dq model of IM machine is shown in fig 3.5, referring all parameters to the stator. The Γ type equivalent circuits are used, with all leakage inductances considered on the rotor side and stator resistances omitted.

Such stator resistance as well as all 3D parameters are not included in the FE model of the motor, but they are computed analytically and added

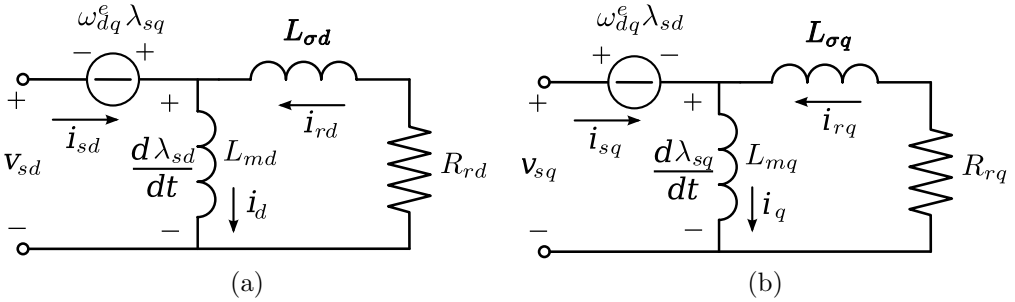

Figure 3.5: Dynamic dq equivalent circuits of the IM.

to the circuits in a second time [11].

At steady state, the voltages and currents are considered to be sinusoidal with time. In the dq reference frame, they vary at the electrical speed $(\omega - \omega^e_{dq})$, where $\omega = 2\pi f$, with f the line frequency. It follows that the complex notation can be used. Overline symbols will be used to highlight complex quantities. Thus, (3.13) are rewritten as

$$\begin{aligned} \overline{V}_{sd} &= R_s\overline{I}_{sd} + \jmath(\omega - \omega^e_{dq})\overline{\Lambda}_{sd} - \omega^e_{dq}\overline{\Lambda}_{sq} \\ \overline{V}_{sq} &= R_s\overline{I}_{sq} + \jmath(\omega - \omega^e_{dq})\overline{\Lambda}_{sq} + \omega^e_{dq}\overline{\Lambda}_{sd} \end{aligned} \tag{3.14}$$

3.3.1 dq Magnetizing inductances

For the computation of the magnetizing inductances, it is convenient to choose the speed of the dq reference frame (that is the rotor speed) equal to the line electrical speed, i.e., $\omega^e_{dq} = \omega$.

It results that the electrical quantities (currents, voltages, flux linkages) exhibit zero frequency, that is, they have constant values. The voltage equations (3.14) are rewritten as

$$\begin{aligned} V_{sd} &= R_s I_{sd} - \omega\Lambda_{sq} \\ V_{sq} &= R_s I_{sq} + \omega\Lambda_{sd} \end{aligned} \tag{3.15}$$

without overline, they being constant. Since the frequency is zero, there are no currents induced in the rotor.

The dq flux linkages correspond to the magnetizing dq flux linkages of the motor.They depend on the dq currents imposed in the stator, since the iron is non linear. It is worth noticing that d and q axis currents can be imposed simultaneously. Then, both d and q axis flux linkages, and d and q axis inductances, can be computed from the same field solution.

Therefore, not only the saturation effect is considered, but also the mutual effect between the d and the $q$axis, that is the dq cross saturation effect. In

this condition, the dq circuits of IM model (see fig 3.5) are not independent. Starting from the dq axis magnetizing currents, i.e., I_d and I_q, the phase currents are obtained from the Park transformation. The dq flux linkages are obtained from field solutions. The magnetizing inductances are defined as

$$\begin{aligned} L_{md}(I_d, I_q) &= \frac{\Lambda_{md}(I_d, I_q)}{I_d} \\ L_{mq}(I_d, I_q) &= \frac{\Lambda_{mq}(I_d, I_q)}{I_q} \end{aligned} \tag{3.16}$$

and they are functions of both magnetizing currents.

3.3.2 Rotor parameters

For the computation of the rotor parameters, it is convenient to refer to the rotor reference frame, in which the steady state quantities vary at the rotor frequency. In the adopted reference frame, in which $\omega^e_{dq} = \omega^e_m$, such a rotor frequency results in $\omega_r = (\omega - \omega^e_{dq}) = (\omega - \omega^e_m)$. Neglecting the stator resistance, R_s, the voltages (3.14) are rewritten as

$$\begin{aligned} \overline{V}_{sd} &= +\jmath\omega_r\overline{\Lambda}_{sd} - \omega^e_m\overline{\Lambda}_{sq} \\ \overline{V}_{sq} &= +\jmath\omega_r\overline{\Lambda}_{sq} + \omega^e_m\overline{\Lambda}_{sd} \end{aligned} \tag{3.17}$$

and they vary at the electrical frequency ω_r.

In order to compute the rotor parameters, a time harmonic FE simulation is carried out, setting the frequency $f_r = \omega_r/2\pi$. The FE simulations are carried out with fixed rotor and stator (as at standstill), supplying the d–q stator windings at the rotor frequency f_r. Since rotor parameters depend on the rotor frequency, they are obtained from various time harmonic FE simulations imposing different rotor frequencies.

Since the rotor is at standstill, the dq circuits of fig 3.5 reduce to those shown in fig 3.6. In order to estimate the rotor parameters, the dq stator currents in the simulations are fixed to

$$\overline{I}_{sd} = \overline{I}$$

and

$$\overline{I}_{sq} = -\jmath\overline{I}$$

where

$$|\overline{I}| = \sqrt{2}\, I_{rms}$$

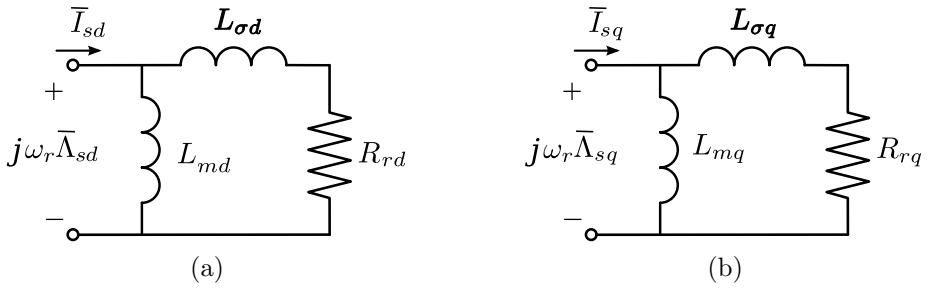

Figure 3.6: Steady state dq equivalent circuits

is the current amplitude.

Thus, the magnetic field is rotating, but modulated by the rotor anisotropy. Currents are induced in the rotor bars, and the rotor parameters of the dq model of fig 3.6 can be computed. The flux linkages $\overline{\Lambda}_{sd}$ and $\overline{\Lambda}_{sq}$ are determined from the field solution.

The voltages can be achieved from (3.17). Therefore, the equivalent parameters of the circuits of fig 3.6 are computed from flux linkages, as

$$\begin{aligned} L_{eq,d} &= \Re_{eal}\left(\frac{\overline{\Lambda}_{sd}}{\overline{I}_{sd}}\right) \\ R_{eq,d} &= -\omega_r \Im_{mag}\left(\frac{\overline{\Lambda}_{sd}}{\overline{I}_{sd}}\right) \end{aligned} \tag{3.18}$$

and

$$\begin{aligned} L_{eq,q} &= \Re_{eal}\left(\frac{\overline{\Lambda}_{sq}}{\overline{I}_{sq}}\right) \\ R_{eq,q} &= -\omega_r \Im_{mag}\left(\frac{\overline{\Lambda}_{sq}}{\overline{I}_{sq}}\right) \end{aligned} \tag{3.19}$$

Finally, the rotor parameters R_{rd}, $L_{\sigma d}$, R_{rq} and $L_{\sigma q}$ are computed with

$$
\begin{aligned}
L_{\sigma d} &= L_{md}\frac{L_{eq,d}(L_{md}-L_{eq,d})-\left(\frac{R_{eq,d}}{\omega_r}\right)^2}{(L_{md}-L_{eq,d})^2+\left(\frac{R_{eq,d}}{\omega_r}\right)^2} \\
R_{rd} &= R_{eq,d}\frac{(L_{md}+L_{\sigma d})}{L_{md}-L_{eq,d}} \\
L_{\sigma q} &= L_{mq}\frac{L_{eq,q}(L_{mq}-L_{eq,q})-\left(\frac{R_{eq,q}}{\omega_r}\right)^2}{(L_{mq}-L_{eq,q})^2+\left(\frac{R_{eq,q}}{\omega_r}\right)^2} \\
R_{rq} &= R_{eq,q}\frac{(L_{mq}+L_{\sigma q})}{L_{mq}-L_{eq,q}}
\end{aligned}
\tag{3.20}
$$

It is worth noticing that $|I_{sd}| = |I_{sq}|$ are imposed in the FE simulation. As a consequence $|V_{sd}| \neq |V_{sq}|$, since the flux linkages and the corresponding voltages are modulated by the rotor anisotropy. In the actual operating conditions, it is $|V_{sd}| = |V_{sq}|$,while $|I_{sd}| \neq |I_{sq}|$.

3.4 Simulation results in dq reference frame

The parameter here calculated are referred at frequency f=300 Hz, so they are different than the analytically calculated. The leakage inductance of prototype 01 present a mean value higher than prototype 02, due to the rotor slot open geometry. The difference of leakage inductance between d and q axis, respect to the mean value is $\Delta L_{01} = \frac{9}{38} = 23\%$ and $\Delta L_{02} = \frac{7.5}{20} = 37.5\%$. The variation ΔL is as expected higher for the prototype 02, because the rotor 02 present two degree of anisotropy instead of only one. (see figs 1.2 and 1.3.

For investigate the rule of the skew on parameter harmonic reduction, a simulation with only 1 rotor slot is made. The other are made with 1.5 rotor slot, like in the real prototype.

3.5 Induction motor model in $\alpha - \beta$

For providing the measure of the high frequency rotor parameter, a fix reference frame is choose. Starting from the dq model and using the transformation is simple to obtain the stator voltage equation in the $\alpha\beta$ reference frame.

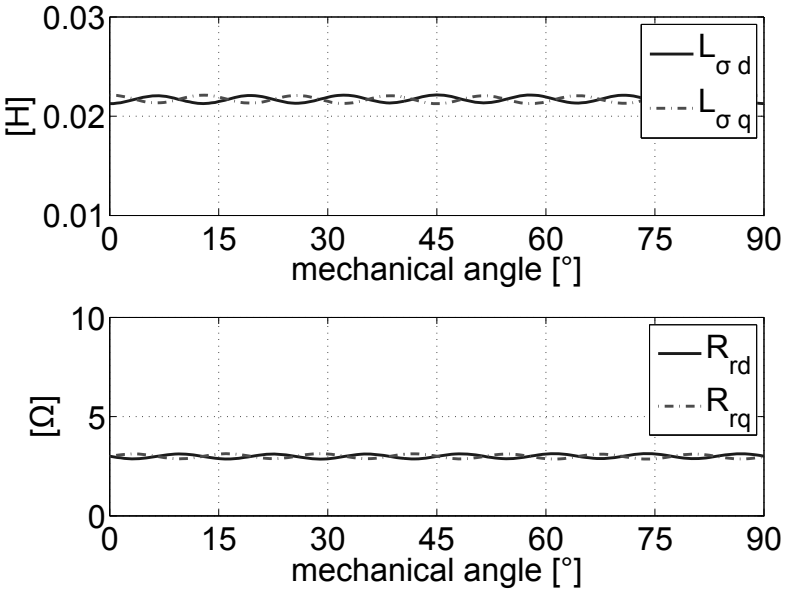

Figure 3.7: Inductance and resistance vs θ_m of standard motor.

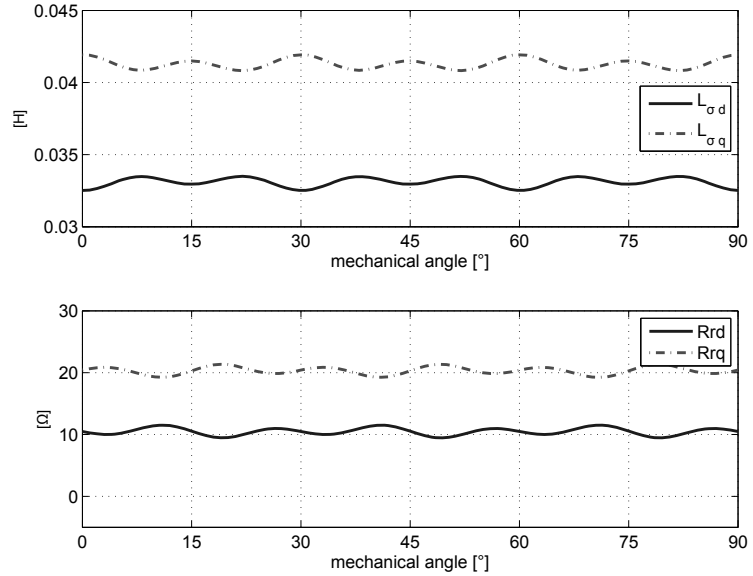

Figure 3.8: Inductance and resistance vs θ_m of prototype 01.

$$V_{\alpha\beta} = [R_{\alpha\beta}] \cdot i_{\alpha\beta} + [L_{\alpha\beta}] \cdot i_{\alpha\beta} \tag{3.21}$$

Supposing the inductance matrix in dq like:

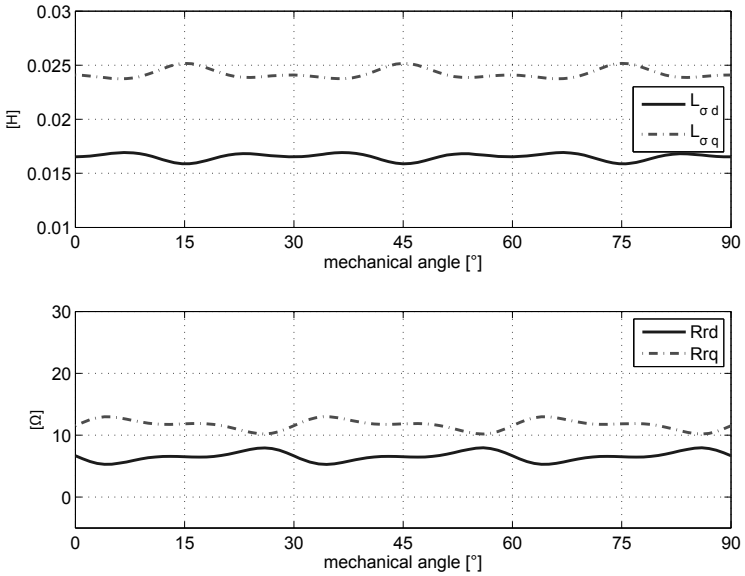

Figure 3.9: Inductance and resistance vs θ_m of prototype 02.

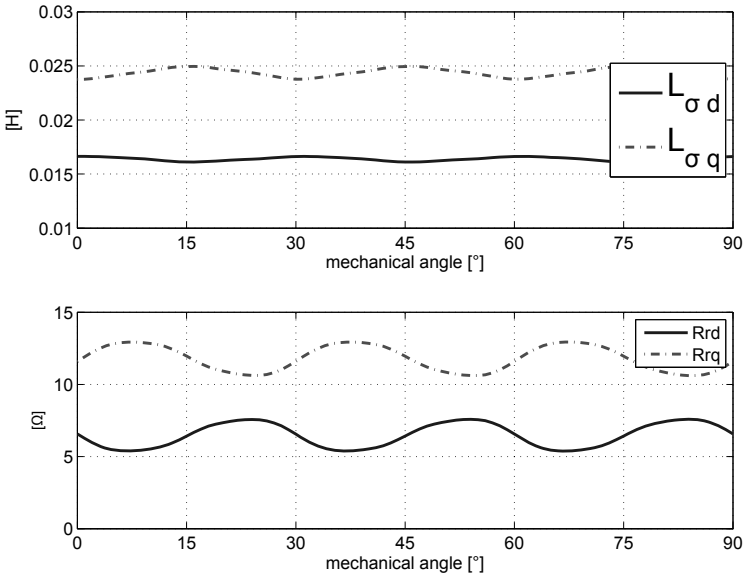

Figure 3.10: Inductance and resistance vs θ_m of prototype 02 with 1 rotor slot skew

$$[L_{dq}] = \begin{bmatrix} L_d & 0 \\ 0 & L_q \end{bmatrix} \tag{3.22}$$

The corresponding matrix in $\alpha\beta$ is:

$$[L_{\alpha\beta}] = \begin{bmatrix} cos(\theta_m^e) & -sin(\theta_m^e) \\ sin(\theta_m^e) & cos(\theta_m^e) \end{bmatrix} \cdot \begin{bmatrix} L_d & 0 \\ 0 & L_q \end{bmatrix} \cdot \begin{bmatrix} cos(\theta_m^e) & sin(\theta_m^e) \\ -sin(\theta_m^e) & cos(\theta_m^e) \end{bmatrix} \tag{3.23}$$

And the resultant inductance matrix is:

$$[L_{\alpha\beta}] = \begin{bmatrix} \frac{L_{\sigma q}+L_{\sigma d}}{2} - \frac{L_{\sigma q}-L_{\sigma d}}{2} \cdot cos(2\theta_m^e) & -\frac{L_{\sigma q}-L_{\sigma d}}{2} \cdot sin(2\theta_m^e) \\ -\frac{L_{\sigma q}-L_{\sigma d}}{2} \cdot sin(2\theta_m^e) & \frac{L_{\sigma q}+L_{\sigma d}}{2} + \frac{L_{\sigma q}-L_{\sigma d}}{2} \cdot cos(2\theta_m^e) \end{bmatrix} \tag{3.24}$$

This notation however is difficult and is better rewrite the matrix in a simplest form:

$$[L_{\alpha\beta}] = \begin{bmatrix} L_{\sigma avg} - L_{\sigma diff} \cdot cos(2\theta_m^e) & -L_{\sigma diff} \cdot sin(2\theta_m^e) \\ -L_{\sigma diff} \cdot sin(2\theta_m^e) & L_{\sigma avg} + L_{\sigma diff} \cdot cos(2\theta_m^e) \end{bmatrix} \tag{3.25}$$

with:

$$L_{\sigma avg} = \frac{L_{\sigma q} + L_{\sigma d}}{2} \tag{3.26}$$

and

$$L_{\sigma diff} = \frac{L_{\sigma q} - L_{\sigma d}}{2} \tag{3.27}$$

Is simple observe that in $[L_{\alpha\beta}]$ are present also the two terms that corresponds to the mutual inductances between the two axis α *and* β.

This fastidious effect can be neglected if the motor is supplied using only the current i_α or i_β.

3.5.1 Rotating field simulation

If the stator is supplied with a rotating field instead of only pulsating, both axis parameters can be extract from field solution. For the three motors the results are shown in fig 3.11, 3.12, 3.13.

The parameter are variable with the rotor position, due to the adopted reference frame. So from rotor parameter value, is possible obtain the rotor position.

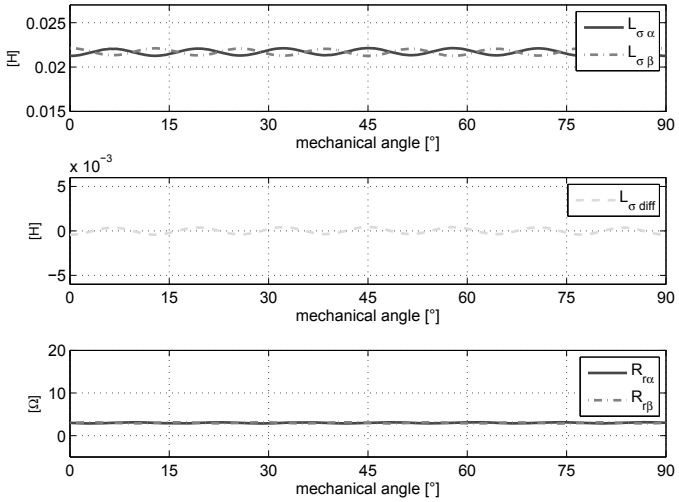

Figure 3.11: $\alpha\beta$ parameter of standard motor with rotating field

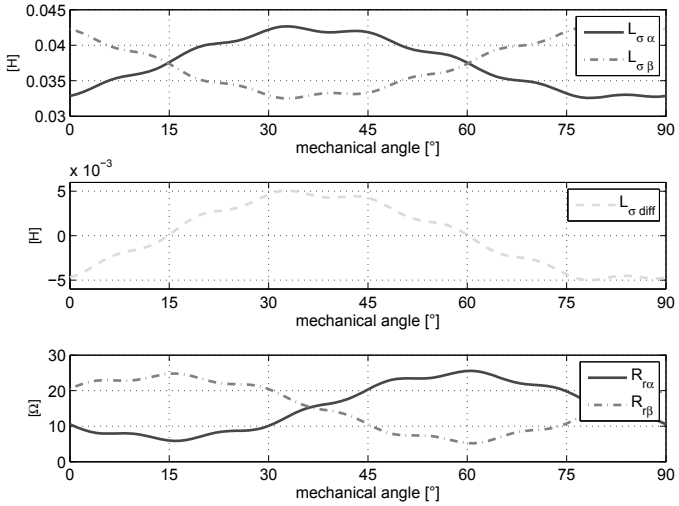

Figure 3.12: $\alpha\beta$ parameter of prototype 01 with rotating field

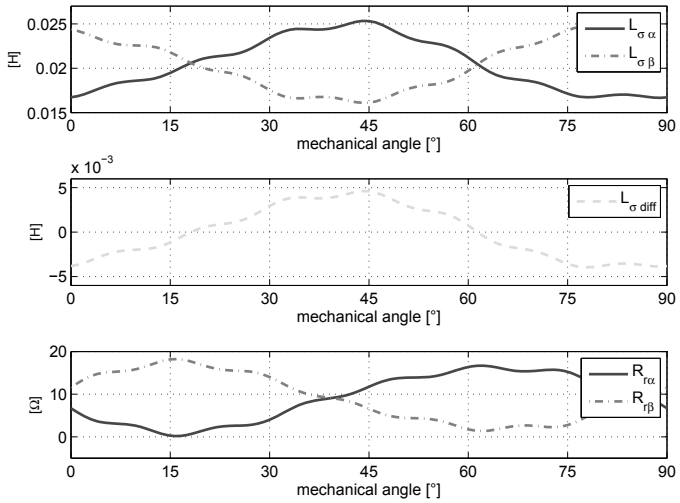

Figure 3.13: $\alpha\beta$ parameter of prototype 02 with rotating field

3.5.2 Pulsating field on β axis

For comparison between simulation and measurement, the same electrical situation has to be reproduce. The measure is made with a pulsating field on β-axis, so also the simulation have to been made with a pulsating field. If only a current on β axis is imposed and if the stator resistance is neglected, the voltages equation are:

$$\begin{cases} V\alpha = Z_{M\alpha\beta} \cdot I_\beta \\ V\beta = Z_\beta \cdot I_\beta \end{cases} \tag{3.28}$$

with $I_\alpha = 0$

Similar results are obtained if $I_\beta = 0$ and $I_\alpha \neq 0$. Is possible to use two not coupled equivalent circuit like in the dq model. Is immediate see that also the formulation for rotor parameter are the same that in the other model.

Obviously with only one pulsating field from those simulation is possible obtain only one parameter, related to the excitating axis. If one want to obtain the parameter of the other axis must be simple invert the supply. The trend of the parameter in relation with mechanical angle is the same for the two simulation. The difference is only the translation by $45deg$, due to the periodicity of the motor.

The results for the three motors are shows below in figs 3.14, 3.15, 3.16.

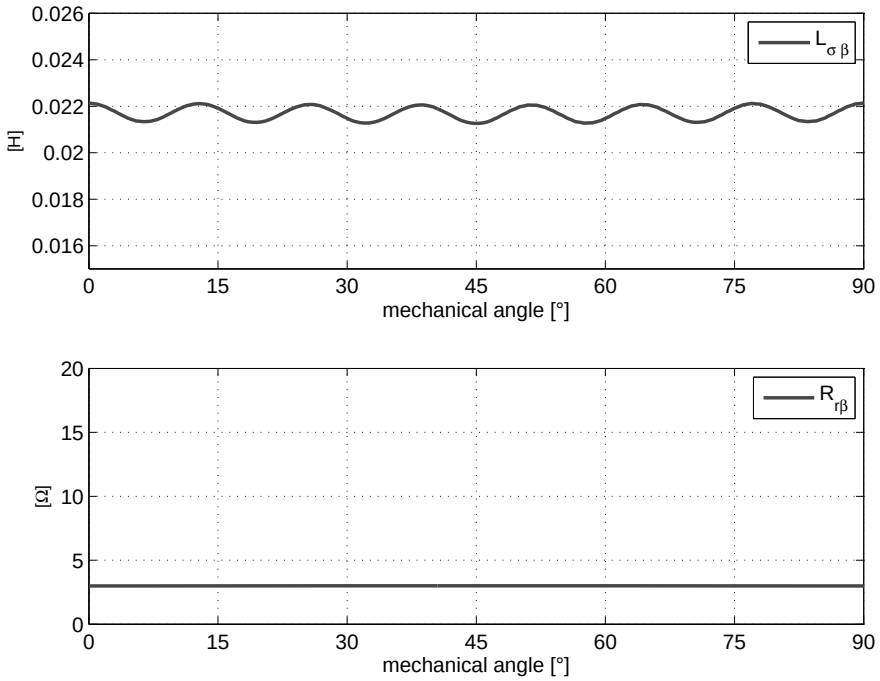

Figure 3.14: Rotor parameter on β axis with pulsating field of Standard motor

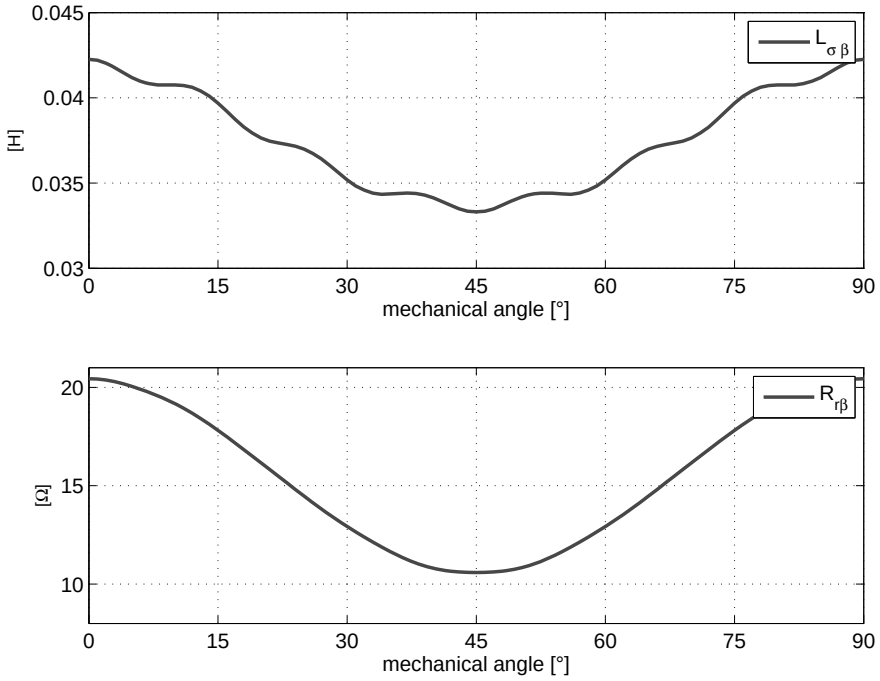

Figure 3.15: Rotor parameter on β axis with pulsating field of Prototype 01

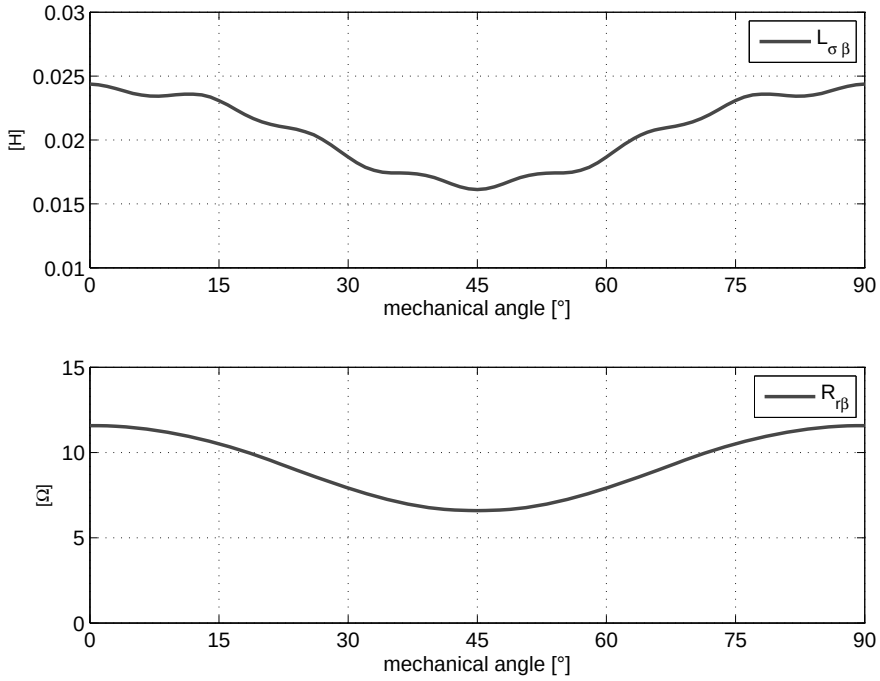

Figure 3.16: Rotor parameter on β axis with pulsating field of Prototype 02

3.6 Mutual coupling of $\alpha\beta$ rotor axis

From (3.28), and supplying the motor with pulsating current, the mutual effect between α and β axis can be obtained. Observing fig 3.17 it can be see that the mean value is zero over the period, as can be expected.

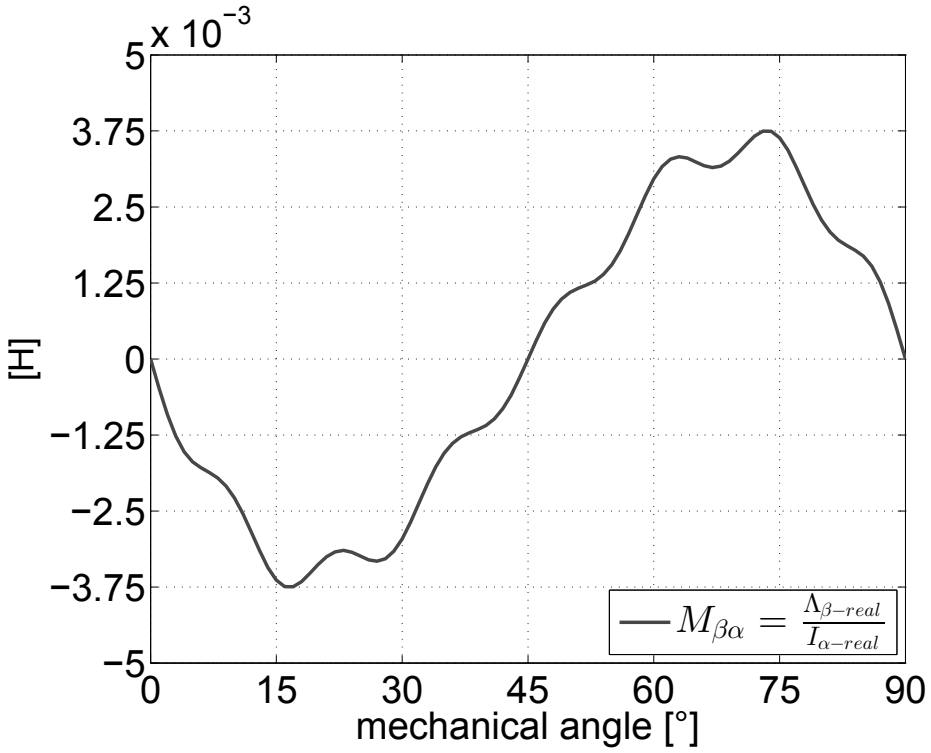

Figure 3.17: Mutual Impedance $\Lambda_{\alpha\beta}$ of prototype 02 with 19° skew

3.7 Linkage Flux with pulsating field

The Flux obtained from finite element simulation with a pulsating field is visible in fig 3.18. Only β axis current is imposed and the linkage flux present real and imaginary part of both axis. This means that there is a mutual coupling between α and β axis.

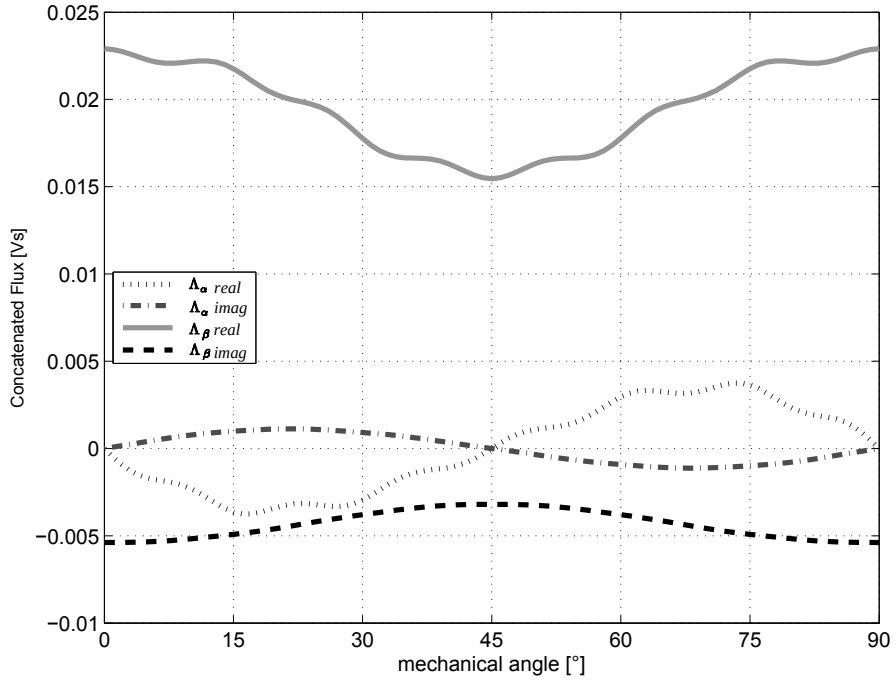

Figure 3.18: Flux Linkage of skewed prototype 02 with pulsating field on β axis

The flux can also be plotted in complex plane, in order to observe the same thing by another point of view. In fig 3.19 is shown the resultant flux with a signal injection frequency of 300 Hz.

For investigate the variation of concatenated flux with frequency in fig 3.20 and in fig 3.21 are shown the flux in the complex plane for 100 Hz and 600 Hz.

It can be note that, at low frequency, fig 3.20 the resistive effect in not very important while the inductive a large variation has. If the signal injection has an higher frequency,fig 3.21 the variation of resistive effect is almost large than the variation of inductive effect.

The same simulation is performed also for the standard motor without the anisotropy. As expected, there is any variation on the concatenated flux, and the flux of both axis is almost constant.

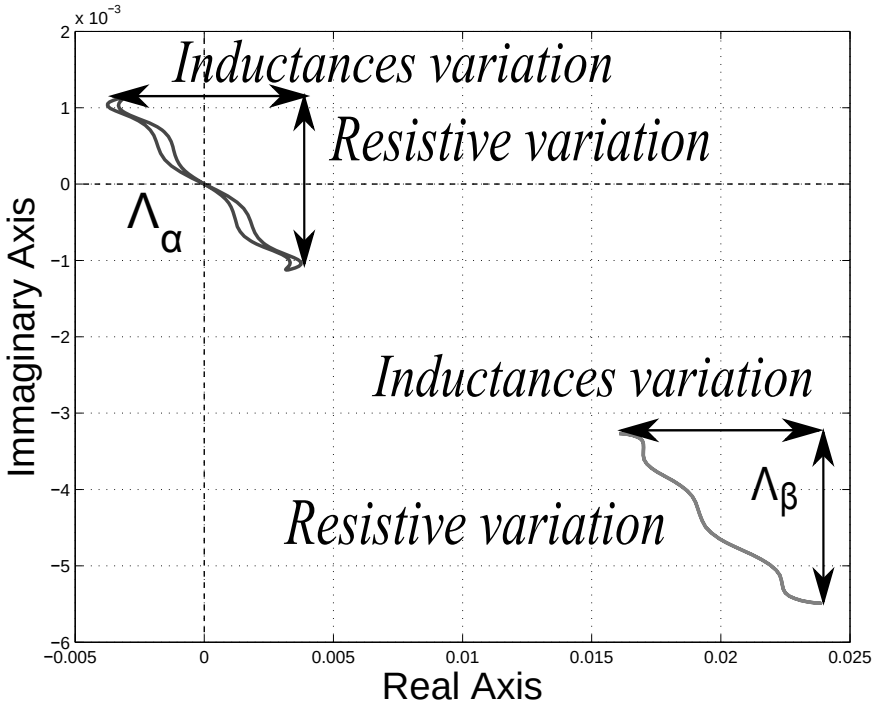

Figure 3.19: Flux Linkage on complex plane at 300 Hz

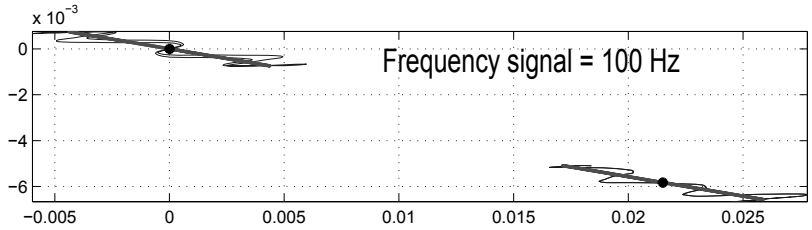

Figure 3.20: Flux Linkage on complex plane at 100 Hz

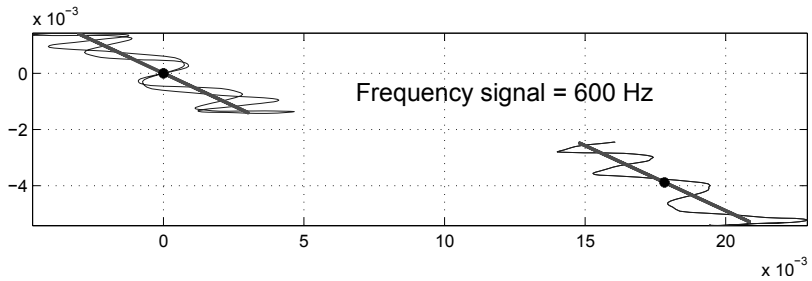

Figure 3.21: Flux Linkage on complex plane at 600 Hz

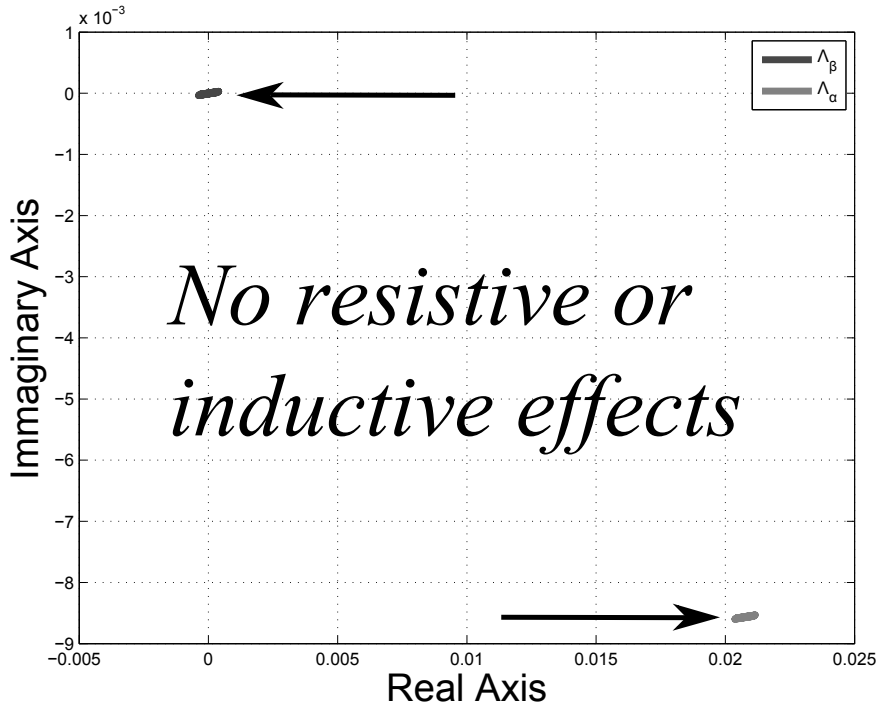

Figure 3.22: Flux Linkage for standard motor

An investigation on the impact of resistive effect for sensorless application could be in a future made. Maybe the resistive effect could be better instead of inductive for rotor position recognizing.

3.8 Frequency of signal injection

In this section, the variation of the L_{diff} parameter with the frequency is investigate. A set of simulation in the same condition with variable frequency are made. The results are then elaborated and are observable in fig 3.23.

Is clearly visible that there isn't a substantial difference on $L_{\sigma diff}$ with frequency variations. In the simulation a fixed current of $1A$ is set, and in according to the measure in 5.12 is correct that any variation is present.

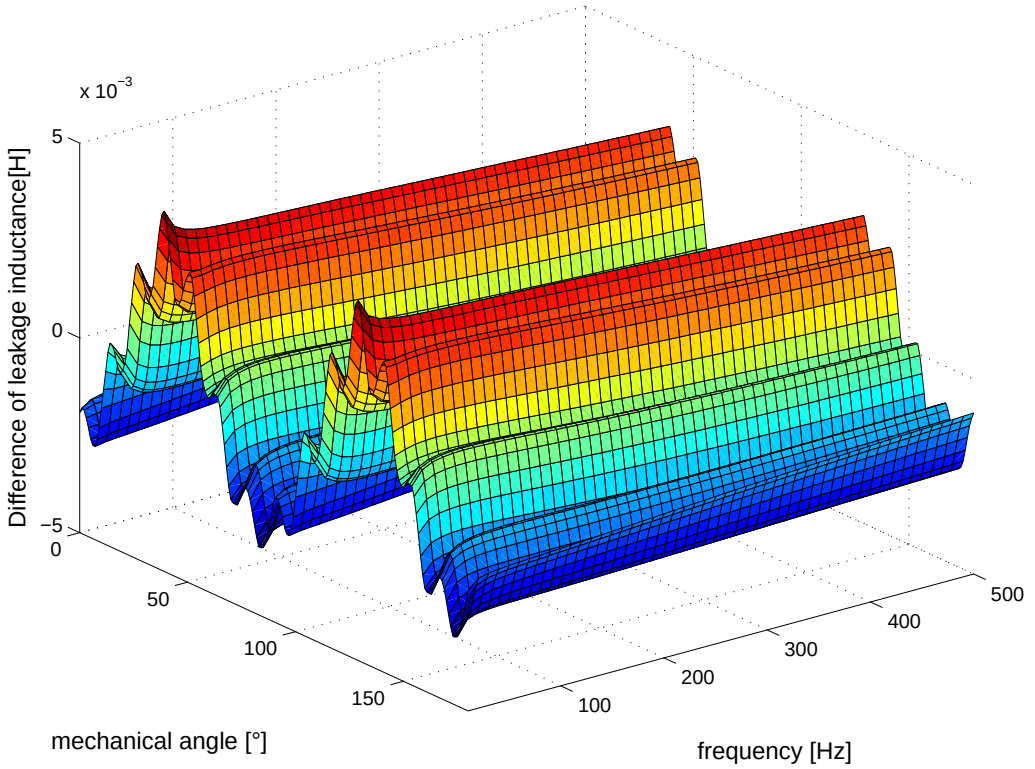

Figure 3.23: Difference inductance function of frequency and mechanical angle

3.9 Effect of the number of rotor slot on inductance matrix

3.9.1 Influence on mutual flux

The mutual flux $\Lambda_{\alpha\beta}$ derived from equation (3.24) contain only one factor modulated by $2\theta_m^e$ angle. By observing the fig 3.17 is clear that there is another factor that contributes at the mutual flux linkage. The flux is hence decomposed with fourier transformation, and the result for skewed motor and non-skewed motor can be observed in fig 3.24.

On the non-skewed motor, the influence of the 7th harmonic present a very important value, but in the skewed motor it is very little.

Some simulations with different rotor slot number are done in order investigate how the rotor slot number (Qr) influence the mutual flux. The simulations are visible in fig 3.25.

The conclusion is that the mutual flux is strongly influenced by the num-

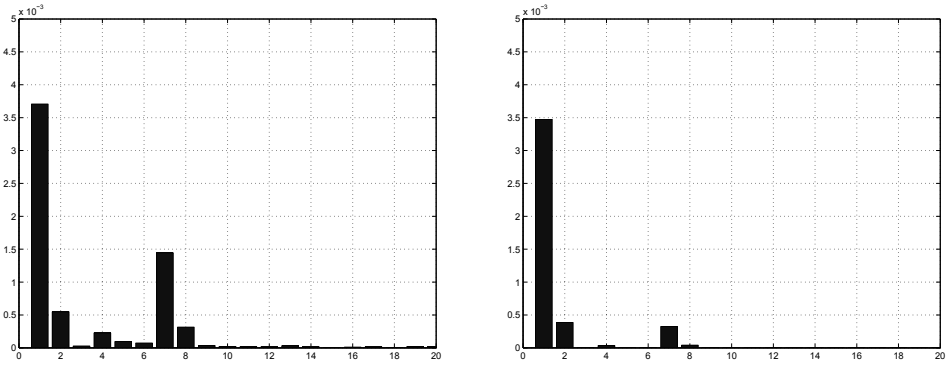

Figure 3.24: Mutual Flux in non-skewed and skewed 28 slot Prototype 02

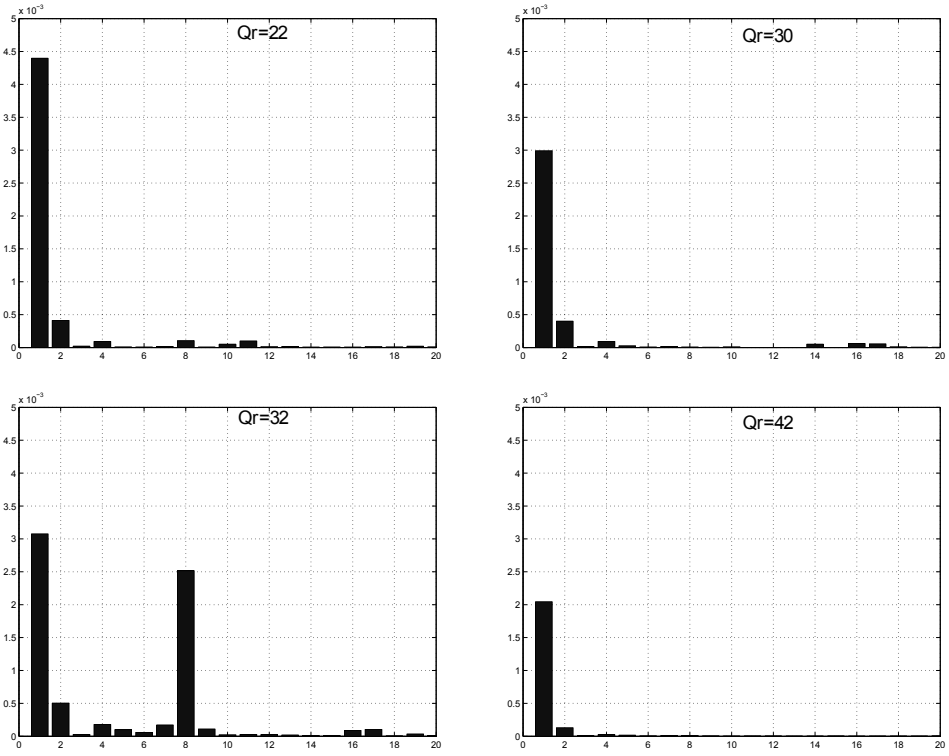

Figure 3.25: Mutual Flux in non-skewed slot Prototypes

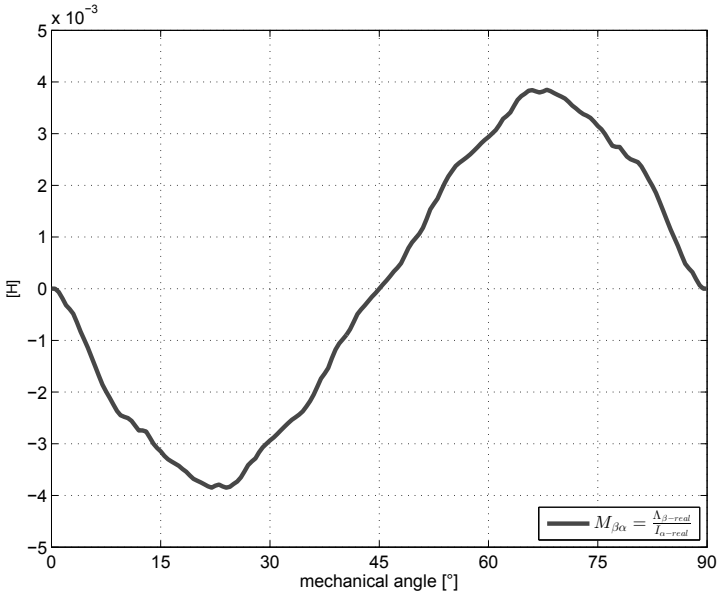

Figure 3.26: Mutual Impedance with current point and iron stator slot of motor 02

ber of rotor slot. Is simple observe that, if the number of rotor slot:

$$\frac{Q_R}{2p} = integer$$

an harmonic of order $h = \frac{Q_R}{2p}$ is present. If $\frac{Q_R}{2p}$ is not an integer, the flux harmonics are highly reduced. The influence of these harmonics on mutual flux, can then be neglected.

3.9.2 Current point simulations

To investigate if the influence on mutual coupling, is also due to the stator slot, a simulation with current point is made. The air gap induction is not created with stator winding, but imposing the current in points placed in the middle of air gap. This allow us also to use the stator only also for re-closing the magnetic field.

First, the stator slots are filled with iron to observe how copper winding influence the mutual flux. The result is show in fig 3.26.

The mutual impedance has almost exclusively the first harmonic and the high level harmonics aren't present.

Second, the stator slot are filled with copper, like in the real motor. The air gap induction is also made with current point and in the stator any current

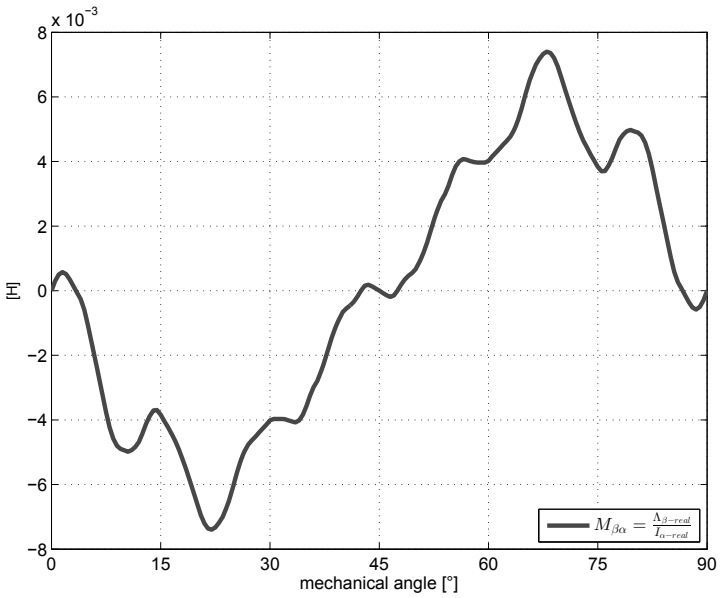

Figure 3.27: Mutual Impedance with current point and copper stator slot of motor 02

is present. The result is in fig 3.27.

The copper stator slots influence the mutual flux very much. It can be seen that not only the first harmonic is present, but also the $\frac{Q_R}{2p}$ harmonic.

The conclusion is that is better use motors with number of slot per pole not integer, in order to break down the superior order harmonic.

3.9.3 Skewing of the rotor

The real motor has a skewed rotor. Is necessary therefore implement the same situation also in the finite element analysis, to make a valid comparatione of the results.

To simulate the skew, in this case $\approx$ 19 degree, a series of stationary simulation are performed. The total simulations are 19 for each step of the rotor, 9 before the effective position and 9 after the actual position of the rotor. For each angular position, the results of this simulation is averaged and the mean value is referred at the actual position of the rotor.

3.10 Investigation about measure and simulation differences

In this section the difference between simulated and measured parameters for prototype 02 are investigated. To understand why the measure (explained in chapter 7) don't match the simulation, some constructive problem are hypothesized.

In particular, in fig 3.28 is worth noticing that the greatest problem is on the d axis of the rotor. Indeed at 45 $degree$, the measured parameters are comparable with the simulated one.

Starting from this consideration and looking only at the prototype 02, is clear that the slot opening width on d-axis is very small and maybe the die-casted aluminium cannot enter and fill entirely the slot opening. In order to explanation the difference, some simulations are performed:

- only the thin opening slot on d axis without aluminium
- three slot openings around d axis without aluminium
- the thin opening slot on d axis filled with iron and other with aluminium

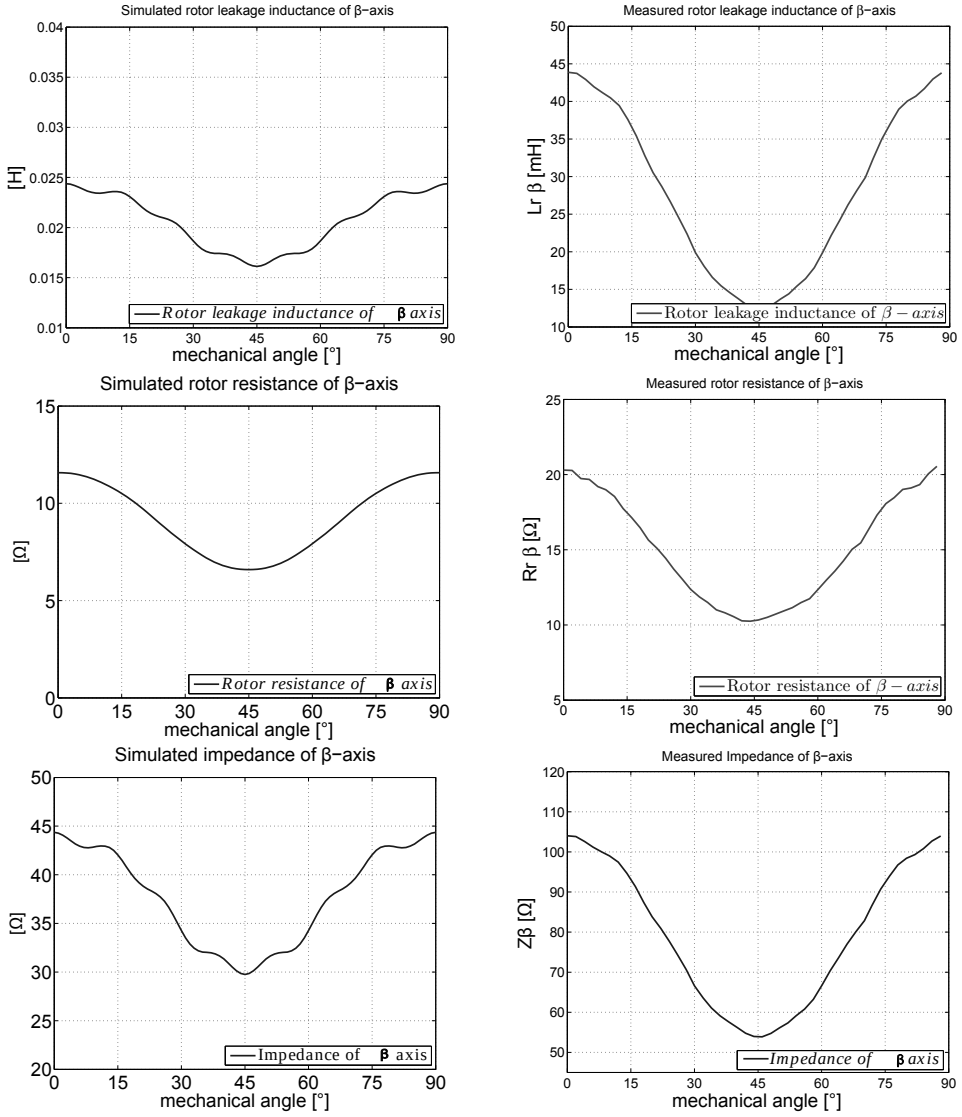

Figure 3.28: Difference between simulation and measure

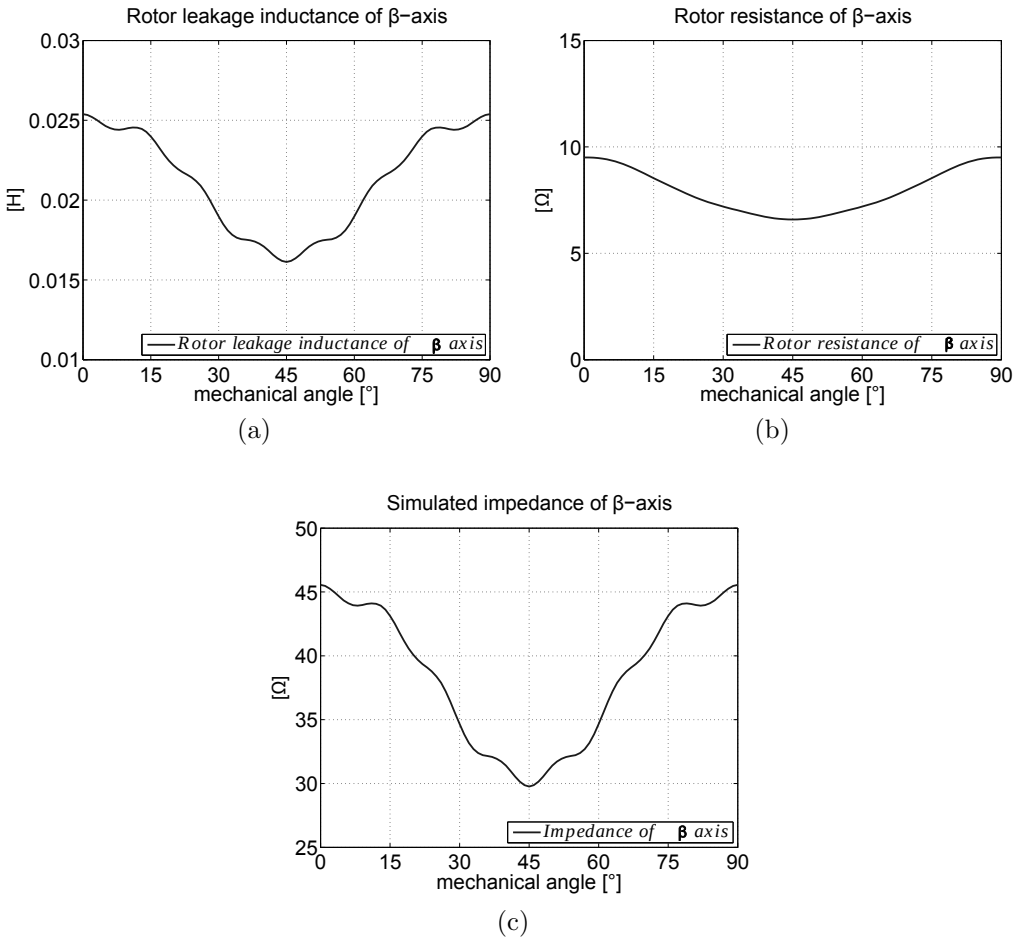

Figure 3.29: Parameter of β axis with the thin slots not filled by aluminium

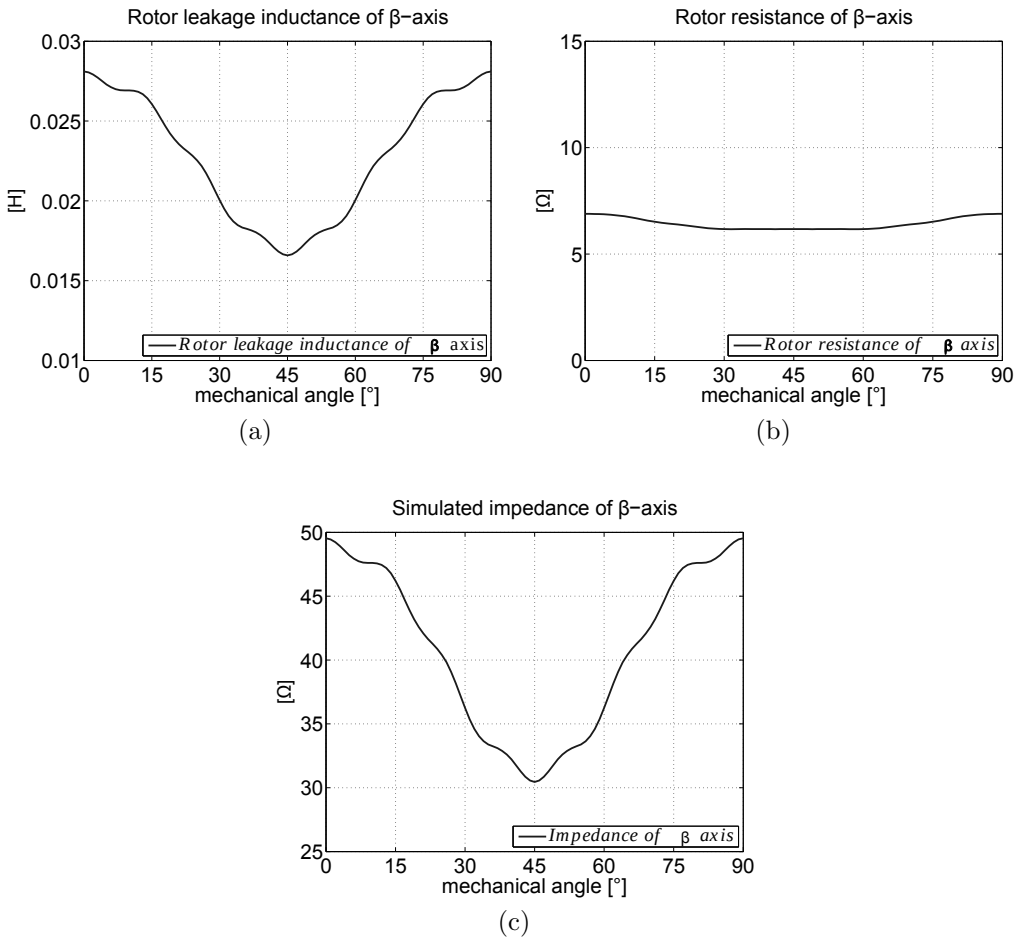

Figure 3.30: Parameter of β axis with three slot around d axis not filled by aluminium

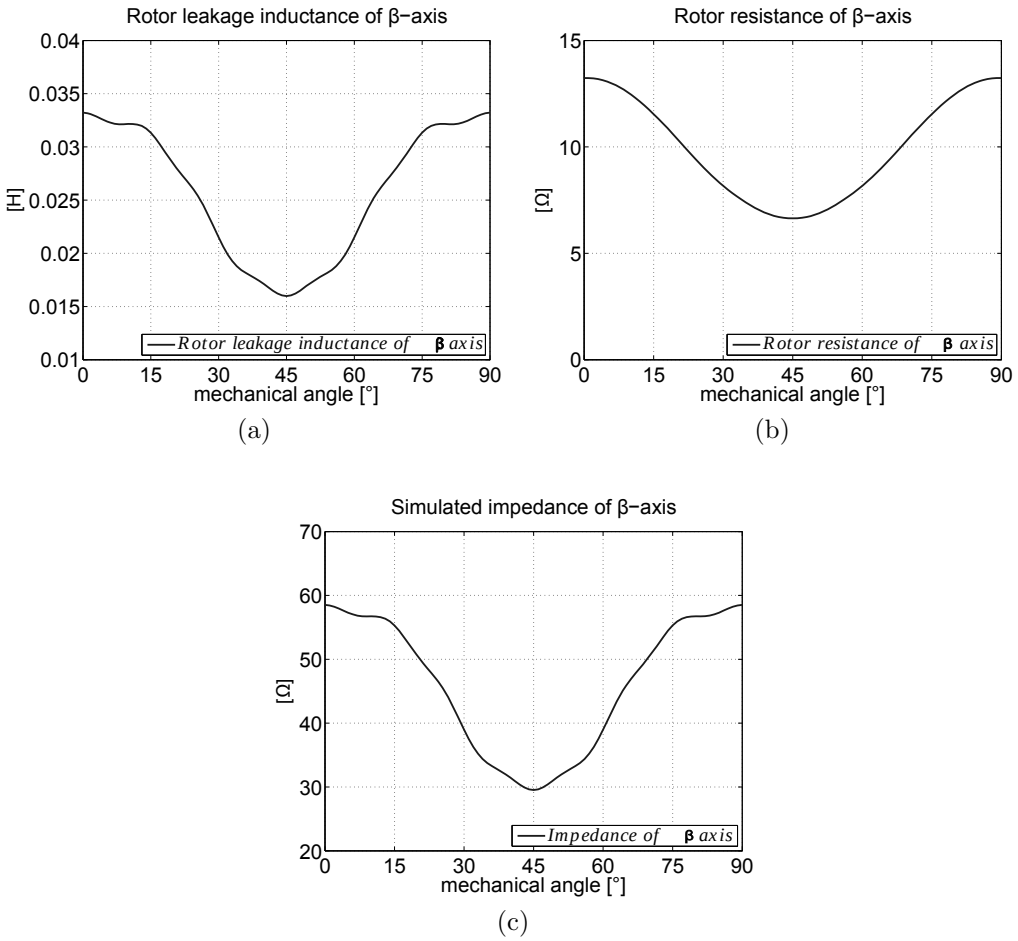

Figure 3.31: Parameter of β axis with the thin slot fill by iron

Chapter 4

Optimization

This chapter examines the potential of the optimization algorithms, to investigate deeply the possibilities of increasing the sensorless capability of the induction motor with the decided geometry. The optimizer also takes in account the mean torque of the motor, in order to consider the maximization of both objectives.

4.1 General information

4.1.1 Introduction

Optimization problems are common in many disciplines and various domains. In optimization problems, solutions which are optimal or near-optimal with respect to some goals are to find. Often, the solution process is separated into different steps which are executed one after the other.

Commonly used steps are recognizing and defining problems, constructing and solving models, evaluating and implementing solutions.

Differential evolutionary non dominated sorting algorithm

The type of algorithm used is a differential evolution (DE). This is a method that optimizes a problem by iteratively trying to improve a candidate solution with regard to a given measure of quality. DE is used for multidimensional real-valued functions but does not use the gradient of the problem being optimized, which means DE does not require for the optimization problem to be differentiable as is required by classic optimization methods such as gradient descent and quasi-newton methods.

DE optimizes a problem by maintaining a population of candidate solutions and creating new candidate solutions by combining existing ones according to its simple formulae, and then keeping whichever candidate solution has the best score or fitness on the optimization problem at hand. In this way the optimization problem is treated as a black box that merely provides a measure of quality given a candidate solution and the gradient is therefore not needed.

4.1.2 Optimization algorithm test function

For testing the real convergence of the algorithm, some test function have been used. In particular the test function take in consideration are:

- Poloni's (2 objective)
- Kursawe (2 objective)

For checking the optimization algorithm, the parameter are:

- Population = 20
- Archive = 200
- Generation = 500

Poloni's

Poloni's is a 2 objective, 2 variable test function. The function to be minimized are:

$$\begin{cases} f_1(x,y) = [1 + (A_1 - B_1(x,y))^2 + (A_2 - B_2(x,y))^2] \\ f_2(x,y) = (x+3)^2 + (y+1)^2 \end{cases} \tag{4.1}$$

where:

$$\begin{cases} A_1 = 0.5sin(1) - 2cos(1) + sin(2) - 1.5cos(2) \\ A_2 = 1.5sin(1) - cos(1) + 2sin(2) - 0.5cos(2) \\ B_1(x,y) = 0.5sin(x) - 2cos(x) + sin(y) - 1.5cos(y) \\ B_2(x,y) = 1.5sin(x) - cos(x) + 2sin(y) - 0.5cos(y) \end{cases} \tag{4.2}$$

and the variable constrain:

$$-\pi \leq x, y \leq \pi$$

The literature and the simulation resultant front are reported in fig 4.1 and in fig 4.2. It can be see that there is a good match between the two curves.

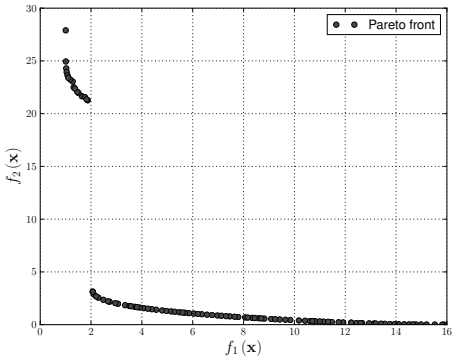

Figure 4.1: Literature Front

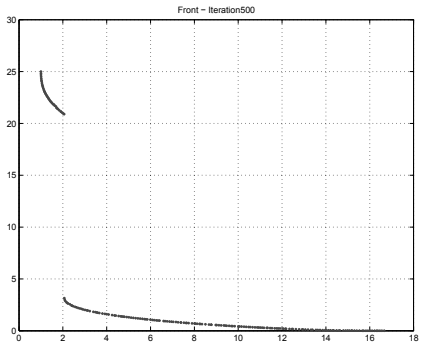

Figure 4.2: Simulated Front

Kursawe

Kursawe is a 2 objective, 3 variable test function. The function to be minimized are:

$$\begin{cases} f_1(x) = \Sigma_{i=1}^{2} \left[-10e^{(-0.2\sqrt{x_i^2 + x_{i+1}})} \right] \\ f_2(x) = \Sigma_{i=1}^{3} \left[|x_i|^{0.8} + 5sin(x_i^3) \right] \end{cases} \tag{4.3}$$

and the variable constrain:

$$-5 \leq x_i \leq 5, 1 \leq i \leq 3$$

The literature and the simulation resultant front of kursawe test function are reported in fig 4.3 and fig 4.4. It can be see that there is a good match between the two curves.

The conclusion of this set of simulation is that the algorithm work very well and is good for starting the Induction Motor Optimization. Now is the algorithm could be coupled with a finite element software that evaluate the motor objective.

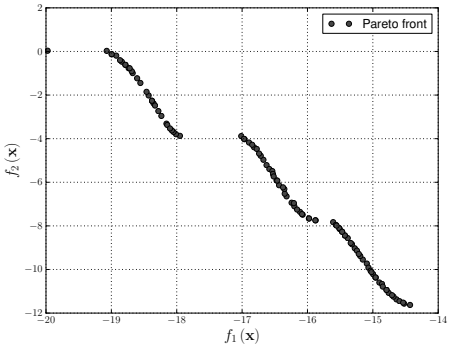

Figure 4.3: Literature Front

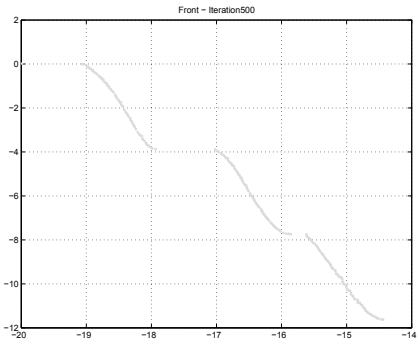

Figure 4.4: Simulated Front

4.2 Optimization Process 36/28

4.2.1 Finite Element Objective evaluation

For objective evaluation, Finite Element are used, so the optimization algorithm has to call external program and function. The language selected for this optimization algorithm is for the great flexibility and simplicity Matlab. However the main script that we use with fem software are write in .lua. A translation of the code in Matlab language was required.

The steps for the optimization are:

- Electric motor drawing
- Objective 1: *dq* high frequency rotor parameter
- Objective 2: Mean Torque computation (with Foc)
- Evaluation of the objective by optimization script

The flowchart for the optimization process can be see in fig 4.5.

The variable of the optimization are, for question of thesis time, only the rotor open slot parameters, and in separated simulations the rotor slot number. The range in that the variable can space are visible in Table 4.1.

The parameter $wsor_d$ and $wsor_q$ are bigger respect of the constructed prototype, in order to avoid possibly problems in die-casting process.

4.2.2 Speed-up optimization process

In optimization process, all the objective are evaluated for all individual of the population. Due to the high computation time, a smart thing is make the simulation not in all domain, but search a sub-domain in which the objective are more significant.

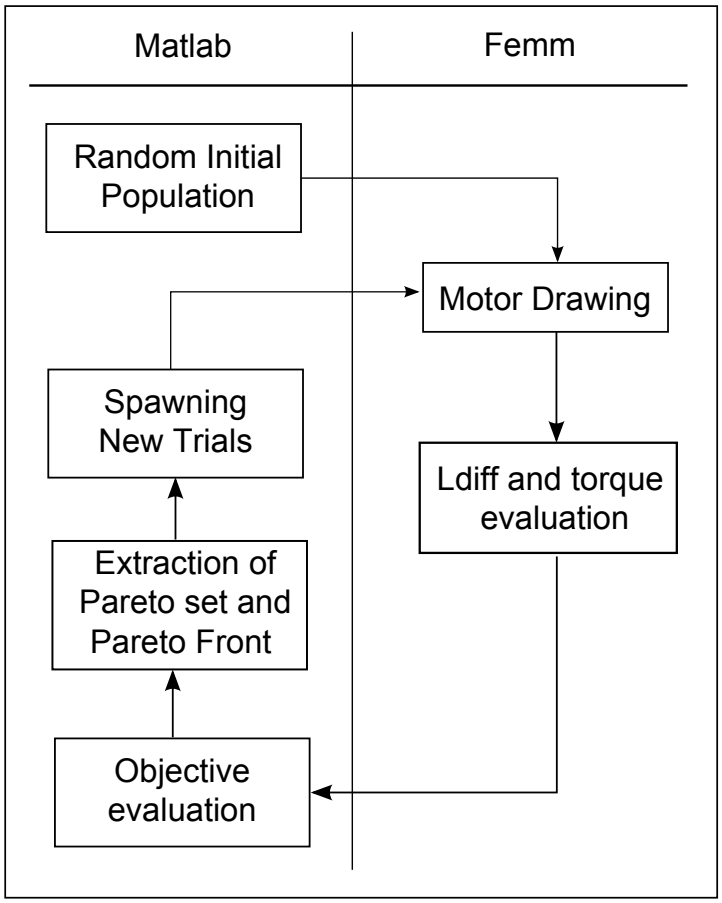

Figure 4.5: Logical scheme about how the algorithm works

Table 4.1: Optimization parameter

parameter	min [mm]	max [mm]
$hsor_d$	0.5	5.0
$hsor_q$	0.5	3.0
$wsor_d$	0.7	3.5
$wsor_q$	0.7	3.5

Leakage difference inductance

The leakage difference inductance at high frequency of the IM, is evaluated in dq reference frame. As seen in fig 3.8, fig 3.9, fig 3.7, the two axis inductance are quite constant. There is a little ripple, so a mean over some position is required. The leakage inductance is calculated from 0 to 15 degree, at 3 degree step. Then a mean of the value us made and the mean of the difference leakage inductance is stored.

Mean torque

After the simulation with the Foc algorithm, the torque calculated with three formulation is observed. At $\Theta_m = 0deg$ the calculated torque is approximately equal to the mean torque so it's possible to do only 1 FE FOC simulation. It's important remember that for each rotor position the FOC script run the FE analysis three or four times, because it try to impose the rotor current in order to obtain $\lambda_{rq} = 0$.

4.2.3 Optimization result of 36/28

The same code used for objective evaluation has been run over the three studied motors. The result are in Table 4.2.

Table 4.2: Results of studied motors

motor	$hsor_d$ [mm]	$hsor_q$ [mm]	$wsor_d$ [mm]	$wsor_q$ [mm]	Ldiff [H]	Torque [Nm]
Prototype 01	4.0	0.95	0.5	0.5	0.0043	12.1
Prototype 02	4.0	0.95	0.5	3.0	0.0039	12.0
Standard	0.5	0.50	1.0	1.0	0.0003	12.7

Is worth noticing that the major influence over $Ldiff$ is due to $wsor_d$ and $wsor_q$. After prototype construction problems identification, the very thin slot on d and q axis could be the main problem of simulations and measures results. Hence, for the optimization problem, those variables are limited to 0.7.

In fig 4.6 the Pareto front of 28 slot rotor can be see.

It can be see a good distribution of the individual in the front, thanks to the good combination of individual across the generation. It's possibly also to see how the two objective are conflicting each others.

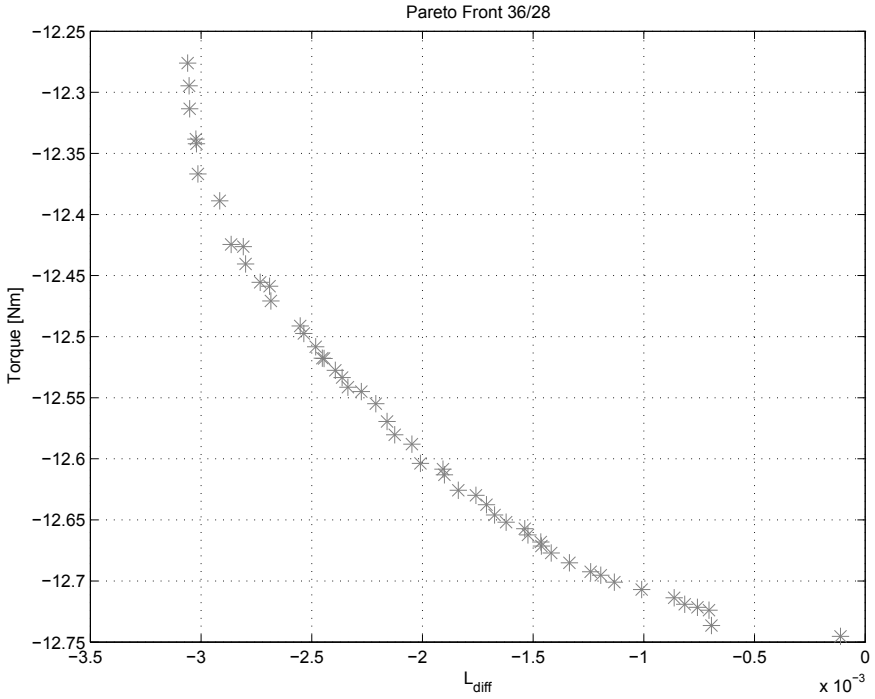

Figure 4.6: Pareto front of 28 rotor slot motor

4.3 Different number of rotor slot

It's interesting now test how can the number of rotor slot influence the sensorless capability of the machine. For this investigation the optimization algorithm, over machine with rotor slot different than 28 is been running. The 36/28 FOC code has to be changed, because the slot matrix of the rotor has a different dimension.

The parameters choose for this optimization are:

- Population = 20
- Archive = 50
- Generation = almost 200

For select the number of rotor slot to be adopt, is useful use the table reported in [12] at pg.336. Only the suggested number of rotor slot are taken in consideration: 22, 26, 30, 46.

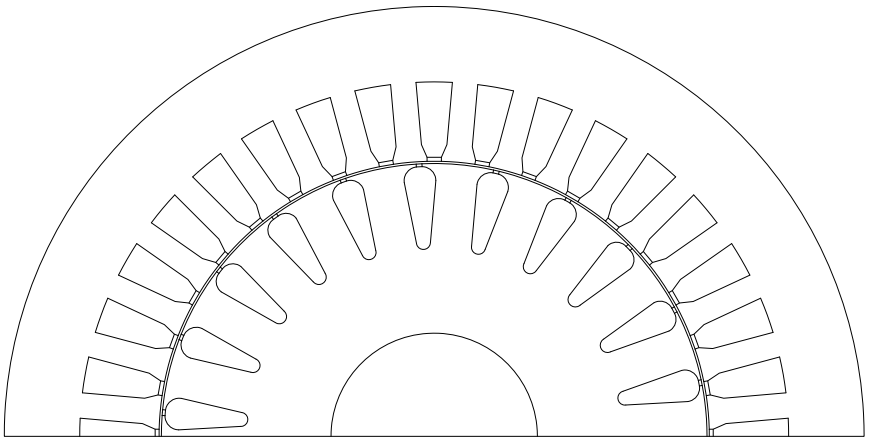

Figure 4.7: Section of 22 rotor slot motor

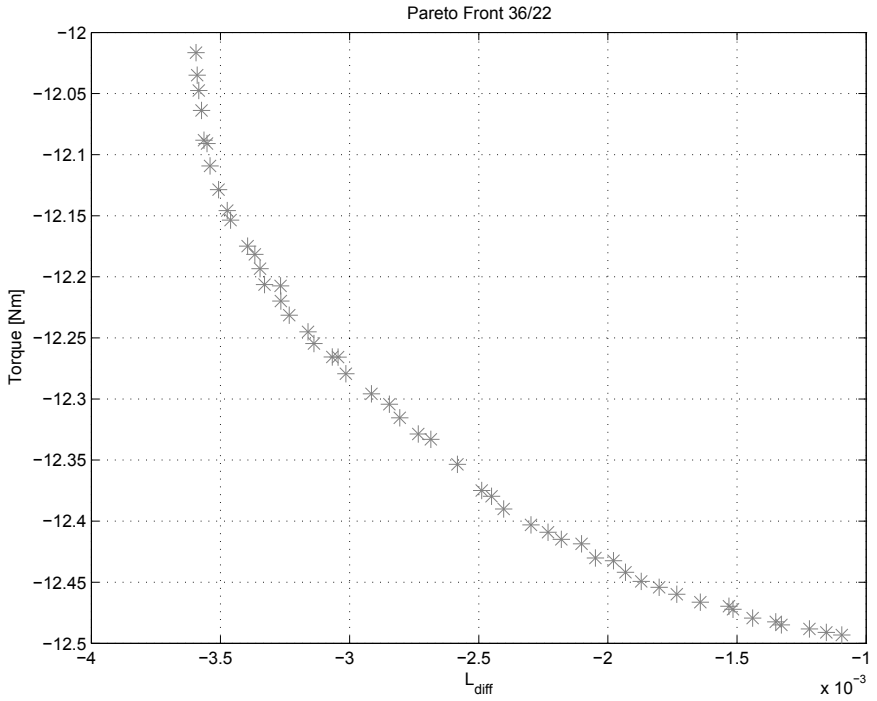

Figure 4.8: Pareto front of 22 rotor slot motor

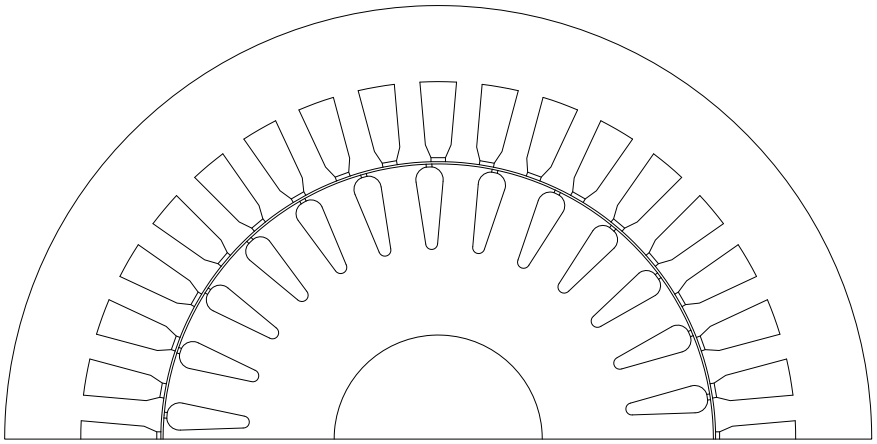

Figure 4.9: Section of 26 rotor slot motor

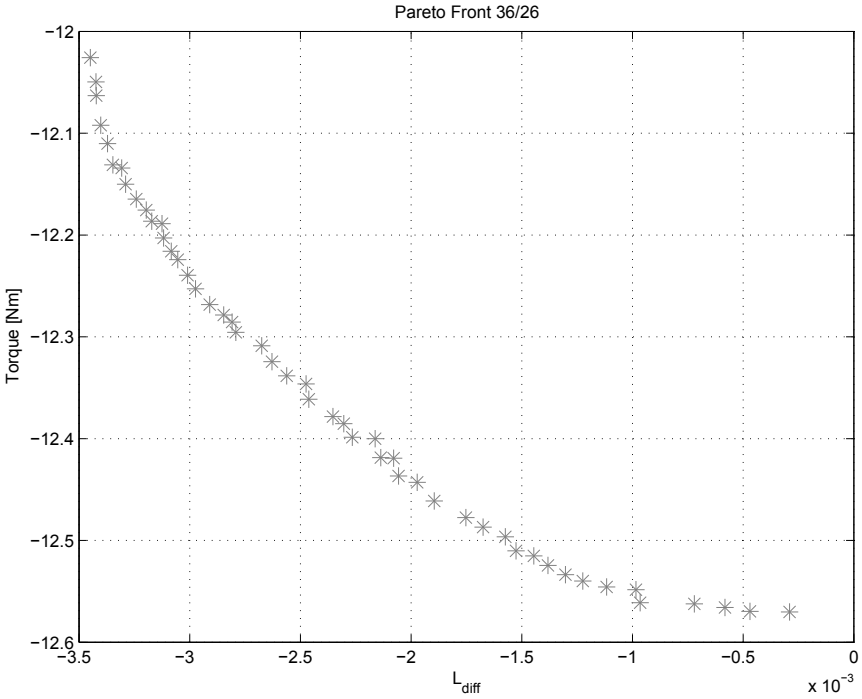

Figure 4.10: Pareto front of 26 rotor slot motor

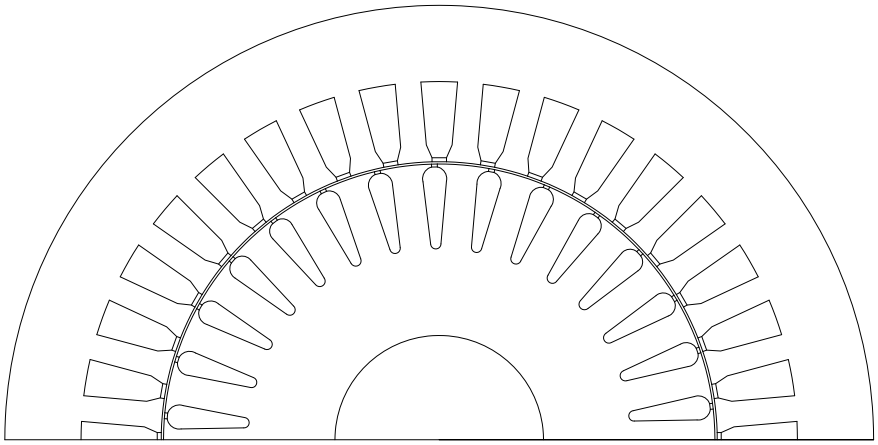

Figure 4.11: Section of 30 rotor slot motor

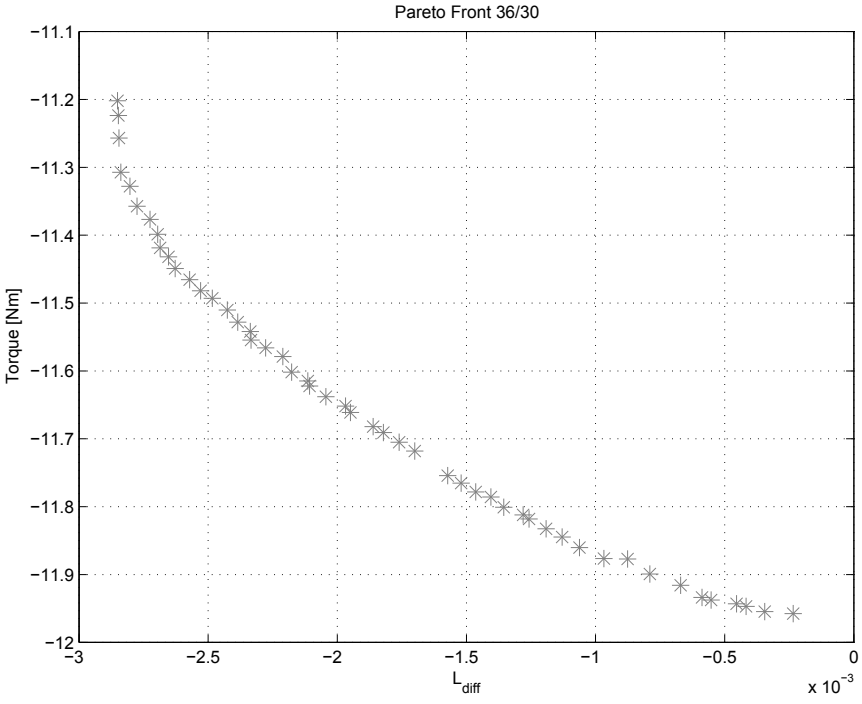

Figure 4.12: Pareto front of 30 rotor slot motor

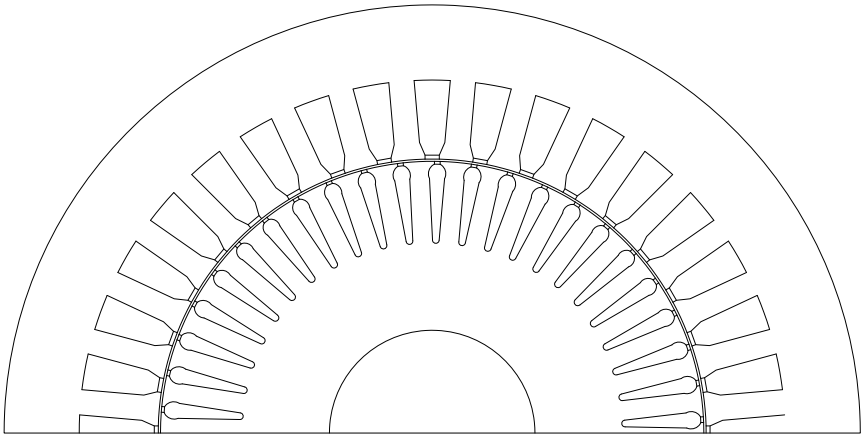

Figure 4.13: Section of 46 rotor slot motor

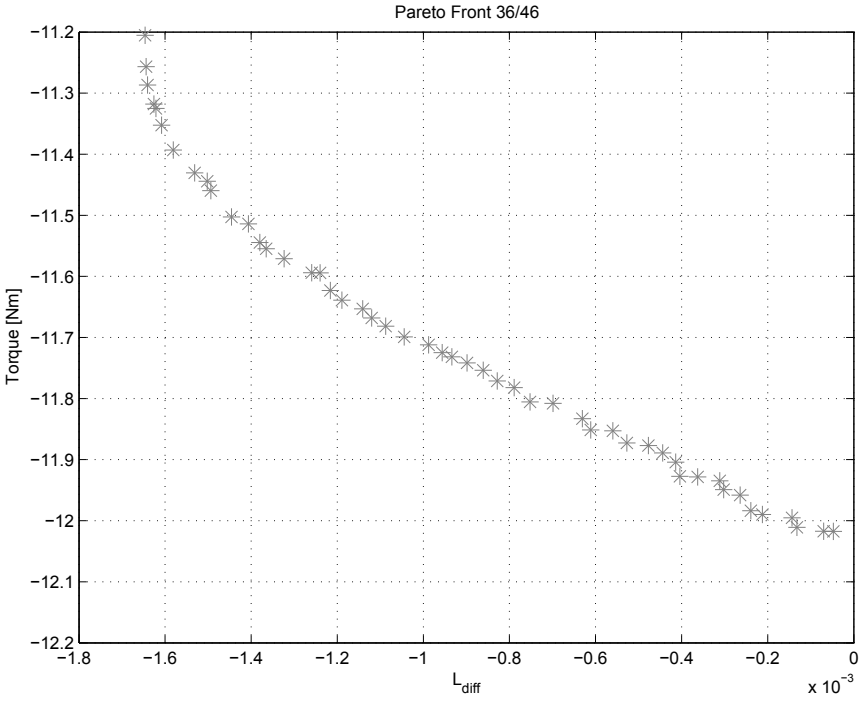

Figure 4.14: Pareto front of 46 rotor slot motor

4.3.1 Optimization Conclusion

The number of rotor slots don't influence the difference inductance of two-axis very much. For 22,26,30 slot rotors the $Ldiff$ value is almost the same. For 46 rotor slot indeed the $Ldiff$ present lower value.

There is also a problem with the number of rotor slot. The number of rotor slots per pole per axis:

$$\kappa = \frac{Q_r}{2p}$$

should be integer.

If this condition is verified, the position of q-axis is superimpose on a rotor slot or is in the middle of two slots. In case of Qr=22,26,30,46 the κ factor don't accord to previous condition.

4.4 Optimized motor

The prototype proposed for a new case of study is indeed a 36/28. The motor choice are circled in fig 4.15, and the objective evaluation are reported in Table 4.3

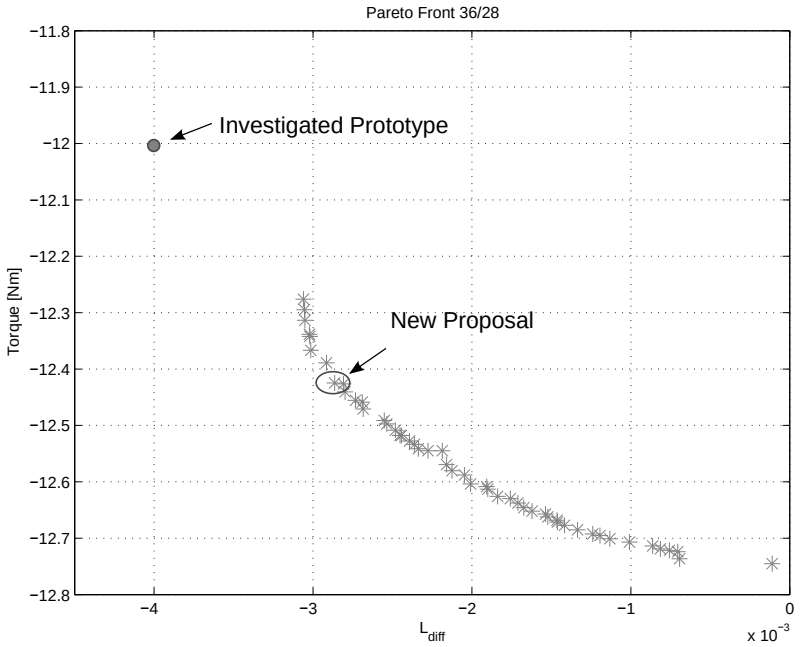

Figure 4.15: Choice of new prototypes

Table 4.3: Proposal for new prototype

motor	$hsor_d$ [mm]	$hsor_q$ [mm]	$wsor_d$ [mm]	$wsor_q$ [mm]
New Proposal	3.14	0.36	0.71	1.19

Table 4.4: Results for new prototype

	$Meantorque\,[Nm]$	$Ldif\,[H]$
New Proposal	12.4	0.003

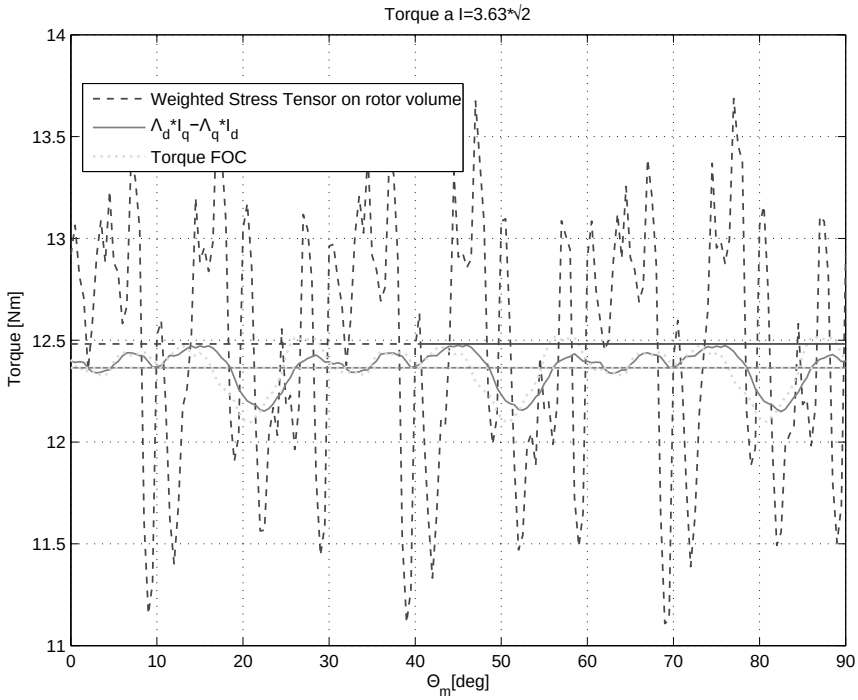

Figure 4.16: Torque of new proposal

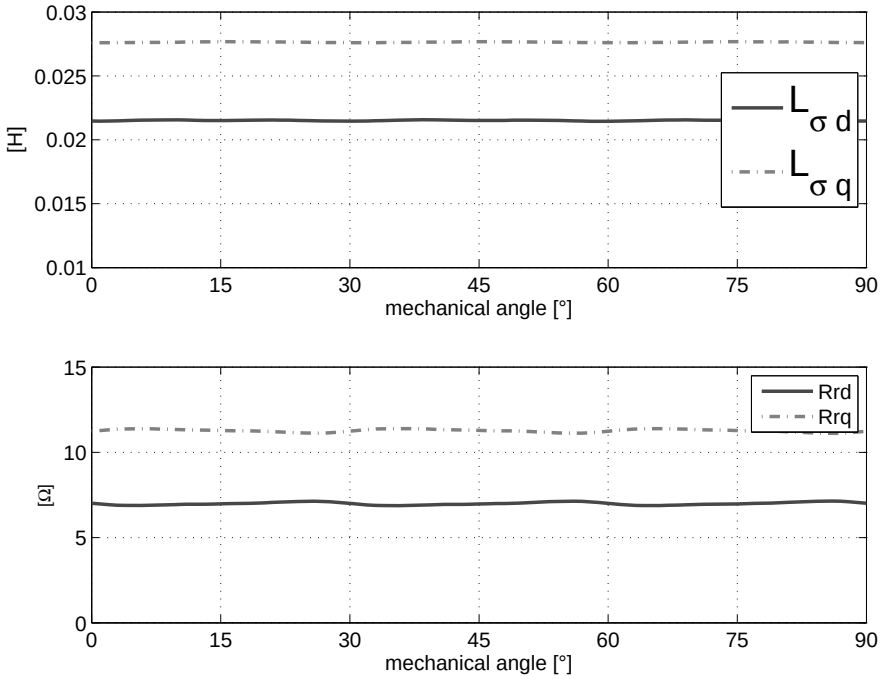

Figure 4.17: Rotor Parameter of new proposal

Chapter 5

Motor Parameter Measurement

This chapter would explain the measurement procedures used for characterization of induction motor prototypes. First the classical measure procedures and then the measure made for retrieve the rotor parameter at high frequency are explained. The high frequency parameter can be used to implement a sensorless field oriented control of the induction motor.

5.1 Classical Measurement

5.1.1 No-load Test

The no-load test is the classical measure used to obtain:

- mechanical losses
- stator resistance
- magnetizing inductance
- resistance R_0 (iron losses)

The mechanical losses are obtain with some measures (Table 5.1) at decreasing voltage at constant speed. When the speed decrease the measure is stopped and a data interpolation is made. The power at zero voltage is the mechanical loss (fig 5.1).

In Table 5.4 are itemized the obtained data by no-load test for the three induction motor.

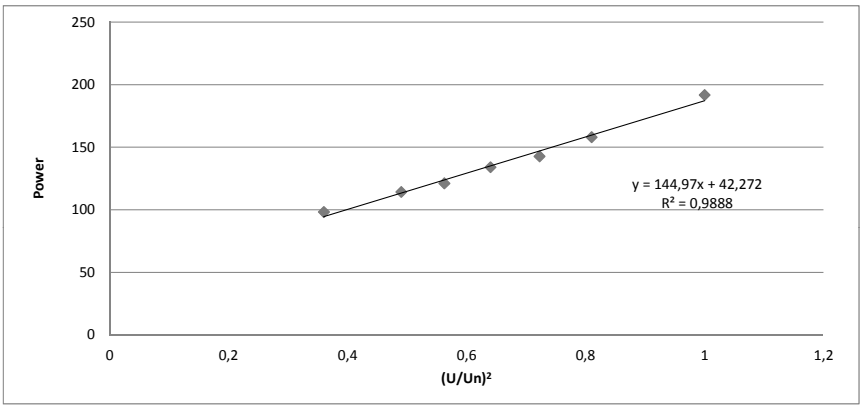

Figure 5.1: Mechanical loss of standard motor

Table 5.1: Decreasing Voltage No-Load Test of Standard Motor

$Voltage[V]$	$P_0[V]$	$I_0[A]$	$Speed[rpm]$
400	191.8	2.37	1497.0
360	158.1	1.95	1497.0
340	142.8	1.77	1497.0
320	134.1	1.64	1497.0
300	121.2	1.52	1497.0
280	114.3	1.40	1496.4
260	—	—	—
240	98.3	1.20	1495.8
Mechanical Losses			42 W

Table 5.2: Decreasing Voltage No-Load Test of Motor 01

$Voltage[V]$	$P_0[V]$	$I_0[A]$	$Speed[rpm]$
400	175.5	2.46	1497.6
360	143.9	1.97	1497.3
340	130.9	1.84	1497.0
320	120.4	1.67	1497.0
300	111.5	1.55	1496.4
280	103.6	1.44	1496.3
260	96.2	1.31	1496.2
240	89.2	1.20	1495.2
Mechanical Losses			38 W

Table 5.3: Decreasing Voltage No-Load Test of Motor 02

$Voltage[V]$	$P_0[V]$	$I_0[A]$	$Speed[rpm]$
400	200	2.56	1497.4
360	164.2	2.09	1497.4
340	151.9	1.91	1497.0
320	140	1.85	1497.0
300	132.2	1.60	1496.0
280	128.3	1.52	1496.0
260	110	1.42	1496.0
240	102	1.28	1495.5
Mechanical Losses			50 W

Table 5.4: No-Load Data

	$Vn\,[V]$	$I_0\,[A]$	$P_0\,[W]$	$P_{mecc}\,[W]$
Standard	400	2.37	191.8	42
#01	400	2.47	175.5	38
#02	400	2.56	200.0	50

5.1.2 Motor test at 50 Hz without rotor

For this test the rotor is pulled out and then a Voltamperometric measure at 50 Hz on one phase circuit is made. The result are shown in Table 5.5 The test was made for the Stator of Motor 01 and for the other motor is assumed that the parameter has the same value.

Table 5.5: Pulled Out Rotor Test

$V\,[V]$	$I\,[A]$	$P\,[W]$	$S\,[VA]$	$Q\,[VAr]$	$cos\varphi$	deg	$R_s\,[\Omega]$	$X_s\,[\Omega]$
13.5	2.44	19.6	32.9	26.5	0.59	53	3.29	4.45

The Stator leakage inductance is then equal to:

$$L_{\sigma s} = \frac{X_s}{2 \cdot \pi \cdot 50} = 14.16\,mH$$

The analytical prediction of the stator leakage inductance is $11.5\,mH$ and the femm result is $14.1\,mH$. The three value are comparable.

Figure 5.2: Stator and rotor

5.1.3 Locked-rotor Test

The locked rotor test is the classical measure used to obtain:

- rotor resistance
- rotor leakage inductance

The rotor is locked in one position and then with a low voltage power supply, the current is set at the nominal value. In this condition the measure of the power absorbed by the motor is done and the data for the three induction motor are itemized in Table 5.6.

Table 5.6: Locked Rotor Parameter

	$V_{cc}\,[V]$	$I_{cc}\,[A]$	$P_{cc}\,[W]$	$S_{cc}\,[VA]$	$Q_{cc}\,[VAr]$	$cos\varphi_{cc}$	deg
Standard	60.87	3.418	217.6	361	285.5	0.60	52.9
#01	110.97	3.424	281.6	658	624.1	0.43	64.7
#02	69.54	3.452	234.8	415	333.7	0.57	55.6

5.1.4 Summarize of the data of the three Motor

The Formulation and the equivalent circuit used in for calculate the parameter are reported below.

For no load test the equivalent circuit is 5.1

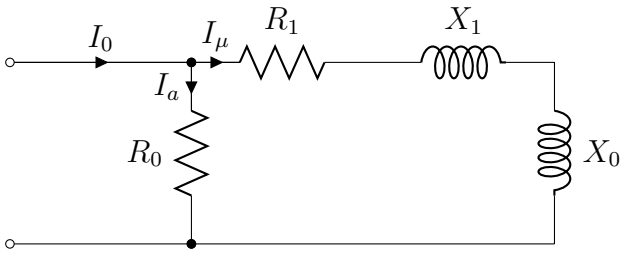

Circuit 5.1: IM No Load circuit

The procedure used for obtain the motor data are:

$$P_{fe} = P_0 - P_{mecc} - 3 \cdot P_{js} \tag{5.1}$$

$$I_a = P_{fe}\sqrt{3} \cdot U_N \tag{5.2}$$

$$R_0 = \frac{U_N}{\sqrt{3} \cdot I_a} \tag{5.3}$$

$$I_\mu = \sqrt{I_0^2 - I_a^2} \tag{5.4}$$

$$\dot{Z_{TOT}} = R_1 + j(X_1 + X_0) \cong j(X_1 + X_0) \tag{5.5}$$

$$U_N = Z_{TOT} \cdot \sqrt{3} \cdot I_\mu \tag{5.6}$$

$$(X_0 + X_1) = \frac{U_N}{\sqrt{3} \cdot I_\mu} \tag{5.7}$$

and from the 5.7 is simple obtain the X_0.

In locked rotor test instead, the equivalent circuit is shown in circuit 5.2

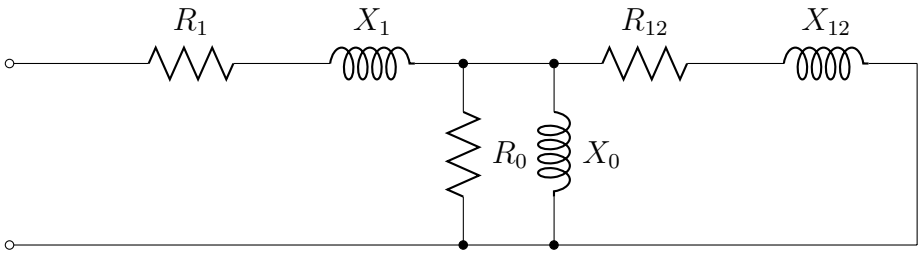

Circuit 5.2: IM Locked Rotor circuit

The procedure used for obtain the rotor data are:

$$\dot{Z}_1 = R_1 + jX_1 \tag{5.8}$$

$$\dot{Z}_{cc} = \frac{\bar{V}_{cc}}{\sqrt{3} \cdot \bar{I}_{cc}} \tag{5.9}$$

and neglecting for the low voltage, the R_0 resistance:

$$\dot{Z}_0 = jX_0 \tag{5.10}$$

$$\dot{Z}_{12} = \frac{(\dot{Z}_{cc} - \dot{Z}_1) \cdot \dot{Z}_0}{(\dot{Z}_1 + \dot{Z}_0 - \dot{Z}_{cc})} \tag{5.11}$$

The resistance now must to be correct with the temperature coefficient, because the measures are made at 20 Celsius degree.

In Table 5.7 are listed the Value of the equivalent circuit of the three motor. There is a strange discrepancy of the data for the motor #01 respect to the other, especially to the motor #02, that should be very similar.

The resistance are expressed at 120 Celsius Degree, because the simulation are carried out with material at this temperature.

Table 5.7: Parameter of equivalent circuit of the 3 motor

	$R_1[\Omega]$	$X_1[\Omega]$	$R_0[\Omega]$	$X_0[\Omega]$	$L_m[H]$	$R_{12}[\Omega]$	$X12[\Omega]$
Standard	4.615	4.45	1684	93.15	0.296	4.55	3.80
#01	4.615	4.45	2051	89.14	0.283	9.08	14.09
#02	4.615	4.45	1858	85.87	0.273	5.32	5.31

The value of R_0 resistance is influenced by the mechanical losses. When the no-load test has been made, the motors bearings and water-block was new, then the friction on the shaft and the mechanical losses on bearing are not equal. Probably after many hours of operation the mechanical losses are almost the same and the resistance R_0 has the same value.

5.2 High frequency measurement

5.2.1 Only stator measure

We have pulled out the rotor from the motor and then the high frequency measurement to investigate the stator parameter at frequency different than $50\,Hz$ are made.

Preliminary a stator resistance measure is made. With this value is possible to make some considerations. The resistance measure between phase-phase has a value of 6.5Ω, so for one phase the resistance is

$$R_s = 3.25\Omega$$

.

The measurement are done in two different supply condition. In 5.3 are shown the electrical connection and in the Table 5.8 are reported the results.

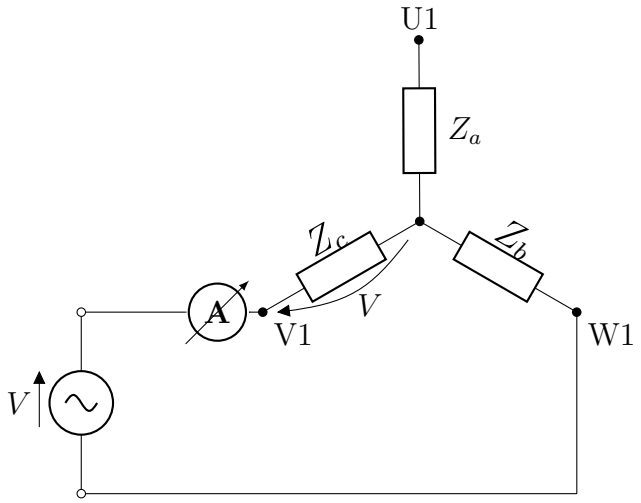

Circuit 5.3: Measure Circuit Nr 1

The measured resistance is almost the same for the two frequencies. At 500 Hz the resistance is a bit greater, due to the current distribution inside the slot. The reactance instead are closely related with the frequency, and is rightful that at 500 is bigger. The measured leakage inductance is not influenced by the frequency.

Table 5.8: Measurement of the V1 phase

Parameter	300 Hz	500 Hz
V [V]	21.28	20.30
I [A]	0.7127	0.4110
P [W]	1.8	0.6
S [VA]	15.2	8.3
Q [VAr]	15.1	8.3
R [Ω]	3.488	3.767
X [Ω]	29.65	49.24
Z [Ω]	29.85	49.39
PF	0.117	0.0763
deg	83.3	85.6
$L\sigma s\,[mH]$	15.73	15.67

For validate the results another measure is made in the supply condition reported in circuit 5.4 and the result are reported in Table 5.9

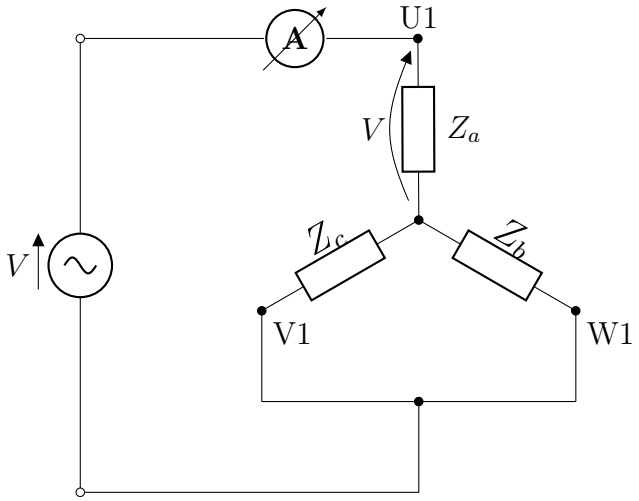

Circuit 5.4: Measure Circuit Nr 2

The leakage inductance of the only stator has circa the same value in both supply condition. This value is referred at high frequency sinusoidal supply and match very good with the value obtained with the test carried out at 50 Hz. This is a very good things, because only a 50 Hz measure is necessary to obtain the parameter.

Table 5.9: Measurement of the U1 phase

Parameter	300 Hz	500 Hz
V [V]	39.22	27.92
I [A]	1.25	0.57
P [W]	5.4	1.2
S [VA]	49.1	15.9
Q [VAr]	48.8	15.9
R [Ω]	3.463	3.651
X [Ω]	31.15	48.83
Z [Ω]	31.34	48.97
PF	0.11	0.075
deg	96.3	94.3
$L\sigma s\,[mH]$	16.52	15.54

5.2.2 Mutual coupling of $\alpha\beta$ reference frame

For investigating the mutual coupling of the stator axis in $\alpha\beta$ reference frame, the adopted supply condition is in circuit 5.5:

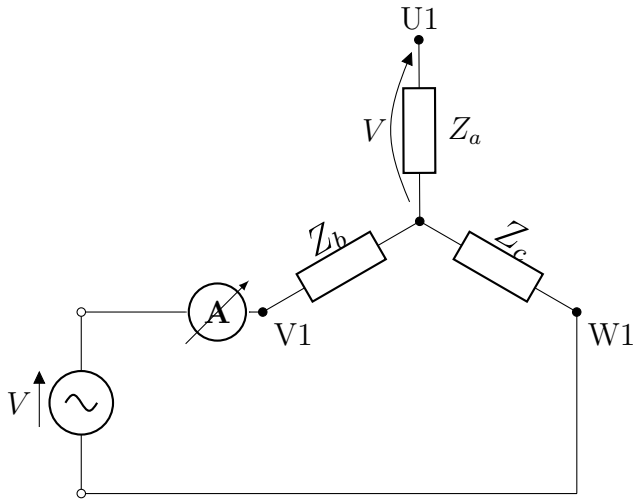

Circuit 5.5: Mutual coupling measure circuit

In the Table 5.10 are reported the measure made at different frequency. In this way is possibly to see the influence of the frequency to the mutual coupling.

I've take the maximum value of the measured voltage, because at the

time in which the measure is done, I have not a recording instrument. For a simple check is by the way sufficient.

Table 5.10: Measurement of the Mutual Coupling

$Frequency[Hz]$	$Voltage[V]$	$Current[A]$	$\Lambda[mVs]$	$M_{\alpha\beta}[mH]$
900	5.79	0.083	1.024	8.74
800	5.73	0.095	1.140	8.48
700	5.69	0.112	1.294	8.21
600	5.61	0.134	1.487	7.83
500	5.44	0.168	1.733	7.31
450	5.32	0.190	1.882	6.99
400	5.16	0.219	2.052	6.22
350	4.95	0.256	2.253	6.22
300	4.69	0.306	2.490	5.76
250	4.37	0.374	2.779	5.25
200	3.95	0.475	3.145	4.68
150	3.42	0.636	3.623	4.03
100	2.70	0.933	4.291	3.25
50	1.73	1.626	5.507	2.39

From Table 5.10 it can be seen that the mutual inductance $M\alpha\beta$ it's not a constant value as expected, but it is variable with the frequency or the current. This result maybe is due to the saturation of iron and it must deeply investigate.

5.2.3 Automatic measure with D-Space Software

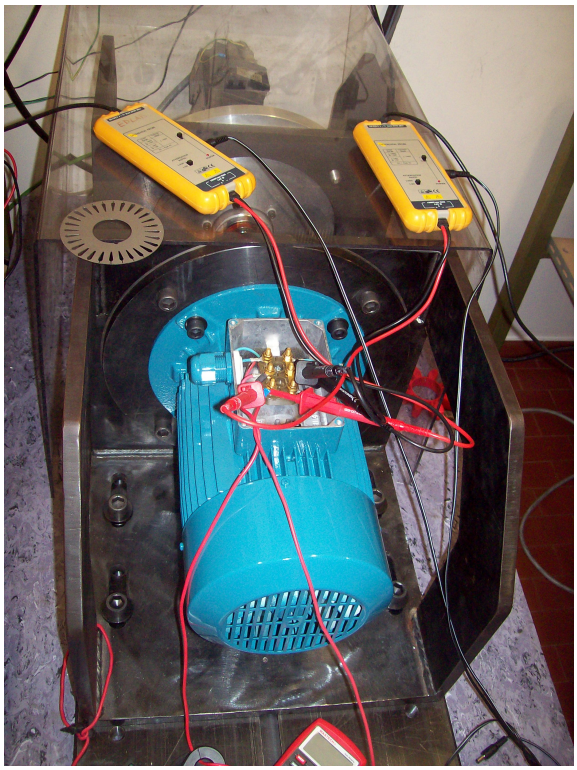

Figure 5.3: Test Bench

An automatic measurement with an automated software that use a D-Space Card and a Matlab script is made. The motor under test is the prototype 02.

The object of the measure is to obtain the motor data at different angular position and reproduce the same result of the simulation made with finite element.

The step are:

- acquire measure (voltage and current)
- moving the rotor of 2 degree
- acquire measure
- ...

for one complete rotation of the rotor.

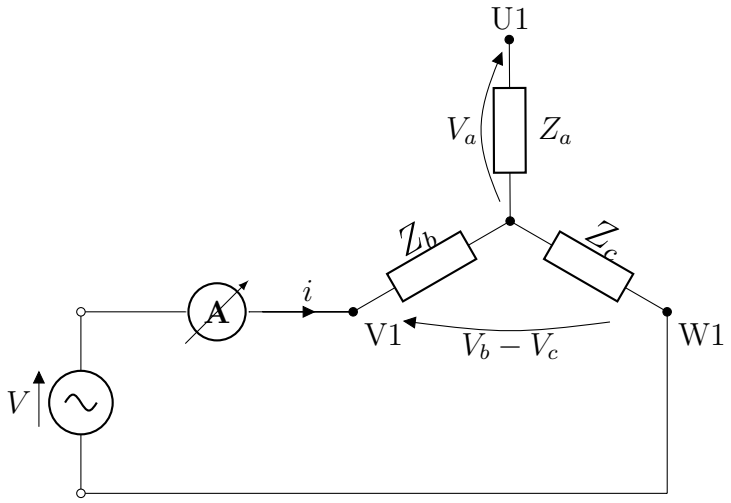

Circuit 5.6: Automatic measure electric connection

The electrical connection adopted for automatic measure is reported in circuit 5.6.

The $\alpha\beta$ transformation use the sign convention reported in circuit 5.7.

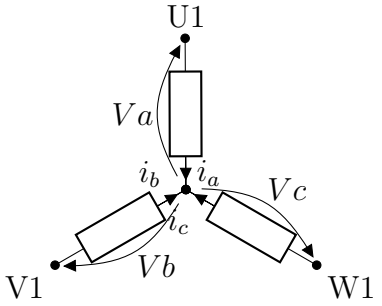

Circuit 5.7: $\alpha\beta$ transformation sign convention

For the v_β the transformation give us:

$$v_\beta = \frac{1}{\sqrt{3}} (v_b - v_c) \tag{5.12}$$

and for the v_α the transformation give us:

$$v_\alpha = \frac{2}{3} \cdot v_a \tag{5.13}$$

the current instead is simple to obtain and is:

$$i_\beta = \frac{2}{\sqrt{3}} \cdot i \tag{5.14}$$

where i is the current measured by the current meter.

In the measure, the voltage is imposed and the current is measured. In fig 5.4 the imposed voltage can be see and in fig 5.5 the measured current is reported.

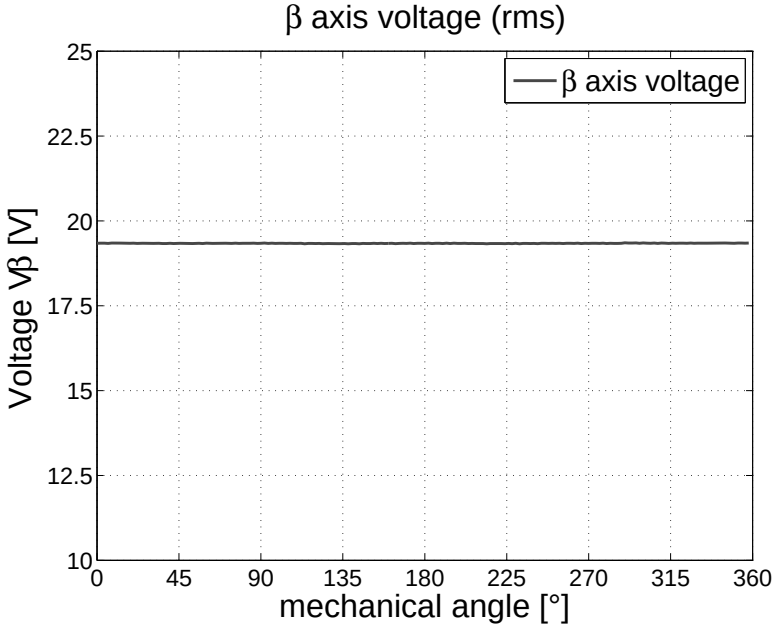

Figure 5.4: Imposed voltage on β axis

Mutual Coupling

The measure circuit is the Circuit 5.6. The mutual leakage inductance between α and β axis come from:

$$M_{\alpha\beta} = \frac{v_\alpha}{\omega \cdot i_\beta} \tag{5.15}$$

The result of this measure are compared with the simulation result in a similar supply situation. The value of the mutual leakage inductance is reported in fig 5.6. The straight line is referred to the simulation result while, with the dots, the measurement is reported. It can be note that there is a difference between the maximum value of the two curves. The shape is the same.

The measure over a complete rotation of the rotor is reported in fig 5.7.

The trend is the same every 90 degree and maybe also this affect could be used for the rotor position recognising.

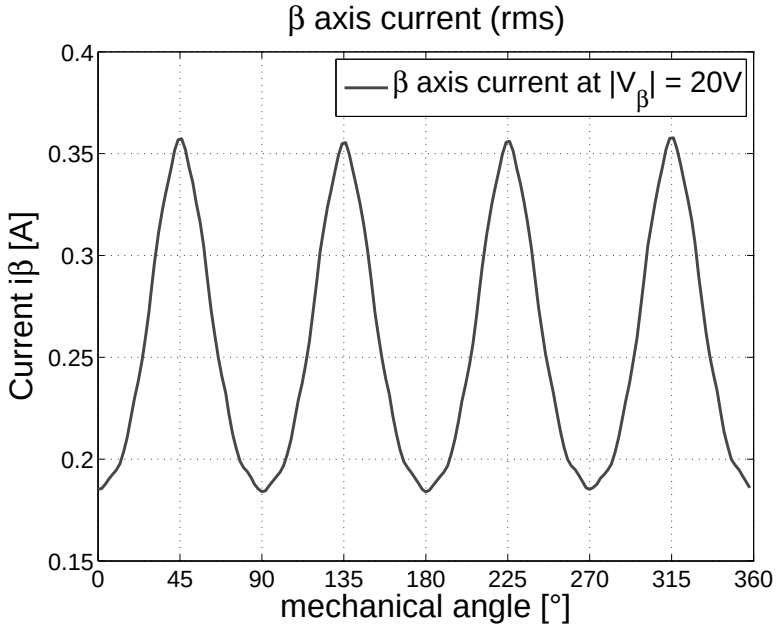

Figure 5.5: Measured current on β axis

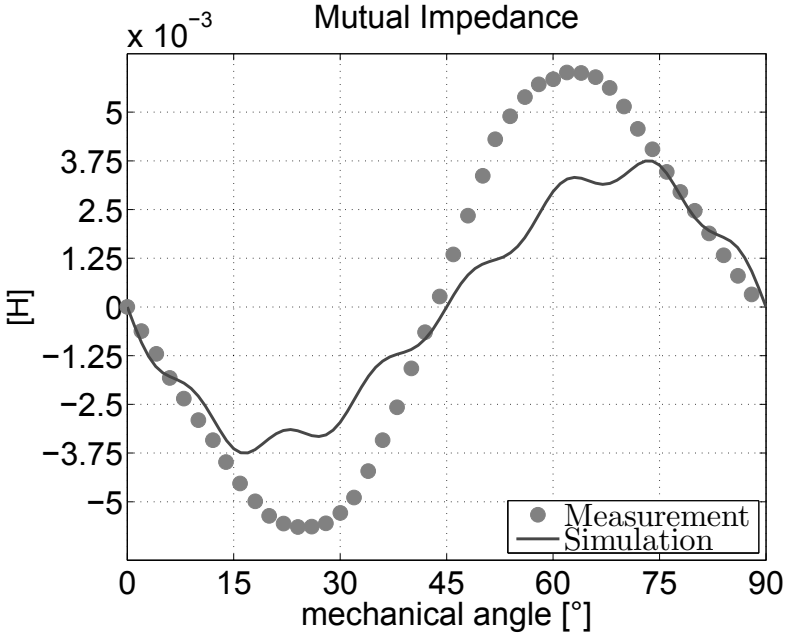

Figure 5.6: Comparison of measured and prototype 02 mutual impedance

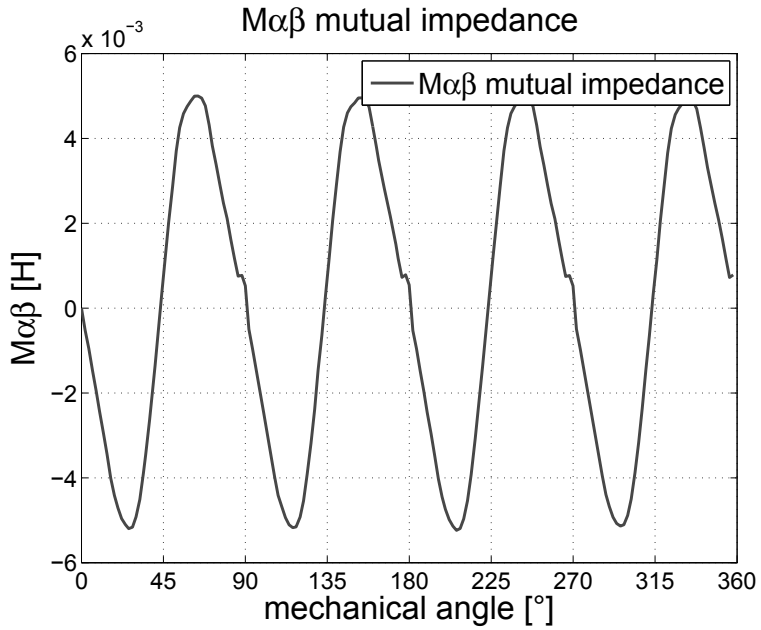

Figure 5.7: Measured mutual inductance over 360

Impedance of β axis

For calculating the impedance Z_β the formula is:

$$Z_\beta = \frac{v_\beta}{i_\beta} = \frac{v}{2 \cdot i} \tag{5.16}$$

From circuit 5.7 is simple to observe that the V_β is exactly the voltage between the phase V1 and W1. For a check of this assertion a measure of the V_b and V_c is made and the V_β is computing through the complex notation of those voltage. Separately a measure of the V_{VW} is made and then the result of the two way are plotted in fig 5.8 and compared. It can be observe that there is no substantial difference between the two measure method.

The Measure is made over one complete rotation of the motor. It can be observe that the the imposed voltage has a slightly deformation with the number of motor pole. This is simply caused by the current that flow in the winding; in particular the minimum of the voltage correspond with the maximum of the current. A possibly explanation is that the power supply used for this measure isn't able to maintain the voltage constant. Nevertheless the variation is little and not intake the measure result.

The impedance of β axis obtained with this measure is reported in magnitude and phase in fig 5.9

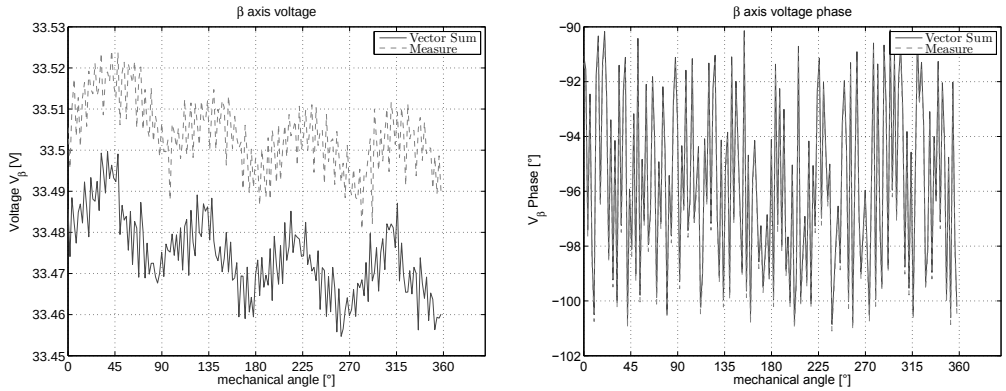

Figure 5.8: Comparison of two measure methods of V_β

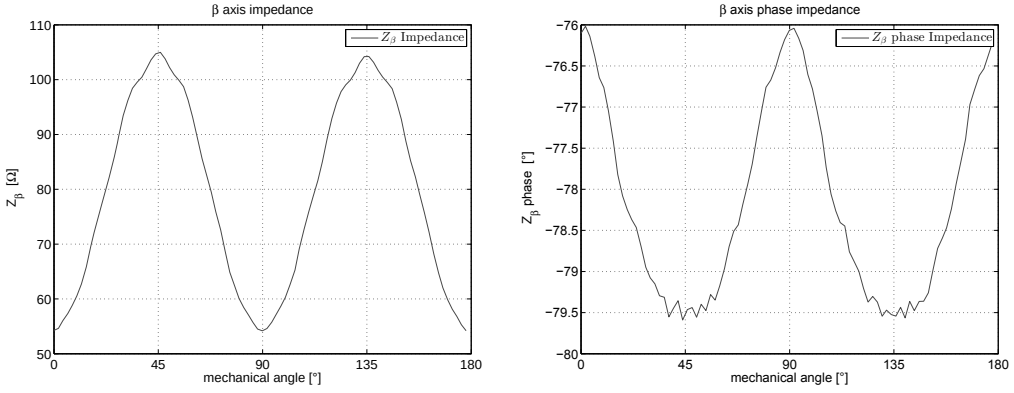

Figure 5.9: Measured Z_β magnitude and phase of prototype 02

It's possible now obtain the rotor parameter from the equivalent circuit in $\alpha\beta$ axis. The parameter result from the measure can be compared with the simulation result. The parameter are reported in fig 5.10.

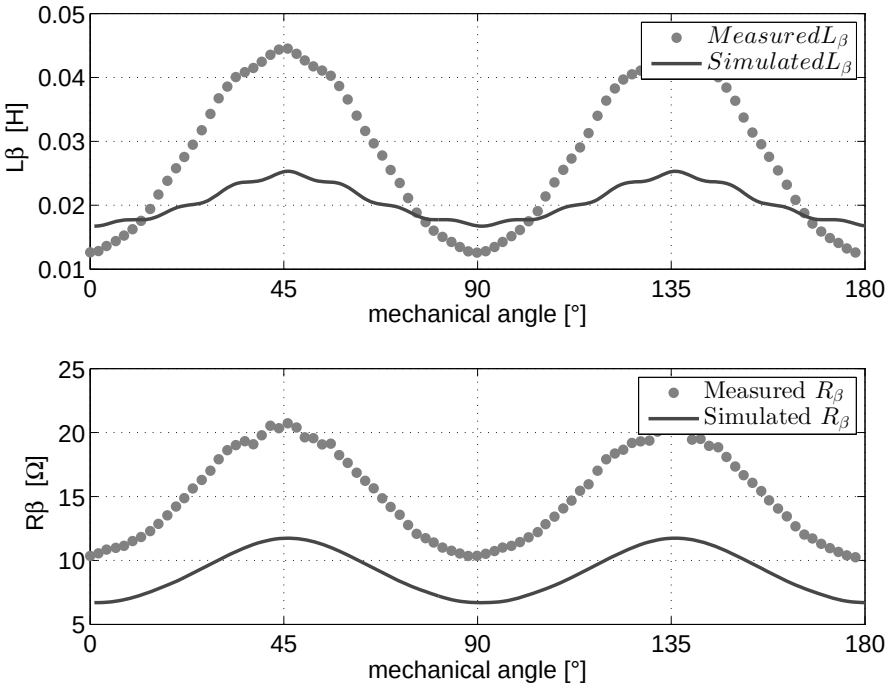

Figure 5.10: Comparison of $\beta axis$ Rotor Parameter of prototype 02

For better note the difference between the measure and simulation only the inductance is reported in fig 5.11. The shape is the same in the two line but there is a difference in the maximum value. This is probably caused by a non optimal die-casting of the rotor slot.

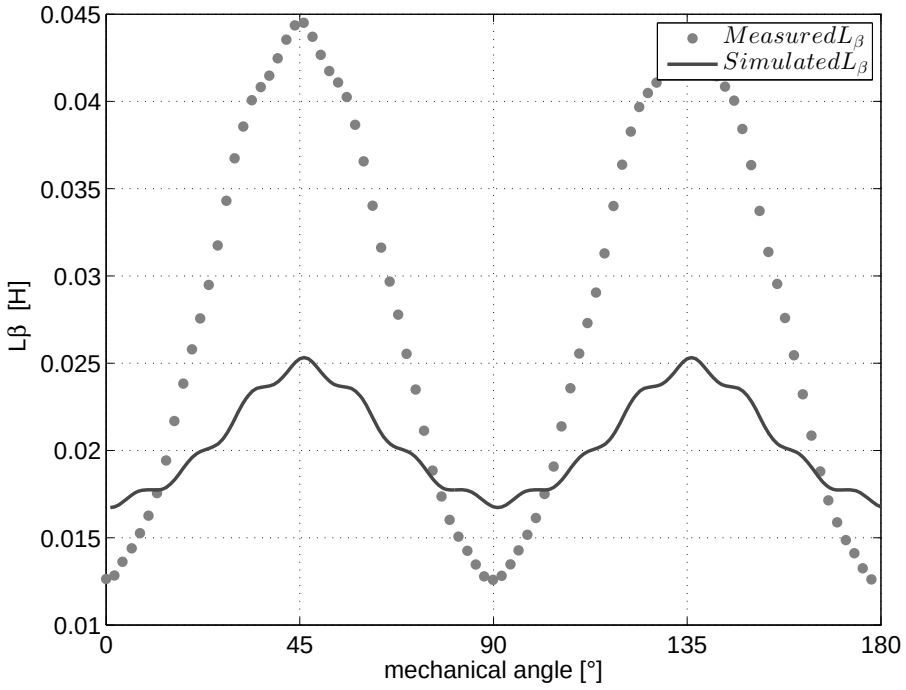

Figure 5.11: Comparison of $\beta axis$ Leakage Inductance of prototype 02

5.2.4 Result of prototype 01

The automatic measure are made also for the prototype 01, in spite of the result of the locked rotor test.

Already from the classical test, is possibly to see that the motor has some problem. The rotor leakage inductance in fact is too big respect to the other two motor. The results of this test are reported in fig 5.12. The prototype 01 seems therefore unusable for nothing, and not sure for a sensorless control.

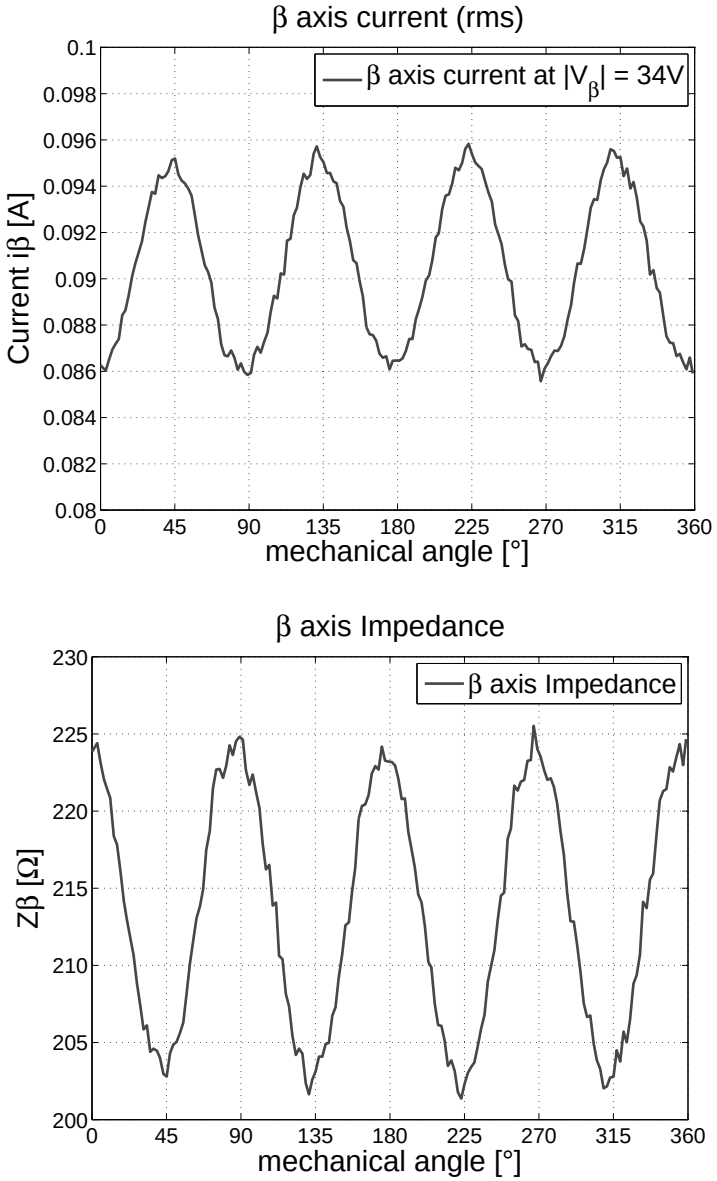

Figure 5.12: Current and β axis impedance of prototype 01

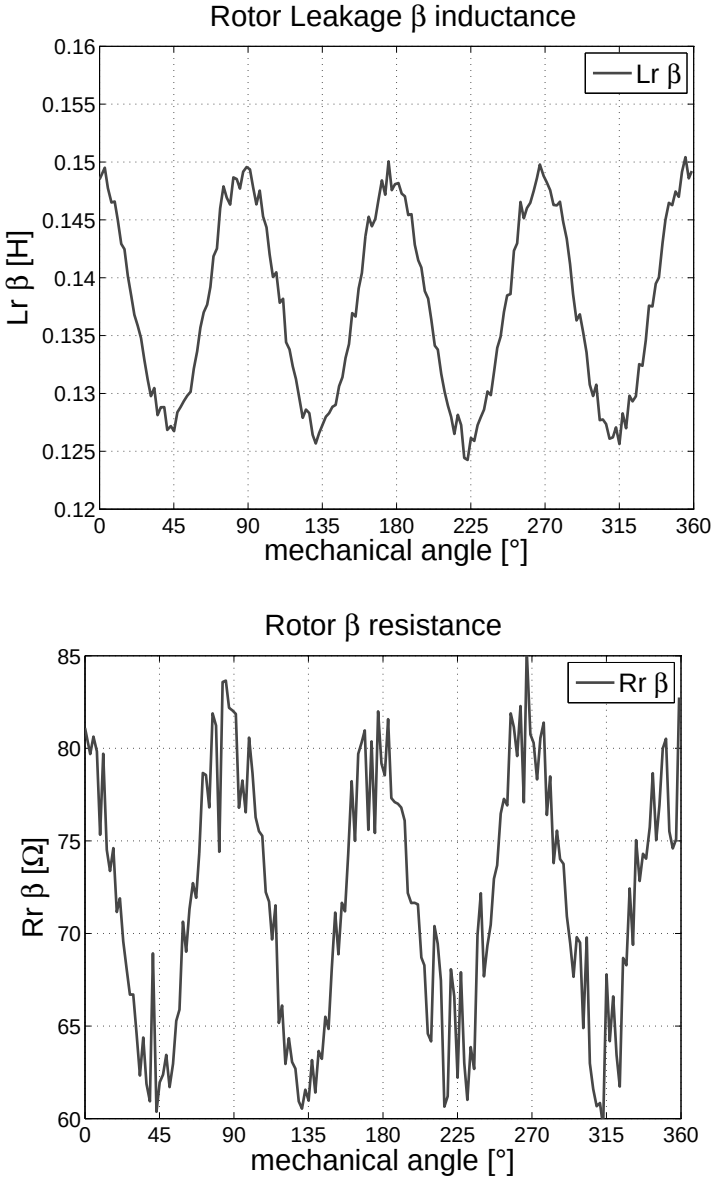

Figure 5.12: Leakage inductance and rotor resistance of prototype 01

5.2.5 Result of Standard motor

For completeness of the measure are below reported the result of the rotor parameter high frequency measure, in order to validate the simulation result, shown in chapter 5. It can be see that the measures are affected by an modulation characterized by rotor slot number. There is any anisotropy present.

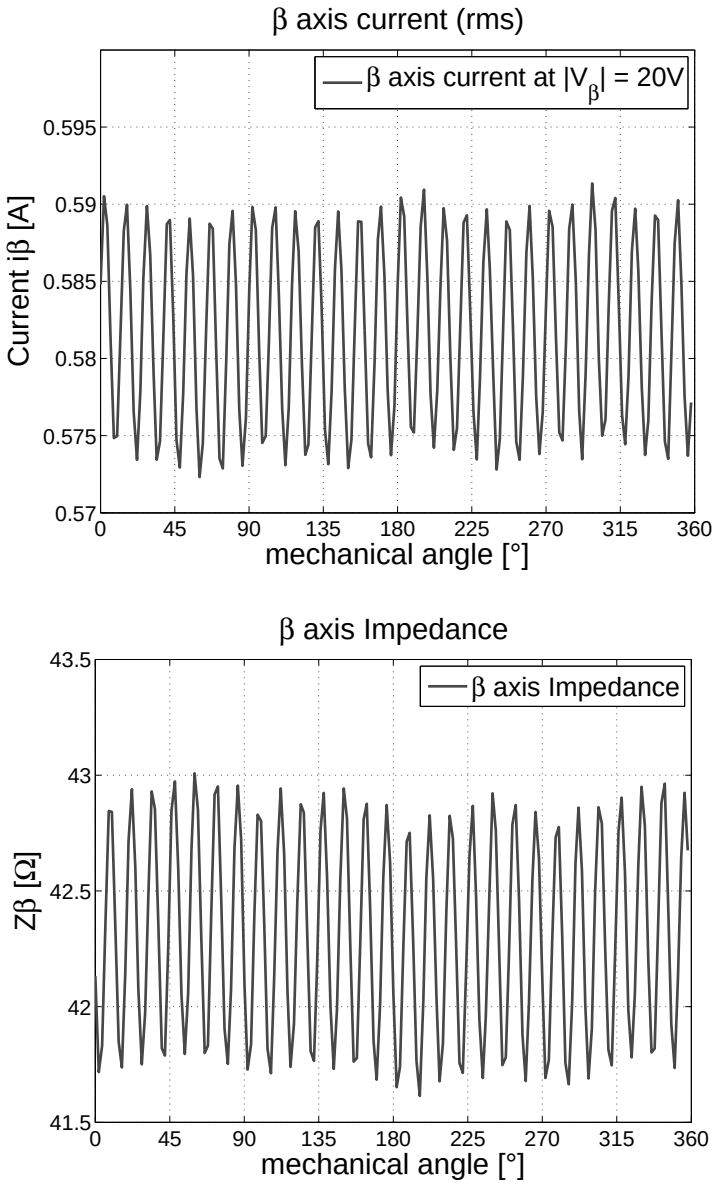

Figure 5.13: Current and β axis impedance of standard motor

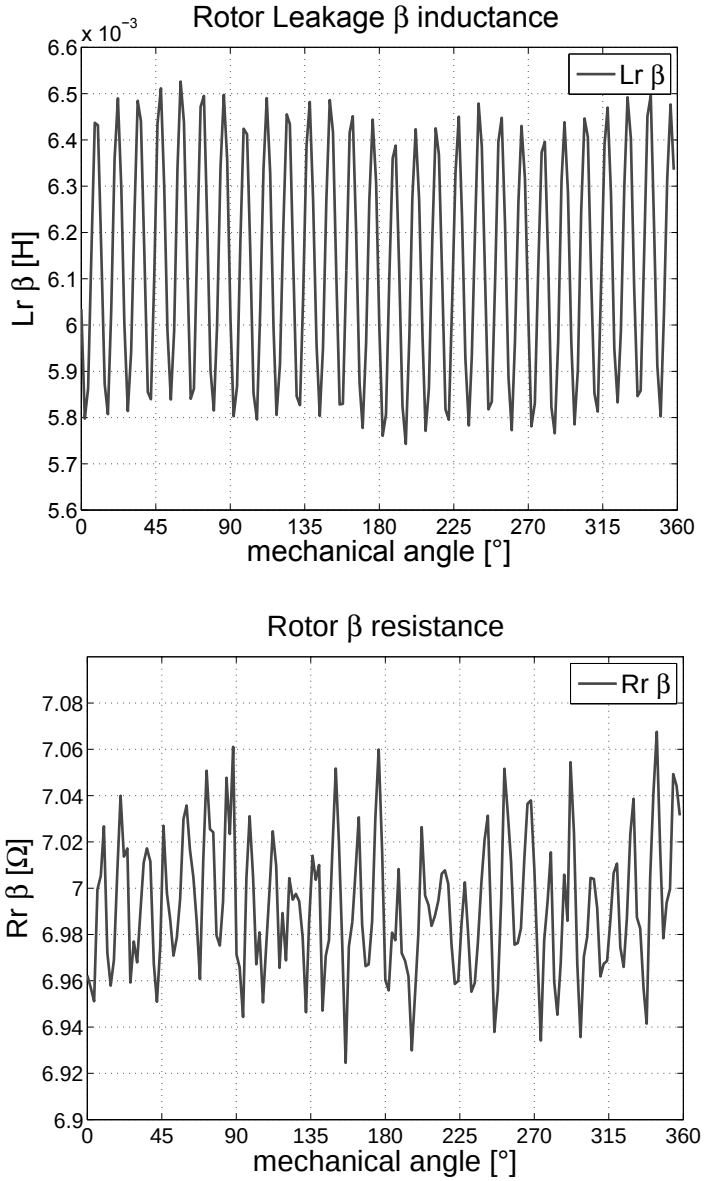

Figure 5.13: Leakage inductance and rotor resistance of standard motor

5.3 Measure with Pacific

Pacific is an instrument that can supply our motor with the desired voltage, variable at will in frequency and in amplitude.

In this section we have made other punctual measure on the prototype 02 with this power supply in order to validate the results obtained with the previous. This allow us also to extend the range of the measure, avoiding the voltage limitation of the used instrumentation.Previous power supply can only create a sinusoidal voltage at variable frequency with maximum voltage value of $\approx 45V_{peak}$. This involves that the maximum β axis voltage is $\approx 19V_{rms}$. The problem is especially remarked at high frequency, because the impedance grow up and the currents are very small.

Table 5.11: Results of pacific measure

		$300[Hz]$		$400[Hz]$		$500[Hz]$		$700[Hz]$	
		$I_\beta[A]$	$Z_\beta[\Omega]$	$I_\beta[A]$	$Z_\beta[\Omega]$	$I_\beta[A]$	$Z_\beta[\Omega]$	$I_\beta[A]$	$Z_\beta[\Omega]$
$V_\beta = 19[V]$	min	196	103	121	157	104	183	81	234
	max	370	55	252	75	195	97	150	126
$V_\beta = 29[V]$	min	336	86	231	126	173	168	115	252
	max	574	50	424	68	335	86	231	126
$V_\beta = 40[V]$	min	525	76	370	108	271	148	173	231
	max	831	48	624	64	492	81	335	119
$V_\beta = 52[V]$	min	740	70	531	98	395	132	254	205
	max	1106	47	845	62	676	77	473	110
$V_\beta = 70[V]$	min	1097	64	785	89	600	117	398	176
	max	1547	45	1174	60	953	73	670	105
$V_\beta = 95[V]$	min					901	105	612	155
	max					1350	70	958	99

Elaborating the data in Table 5.11 the variation of the impedance Z_β in relation of its mean value can be obtain:

$$mean = \frac{max + min}{2}$$

$$diff = max - min$$

$$\Delta = \frac{diff}{mean} \cdot 100$$

The result is in function of the current injected and not with the voltage. Therefore a Table 5.12 with approximated value of current is made and for the variation a linear interpolation is considered.

Table 5.12: Percentage variation of β axis impedance

Current [mA]	$300[Hz]$	$400[Hz]$	$500[Hz]$	$700[Hz]$
≈ 250	64%	62%	64%	64%
≈ 350	56%	58%	60%	60%
≈ 500	50%	51%	54%	52%
≈ 780	41%	45%	46%	44%

The measure wit $V_\beta = 19V$ are comparable with the measure made with our instrumentation. Comparing the impedance in Table 5.11 and fig 5.9 the results are clearly the same. So the conclusion is that our measure instrumentation is good, but has the limitation on the maximum voltage.

The percentage variation of the leakage inductance decrease with increasing current. This is caused by the iron saturation of the rotor.

The leakage inductance is hence influenced by iron saturation; measure with loaded motor and signal injection could be very interesting, to see if the sensorless capability of those motor is still valid. Surely the variation of the leakage inductance is very much influenced by the load of the motor.

5.4 Measure with motors under load

5.4.1 Results of under load condition

For the working point at fixed torque load the results are:

The measure with $1.6Nm$ is referred at no load condition, the load is only the mechanical losses of the motor and the master motor (uses as brake).

The efficiency of the motor is calculated with the formulation:

$$\eta = \frac{P_{mecc}}{P_e} \tag{5.17}$$

and

$$P_{mecc} = T \cdot rpm\frac{2\pi}{60} \tag{5.18}$$

The two prototypes under load condition presents cyclic noise, instead of the standard. This hoarded noise could be interesting to analyze, in order to understand the influence of anisotropy at nominal load condition.

Table 5.13: Working Point of Standard Motor

Torque	1.6	5	7.5	10	12	14	16	20
I [A]	2.30	2.60	3.00	3.47	3.92	4.39	4.90	6.07
V [V]	394.3	394.1	393.7	392.8	392.9	392.9	392.6	392.2
P [W]	404	937	1352	1759	2104	2452	2800	3573
Q [VAr]	1521	1514	1541	1586	1655	1741	1845	2171
S [VA]	1569	1776	2046	2362	2670	2991	3330	4124
PF [-]	0.258	0.528	0.661	0.745	0.788	0.819	0.841	0.866
rpm	1493	1478	1466	1454	1445	1435	1423	1399
slip [%]	0.46	1.46	2.26	3.06	3.66	4.33	5.13	6.73
P_{mecc} [W]	250	774	1151	1522	1816	2104	2384	2930
η [%]	61.88	82.60	85.13	86.53	86.31	85.81	85.14	82.01

Table 5.14: Working Point of Prototype 01

Torque	1.6	5	7.5	10	12	14	16	20
I [A]	2.33	2.69	3.11	3.47	4.20	4.84	5.50	7.03
V [V]	394.4	394.0	394.3	394.1	393.8	393.4	393.2	393.7
P [W]	365	919	1319	1750	2110	2496	2876	3681
Q [VAr]	1550	1587	1668	1800	1952	2172	2423	3116
S [VA]	1593	1832	2124	2505	2868	3298	3748	4795
PF [-]	0.229	0.502	0.621	0.699	0.736	0.757	0.768	0.768
rpm	1492	1474	1462	1447	1434	1419	1403	1365
slip [%]	0.53	1.73	2.53	3.53	4.40	5.40	6.46	9.00
P_{mecc} [W]	234	771	1148	1515	1802	2080	2350	2859
η [%]	64.20	83.98	87.05	86.59	85.40	83.35	81.74	77.67

Table 5.15: Working Point of Prototype 02

Torque	1.6	5	7.5	10	12	14	16	20
I [A]	2.55	2.82	3.19	3.63	4.08	4.56	5.17	6.48
V [V]	396.2	395.9	395.3	398.1	397.1	397.3	394.2	392.9
P [W]	384	922	1322	1733	2093	2442	2846	3684
Q [VAr]	1690	1702	1745	1819	1872	1990	2123	2505
S [VA]	1735	1936	2184	2505	2803	3318	3532	4408
PF [-]	0.221	0.477	0.605	0.692	0.747	0.778	0.806	0.836
rpm	1495	1478	1470	1458	1445	1435	1423	1390
slip [%]	0.33	1.46	2.00	2.80	3.66	4.33	5.13	7.3
P_{mecc} [W]	250	773.8	1154	1526	1816	2104	2384	2911
η [%]	65.10	83.93	87.29	88.05	86.76	86.16	83.76	79.02

5.4.2 Comparison of the motors at nominal current

For better compare the three motors performance, a measure at nominal current is made. The motor is starting and loaded until the current is at the rated value. Then a measure of the mechanical and electrical quantities is made and also a computation of useful comparative data is made. All data are visible in Table 5.16.

Table 5.16: Comparison of the motors at nominal current

Parameter	Standard	Prototype 1	Prototype 2
I [A]	3.62	3.61	3.63
V [V]	396.9	394.4	398.1
P [W]	1869	1703	1733
Q [VAr]	1656	1794	1819
S [VA]	2490	2471	2505
PF [-]	0.750	0.689	0.692
rpm	1455	1449	1458
slip [%]	3.00	3.40	2.80
Torque [Nm]	10.67	9.7	10
Ripple [Nm]	0.03	0.4	-
P_{mecc} [W]	1625	1471	1526
η [%]	86.98	86.38	88.05

5.4.3 Results of dynamic torque

For obtain the real mechanical characteristic of the motor, and not only the steady state, is necessary to measure the mechanical starting transitory of the motor. The starting transitory should be not very quickly, so a speed ramp must be impose. The step for make this are:

- Connect the IM with a bigger well controlled motor
- Impose a starting speed ramp at the master motor
- Supply the induction motor with nominal voltage
- Starting the master motor
- measure speed and torque

The result of this measure is then elaborated and plotted in relation of the slip. In fig 5.14 are reported the mechanical characteristics of the three motors. Is good remember that the prototype 01 present a problem with the rotor, already found with the classical measure (no-load, locked rotor). The dynamic torque for this is made only for completeness, but has nothing value.

The resulting torque is also evaluated at zero speed, for measure the starting torque and the starting current.

The result of this measure are reported in Table 5.17

Table 5.17: Comparison of motors starting torque

Motor	Starting Torque [Nm]	Starting Current [A]
Standard	35.4	25.50
Prototype 1	20.5	19.01
Prototype 2	30.4	22.52

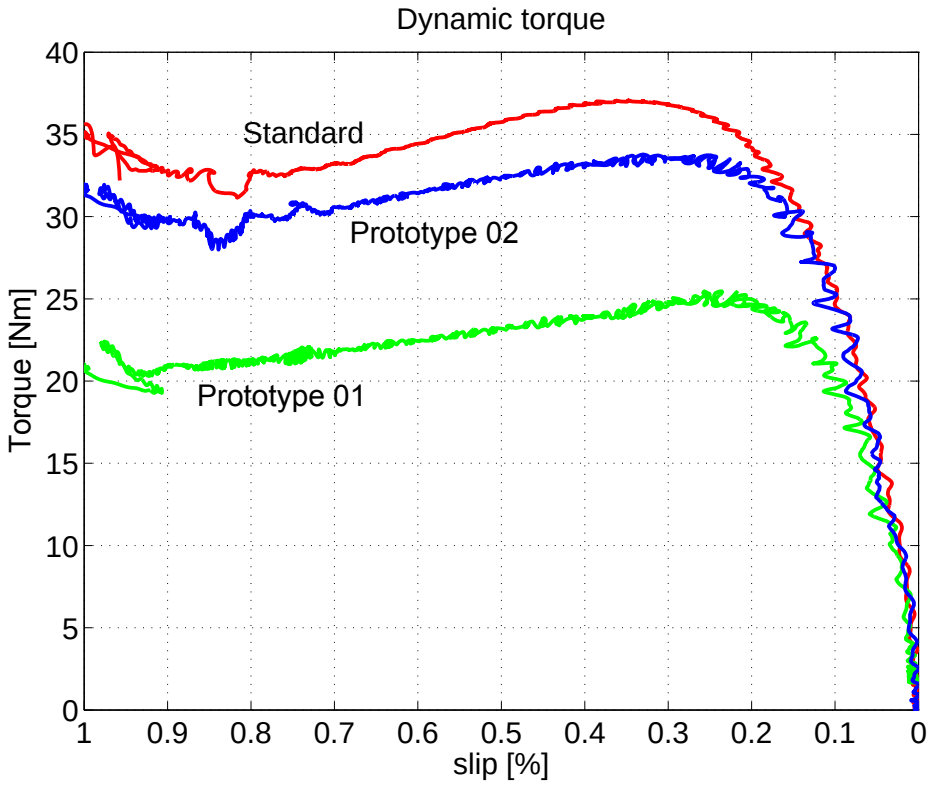

Figure 5.14: Comparison of dynamic torque of the motors

Chapter 6

Motor Parameter comparison

For a better understand the difference of the motors, and validate the measure with analytical model and finite element method, in this chapter a comparison between the investigation methods is reported.

6.1 General remarks

For a valid comparison, the parameter of the motors are to be referred at the same temperature. It is important to make comparison possible. The temperature value has to be a compromise, because when the motor run at no-load the temperature major than the ambient temperature, but smaller than the normal temperature admissible for the temperature class is. So the reference temperature is considered at $40°C$.

6.2 Standard Motor

Table 6.1: Comparison of EC Parameters of Standard Motor

Parameter	Analytical	FEM	Measure
$R_1\,[\Omega]$	3.87	-	3.53
$X_1\,[\Omega]$	7.88	4.43	4.45
$L_m\,[H]$	0.381	0.376	0.296
$R_0\,[\Omega]$	-	1733	1685
$R_{12}\,[\Omega]$	2.9	2.85	3.48
$X_{12}\,[\Omega]$	5.03	2.51	3.80
$I_\mu\,[A]$	1.80	1.8	2.37

The torque, at the nominal current is also different between simulation and measure. It is reported in Table 6.2. It is worth noticing that the Fem torque is the electromagnetic, while the measured one is deducted of mechanical losses.

Table 6.2: Comparison of Torque of Standard Motor

Parameter	Analytical	FEM	Measure
$Torque\,[Nm]$	11.9	12.7	10.67

Table 6.3: Comparison of Rotor HF Parameters of Standard Motor

Parameter	FEM	Measure
Rotor resistance $[\Omega]$	2.95	7
Rotor Leakage inductance $[H]$	0.022	0.006

6.3 Prototype 01

Table 6.4: Comparison of EC Parameters of Prototype 01

Parameter	Analytical	FEM	Measure
R_1 [Ω]	3.87	-	3.53
X_1 [Ω]	7.88	4.43	4.45
L_m [H]	0.381	0.383	0.283
R_0 [Ω]	-	1733	2051
R_{12} [Ω]	2.9	3.32	9.08
X_{12} [Ω]	8.03	11.25	14.09
I_μ [A]	1.80	1.80	2.56

The torque, at the nominal current is also different between simulation and measure. It is reported in Table 6.5

Table 6.5: Comparison of Torque of Prototype 01

Parameter	Analytical	FEM	Measure
$Torque$ [Nm]	11.9	12.1	9.70

Table 6.6: Comparison of Rotor HF Parameters of Prototype 01

Parameter	FEM		Measure	
	d	q	d	q
Rotor resistance [Ω]	10	20	-	-
Rotor Leakage inductance [H]	0.034	0.042	-	-

6.4 Prototype 02

Table 6.7: Comparison of EC Parameters of Prototype 02

Parameter	Analytical	FEM	Measure
R_1 [Ω]	3.87	-	3.53
X_1 [Ω]	7.88	4.43	4.45
L_m [H]	0.381	0.370	0.273
R_0 [Ω]	-	1733	1858
R_{12} [Ω]	2.9	2.90	5.32
X_{12} [Ω]	8.72	3.10	5.31
I_μ [A]	1.80	1.80	2.56

The torque, at the nominal current is also different between simulation and measure. It is reported in Table 6.8

Table 6.8: Comparison of Torque of Prototype 02

Parameter	Analytical	FEM	Measure
$Torque$ [Nm]	11.9	12.0	10.00

Table 6.9: Comparison of Rotor HF Parameters of Prototype 02

Parameter	FEM		Measure	
	d	q	d	q
Rotor resistance [Ω]	7	12	10	20
Rotor Leakage inductance [H]	0.016	0.024	0.012	0.045

6.5 Observation

For all motors the measured no-load current is higher that the estimated and the simulated. Probably there is a difference of the real and the hypothesized air gap.

Prototype 01 From the measure of prototype 01, is clear that always is not correct. The measured rotor parameters are out of usually range and also the dynamic torque is different than the others two. Some construction problems are occurred and the rotor is unusable.

Prototype 02 The measure on prototype 02 are not too much different from the simulation. The good thing is that the variation of high frequency parameters is major than the simulated one. For sensorless application this could be better.

Chapter 7

Conclusion

7.1 General remarks

The analysis on the the sensorless capability of the modified induction motor is positive. Many measure have been carried out and some differences between simulation are investigate. The parameter variation are quite big with respect to the simulated one. This mean that the sensorless capability is better than expected.

The nominal torque of the modified motor is quite small, respect to the standard. The leakage inductance is greater and the nominal torque is reduced. In load condition also some cyclic noise are present, due to the anisotropy of the rotor.

7.2 Identified problems

It is worth noticing that measures on standard and 02 motor make sense. Contrariwise the prototype 01, since from classical measures present signs of constructive problems. The results of locked rotor test are very different than whose of the other two motors. The problem is also present on high frequency measures and it means that probably there is a problem on the rotor prototype 01 external surface.

7.3 Future developments

In this thesis work only the surface of induction motor sensorless drive is investigated. Many others works have also to be performed, in order to

achieve an operating sensorless drive. Neither the effect of saturation at steady state operation on sensorless control of IM has not been studied yet.

Suggestion on possible future works include:

- Investigate the slot influence on $Ldiff$ and creation of a more complete analytical model.
- Investigate the saturation effect at steady state operation on sensorless control of IM. In authors opinion, it would be interesting to simulate the nominal condition and compute the mapping of the relative permeability of the motor. After that such a mapping can be used when applying the high frequency signal, so as to understand the *effect of saturation* on L_{dif}.
- Measure and identification of the prototypes cyclic noise and vibration, in loaded condition.
- Lathing rotor 01, in order to understand the hypothesized construction problems.
- Realize a functioning sensorless drive.

Bibliography

[1] L. Alberti, "A modern analysis approach of induction motor for variable speed applications," Ph.D. dissertation, University of Padova, 2009.

[2] L. Alberti, N. Bianchi, and S. Bolognani, "A very rapid prediction of im performance combining analytical and finite-element analysis," *Industry Applications, IEEE Transactions on*, vol. 44, no. 5, pp. 1505–1512, 2008.

[3] *Finite Element Method Magnetics Version 3.3 User s Manual March 17, 2003.*

[4] *Finite Element Method Magnetics Version 4.2 User s Manual October 16, 2010.*

[5] L. Alberti, N. Bianchi, and S. Bolognani, "A very rapid prediction of im performance combining analytical and finite-element analysis," *Industry Applications, IEEE Transactions on*, vol. 44, no. 5, pp. 1505–1512, 2008.

[6] L. Alberti, N. Bianchi, S. Bolognani, and E. Fornasiero, "Im rotor parameters analysis with an intentionally created saliency," in *Sensorless Control for Electrical Drives (SLED), 2010 First Symposium on*, 2010, pp. 120–126.

[7] J. Holtz, "Sensorless position control of induction motors. an emerging technology," in *Advanced Motion Control, 1998. AMC '98-Coimbra., 1998 5th International Workshop on*, 1998, pp. 1–14.

[8] M. Degner and R. Lorenz, "Using multiple saliencies for the estimation of flux, position, and velocity in ac machines," *Industry Applications, IEEE Transactions on*, vol. 34, no. 5, pp. 1097–1104, 1998.

[9] J. Holtz, "Sensorless control of induction machines - with or without signal injection?" *Industrial Electronics, IEEE Transactions on*, vol. 53, no. 1, pp. 7–30, 2005.

[10] L. Alberti, N. Bianchi, and S. Bolognani, "Variable-speed induction machine performance computed using finite-element," *Industry Applications, IEEE Transactions on*, vol. 47, no. 2, pp. 789–797, 2011.

[11] D. Dolinar, R. De Weerdt, R. Belmans, and E. Freeman, "Calculation of two-axis induction motor model parameters using finite elements," *Energy Conversion, IEEE Transactions on*, vol. 12, no. 2, pp. 133–142, 1997.

[12] S. B. Nicola Bianchi, *Metodologie di progettazione delle macchine elettriche*. Cleup, 2001.

[13] S. Boroujeni, N. Bianchi, and L. Alberti, "Fast estimation of line-start reluctance machine parameters by finite element analysis," *Energy Conversion, IEEE Transactions on*, vol. 26, no. 1, pp. 1–8, 2011.

[14] C.-D. W. Chang-Huan Liu, Horn-Chi Chang, "Very low speed sensorless control of induction motors drives using high frequency signal injection," 2005.

[15] J.-I. Ha and S.-K. Sul, "Physical understanding of high frequency injection method to sensorless drives of an induction machine," in *Industry Applications Conference, 2000. Conference Record of the 2000 IEEE*, vol. 3, 2000, pp. 1802–1808 vol.3.

[16] J. Holtz and H. Pan, "Acquisition of rotor anisotropy signals in sensorless position control systems," *Industry Applications, IEEE Transactions on*, vol. 40, no. 5, pp. 1379–1387, 2004.

[17] P. Lawrenson, "Sensorless vector and direct torque control," *IEE Review*, vol. 45, no. 1, pp. 40–40, 1999.

[18] J. Cilia, G. Asher, and K. Bradley, "Sensorless position detection for vector controlled induction motor drives using an asymmetric outer-section cage," in *Industry Applications Conference, 1996. Thirty-First IAS Annual Meeting, IAS '96., Conference Record of the 1996 IEEE*, vol. 1, 1996, pp. 286–292 vol.1.